Electrical and Optical Characterisation of Bulk Heterojunction Polymer-Fullerene Solar Cells

Von der Fakultät Mathematik und Naturwissenschaften der
Carl von Ossietzky Universität Oldenburg
zur Erlangung des Grades und Titels eines
Doktors der Naturwissenschaften
(Dr. rer. nat.)
angenommene Dissertation.

Von Herrn Zivayi Chiguvare
Geboren am 26. October 1969
in Marondera, Zimbabwe

Erstgutachter: Prof. Dr. Vladimir Dyakonov
Zweitgutachter: Prof. Dr. Juergen Parisi, und
Prof. Dr. Wilfried Tuszynski

Tag der Disputation: 14.02.2005

Erklärung gemäss $8(2) der Promotionsordnung
 Hiermit erkläre ich, dass ich diese Arbeit selbständig verfasst und nur die angegebenen Hilfs-

mittel benutzt habe. Oldenburg, den ...

 Unterschrift

0.1 Technical Summary

Polymer based solar cells are interesting because their fabrication process can be less expensive and less complicated as compared to that of inorganic solar cells. Bulk heterojunction polymer fullerene solar cells consist of an absorber layer of an interpenetrating network of donor (polymer) and acceptor (fullerene) materials sandwiched between two electrodes, carefully chosen to selectively transport one type of the optically generated charge carriers and block the other. Usually Indium Tin Oxide (ITO) and Aluminium (Al) are used as electrodes. For improved performance, a PEDOT:PSS layer is spin-coated between ITO and the absorber layer. The physics of such solar cells is only scarcely understood, and low energy conversion efficiencies have held back their application. If the physics is understood, then it will be possible to optimize device fabrication and performance and hence, improve the efficiency and lifetime of such devices so that high efficiency practical solar cells can be made out of these materials.

In this work, transport properties of the donor poly(hexyl-thiophene) (P3HT), acceptor [6,6]-phenyl-C61 butyric acid methyl ester (PCBM), and P3HT:PCBM blends of selected ratios, were studied, by analysing dark, temperature dependent current-voltage characteristics of P3HT sandwiched between various pairs of electrodes. This was done in order to establish the current limiting mechanisms in the respective devices. Interface potential barriers were estimated from Fowler-Nordheim and /or Richardson-Schottky emission theories. In cases where the contacts were ohmic, the current conduction was found to be limited by bulk transport properties of the P3HT itself, and the trap density could also be estimated from space charge limited current (SCLC) models with traps distributed at different depths within the band gap.

In order to establish the role of the PEDOT:PSS layer spin coated between the positive ITO electrode and absorber layer, studies of solar cells prepared from single layer P3HT, PCBM or blend devices with, and without the PEDOT:PSS layer were done. The obtained parameters could be used to explain some of the features observed in the current-voltage characteristics of solar cells employing P3HT:PCBM blends as absorber. Such understanding leads to some clue as to what must be varied in such solar cells in order to improve their efficiency.

We concluded that besides participating as an electrode, the PEDOT:PSS layer provides the charge separating interface in blend devices. It is suggested that the observed optimum exciton splitting network consists of a homogeneous P3HT:PCBM weight ratio of 1:1 corresponding to 6 monomer units of P3HT per molecule of PCBM. Extra amounts of either material introduce shielding effects which reduce the exciton splitting efficiency.

It was observed that the efficiency of P3HT:PCBM solar cells improves after a thermal annealing step. Experiments were carried out to determine why this is so, by studying *J(V)* characteristics of P3HT, PCBM or P3HT:PCBM blend sandwiched between ITO and Al and/or ITO/PEDOT:PSS and Al electrodes. It was established that the number of traps decreases on annealing P3HT, and this was attributed to oxygen dedoping of the P3HT. It was also established that the hole injecting barrier at the PEDOT interface increases on thermal annealing of all three materials. On thermally annealing the cells, different degrees of conglomeration of pure PCBM islands within the P3HT:PCBM blends were also observed, dependent on the P3HT:PCBM ratio, and commensurate with the observed increase in efficiency.

0.2 Zusammenfassung

Organische Solarzellen sind interessant, da ihre Herstellung im Vergleich zu anorganischen So-
larzellen günstiger und weniger aufwändig ist. Eine "Bulk Heterojunction Polymer - Fullerene"
Solarzelle besteht aus einer Absorberschicht aus einem Donator-Akzeptor Gemisch, das sich zwi-
schen zwei Elektroden befindet, die so ausgewält werden, daß jeweils eine Art der optisch erzeugten
Ladungsträger transportiert wird, während die andere blockiert wird. Üblicherweise verwendet man
Indium-Zinn-Oxid (ITO) und Aluminium (Al) als Kontakte. Zur Verbesserung des Wirkungsgrades
wird zwischen die ITO- und die Absorberschicht PEDOT:PSS aufgebracht. Die Physik solcher So-
larzellen ist noch in den Anfängen und die geringen Wirkungsgrade haben bisher ihre Anwendung
verhindert. Sobald die Physik verstanden ist, kann nicht nur die Herstellung und Funktion dieser So-
larzellen optimiert werden, sondern auch der Wirkungsgrad und die Lebensdauer verbesert werden,
so daß hocheffiziente, praktische Solarzellen produziert werden können.

In dieser Arbeit wurden die Transporteigenschaften des Donators P3HT, des Akzeptors PCBM
und von Gemischen von P3HT:PCBM in verschiedenen Verhältnissen untersucht, indem die tem-
peraturabhängigen Stromspannungskennlinien von P3HT-Dioden mit unterschiedlichen Elektroden
analysiert wurden, um jeweils den strombegrenzenden Mechanismus zu bestimmen. Die Energiebar-
rieren an den Grenzflächen wurden mit Hilfe der Fowler-Nordheim- bzw. der Richardson-Schottky-
Theorie abgeschätzt. Im Falle ohmscher Kontakte wurde festgestellt, dass der Strom durch die Vol-
umeneigenschaften von P3HT begrenzt wurde. Die Störstellendichte konnte dann aus der Theorie
der raumladungsbegrenzten Ströme (SCLC) ermittelt werden.

Um die Rolle der zwischen der ITO Elektrode und der Absorberschicht aufgebrachten PEDOT:PSS
Schicht zu klären, wurden Untersuchungen an Dioden mit P3HT, PCBM und Gemischen aus beiden
Materialen mit und ohne PEDOT:PSS gemacht. Mit den auf diese Weise gefundenen Parametern
konnten einige Aspekte der Stromspannungkennlinien von P3HT:PCBM Solarzellen erkärt werden.
Eine derartiges Verständnis liefert Anhaltspunkte dafür, welche Parameter geändert werden müssen,
um den Wirkungsgrad dieser Solarzellen zu erhöhen.

Wir kamen zu dem Schluß, dass die PEDOT:PSS Schicht nicht nur als Elektrode, sondern auch als
ladungsträgertrennende Grenzfläche fungiert. Die optimale Exziton-Aufspaltung wurde bei einem
homogenen P3HT:PCBM Gewichtsverhältnis von 1:1 beobachtet, was einem Verhältnis von sechs
P3HT Monomer-Einheiten zu einem PCBM Molekül entspricht. Abweichungen von diesem Mis-
chungsverhältnis haben Abschirmungseffekte zur Folge, die zu einer Senkung der Effektivität der
Exziton-Aufspaltung führen.

Es wurde beobachtet, daß es nach einem Temperschritt zu einer Erhöhung des Wirkungsgrades von
P3HT:PCBM Solarzellen kommt. Um die Ursache zu klären, wurden die Stromspannungskennlin-
ien von P3HT, PCBM und P3HT:PCBM-Dioden mit ITO und Al bzw. ITO/PEDOT und Al als
Elektroden untersucht. Dabei stellte sich heraus, dass es durch Tempern von P3HT zu einer Ver-
ringerung der Störstellendichte kommt, die auf Entfernen von Sauerstoff zurückzuführen ist. Zudem
wurde in allen drei Materialen festgestellt, dass die Energiebarriere für die Injektion von Löchern
an der PEDOT:PSS Grenzfläche durch das Tempern erhöht wird. Desweiteren bewirkte das Tem-
pern der P3HT:PCBM-Solarzellen eine unterschiedlich starke Bildung von PCBM-Inseln, die vom
P3HT:PCBM-Verhältins abhing und dem beobachteten Anstieg der Wirkungsgrades dieser Solarzellen
korreliert war.

Contents

Contents

List of Figures

List of Tables

0.3 Preamble

NATURE - the entire universe (including the earth-atmosphere system) is a physical system that is constantly trying to achieve thermal equilibrium. Matter and energy are therefore being constantly exchanged in space and time to try and achieve this equilibrium on local and universal scale. These move from spaces of high to those of lower concentration at speeds determined by external fields and concentration gradients. The media that transport energy and matter, like solids, liquids and gases, as well as man, plant and animal life are vehicles through which local and universal thermal equilibrium is being achieved. Our environment is the earth-atmosphere system fueled by solar energy. The position of the sun in the solar system, the elliptical orbit of the earth around sun, the rotation of the earth about its axis, and the inclination of the earth's axis to the ecliptic plane govern the natural distribution of energy in the earth-atmosphere system. We are all matter transforming into energy and vice versa in the vast infinity of space and time, which also transform one into the other continuously. The only way for man to get enough food and thermal comfort as efficiently as possible, in a sustainable manner, is to live in harmony with nature and with each other within the community, and for communities to live in harmony with each other, countries and continents alike. Man, unlike other animals and plants, can deliberately enact policies that guarantee this sustainability and harmony, and can also destroy these if not careful and considerate enough. Man must acknowledge the importance of living with the deep rhythms of nature and understand that when we conduct our activities aligned with the world's natural cycles, the energy of our actions is blessed by the energies of nature.

0.4 Acknowledgements

I would like to acknowledge the support and guidance offered to me by my supervisors Professor Juergen Parisi, Dr. Vladimir Dyakonov and Dr. Edward Chikuni. In particular I wish to single out the valuable discussions I had with Dr. Dyakonov, and thank him for all the constructive criticism, which benefitted me immensely both during the experimental part, and the compilation of this project. He is a valuable collaborator and a true friend indeed.

To the Photovoltaics group of the University of Oldenburg (UO), in particular: Ingo Riedel, Dana Chirvase, Casten Deibel, Elizabeth von Hauff, Michael Pientka, Verena Mertens, Susanne Boeger, and Britta Bohnenbuck, I thank you all for the fruitful discussions, moral support, and patience as you endured sometimes long hours of listening to my fantasy, or waited for me to complete my measurements so you could do yours. Special mention goes to Holger Koch, Andrea Geisler, Hans Holtorf, Felix Voigt, and Jens Reemts for technical assistance, and to Dr. Achim Kittel (UO), and Prof. Dieter Meissner University of Linz for valuable discussions.

To the German Student Exchange Service (DAAD) and the German Society for Technical Co-operation (GTZ), thank you for providing me with the scholarship within the UZ-UO cooperation in Renewable Energy Programmes, and consistently supporting me throughout my studies. To the University of Oldenburg, I thank you for affording me the time and space to carry out my studies at your prestigious institution, with its state of the art equipment. I am greatly indebted to Dr. Juergen Schumacher, and Mr. Michael Golba (UO), and Prof. A. Wright then Dean of Engineering of the University of Zimbabwe, for supporting my application, even before my probationary period had been completed. It showed that you believed in me. I feel honoured. To the members of the department of Mechanical Engineering UZ, thank you friends for supporting me throughout my studies.

To the organisers of the Quantum Solar Energy Conversion Conference (QUANTSOL) 2004, I thank you for affording me the opportunity to meet, and exchange ideas with the people whose names I have always read in Physics journals and text books. The openness of opinion in your conference is unique and will push polymer and solar cell science a long way. I learnt a lot in that conference.

To members of my immediate, and extended family, I owe you for spending such long periods away from you. We have endured together, thank you very much.

To all those, not mentioned by name, who in one way or the other helped in the successful realisation of the project, I thank you all.

May the good Lord who created us all look after you.

To my wife Theodora, my daughter Dananai, and my son Tadiwa Nashe.

1 Introduction

We discuss the need for research in polymer solar cells and outline the aims and objectives we set out to meet. We describe the structure of the thesis and give small summaries of the main aspects investigated in each chapter.

1.1 Background

In the quest to meet mankind's monotonously increasing energy demand in face of dwindling fossil fuel reserves, renewable energy has been identified as the most environmentally friendly and viable complement. Renewable energy sources comprise of all naturally flowing energy streams, continuous or periodical within time scales ranging from minutes to days. If such natural flows of energy are not harnessed, they are just dissipated in the natural cycles which try to achieve universal thermal equilibrium. Harnessing renewable energy requires technologies that convert the naturally flowing energy streams to forms convenient for human requirements, before allowing the energy to flow back into the natural cycle through a load of our choice.

Renewable energy harnessing technologies include photovoltaic systems, solar thermal applications, wind mills, wind energy electricity generators, micro-hydro power plants, biomass/biogas plants, geothermal, wave and tidal plants, and their associated energy storage components.

Photovoltaic electricity generation has the singular advantage of being modular, thus decentralized electricity generation, and systems of different sizes are possible. The conversion of solar radiation into electrical energy by means of solar cells has been developed as a part of satellite and space travel technology. The theoretical efficiency of solar cells is about 30 percent, and in practice, efficiencies as high as 25 percent have been achieved with silicon photovoltaic laboratory devices. Overall system efficiencies are in the range of 10 to 14 percent [1]. The technology of photovoltaic devices is well developed, but large scale application is hampered by the high price of the cells.

The widespread use of solar power has been elusive because it can be difficult and costly to manufacture the commercial photovoltaic cells, which are made of inorganic crystals such as silicon. One possible alternative to circumvent this problem is to develop photovoltaic cells from materials that can be processed as easily as plastics. Organic solar cells have a singular advantage over their inorganic counterparts, in that they are much less expensive to produce. They do not require the high deposition temperatures or complex processing as required in inorganic devices, and they can be deposited onto large flexible substrates. For example, organic cells might be made in different colors and be flexible enough to use on window blinds, walls, and other materials in buildings. This provides design options that could lower the cost of using the cells. Unfortunately, lagging energy conversion efficiencies have held their application back.

The last few years have seen a tremendous progress in the application of organic materials for photovoltaics following the success of this class of materials in other electrical, electronic and optoelectrical applications. Dye sensitized solar cells as well as Plastic Solar Cells are already on the verge of industrial production. In addition, they have also stimulated further investigations of pure organic solid-state cells as well as new cell structures such as interpenetrating networks of donor and acceptor-type materials.

Conjugated polymers are interesting materials for the fabrication of electronic devices such as light emitting diodes [2] solar cells [3], [4], and thin film field effect transistors [5] on flexible substrates. Poly(3-hexylthiophene) (P3HT) has emerged as one of the very promising materials and is currently a subject of intense research. For instance, power conversion efficiencies of solar cells based on P3HT-fullerene blends of up to 3.5 % have been reported, [6] [7] while P3HT field effect transistors reaching mobilities of 0.05 to 0.1 cm^2/Vs and on - off current ratios of $>10^6$ have been achieved [8]. However the physics of devices based on P3HT is only scarcely understood.

The understanding of the basic physics underlying the electrical, thermal and optical behavior of organic polymeric materials is essential for the optimization of devices fabricated using these materials.

1.2 Aims and Objectives

The aim of this project is to contribute towards the understanding of the operation of organic conjugated polymer electronic devices, like light emitting diodes (PLEDs), field effect transistors (FETs) and polymer solar cells, under different conditions. If the physics is understood, then it will be possible to optimize device fabrication and performance and hence, improve the efficiency and lifetime of such devices so that high efficiency practical solar cells can be made out of these materials in the not so far future. This would go a long way towards cost reduction of solar cell technology, and hence increase the population that can afford them. All benefits that come with cheap electricity would then be made available to more than the 2 billion people of this world who rely mainly on daylight and firewood as main sources of energy.

We proposed that by systematically studying electrical and optical behaviour of separate components that make up the solar cell, useful information can be extracted, which helps in explaining the behaviour of the composite device.

1.3 Factors that affect solar cell performance

The conversion efficiency of a photovoltaic (PV) cell is the proportion of sunlight energy that the cell converts to electrical energy. The efficiency of solar cells is affected by a variety of factors, which are discussed herein. Improving this efficiency is vital to making PV energy competitive with more traditional sources of energy.

1.3.1 Absorption of solar radiation

Absorber materials should be of sufficient band gap to absorb radiation within the UV and visible range of the solar spectrum. Unit absorptance, i.e., ratio of total absorbed flux to incident flux is ideal, but in practice this is lower than 1. The limit of efficiency is first determined by the amount of solar radiation which is incident on the cell but can not be absorbed.

1.3.2 Generation of electron - hole pairs

Only photons with energy greater than or equal to the band gap of the material can excite an electron from valence band to conduction band. All those photons with energy smaller than the band gap are just transmitted through and do not count towards the generation of electron-hole pairs (EHPs) in the device. Those photons with energies greater than the band gap can only generate one electron

hole pair, unless the energy of the photons is two times, or more than, the required, so that it may happen that one photon may generate two EHPs. The fraction of photons with energy equal to twice or greater than band gap energy is however negligible. We may therefore safely assume that each absorbed photon is capable of creating only one electron-hole pair. This means that excess energy is dissipated in the lattice, and may increase the temperature of the cells. It must be possible then to calculate the loss of efficiency only due to unabsorbed radiation, as we describe below.

Planck's law gives the wavelength distribution of radiation emitted by a blackbody, E_λ:

$$E_\lambda = \frac{2\pi h C_o^2}{\lambda^5 [exp(hC_{o/\lambda k_B T}) - 1]}, \tag{1.1}$$

where λ is wavelength, h is Plancks's constant and k_B is Boltzmann's constant. The groups $2\pi\, hC_o{}^2$ and hC_o/k_B are often called Planck's first and second radiation constants, and given the symbols C_1 and C_2, respectively. Recommended values are $C_1 = 3.74 \times 10^{-16}$ m^{2}W and $C_2 = 0.0144$ mK. [9] Equation (1.1) may thus be written as:

$$E_\lambda = \frac{C_1}{\lambda^5 [exp(C_2/\lambda T) - 1]}, \tag{1.2}$$

Equation (1.2) can be integrated to give the radiation between any wavelength limits. The total emitted from zero to any wavelength λ is given by:

$$E_{0-\lambda} = \int_0^\lambda E_{\lambda b} d\lambda, \tag{1.3}$$

Substituting Eq. (1.2) into Eq. (1.3) and noting that by dividing by σT^4, the integral can be made to be only a function of λT,

$$f_{o-\lambda} = \int_0^{\lambda T} \frac{C_1 d(\lambda T)}{\sigma (\lambda T)^5 [exp(C_1/\lambda T) - 1]}, \tag{1.4}$$

where σ is the Stephan-Boltzmann constant. The value of this integral is the fraction of the black-body energy between zero and λT, and has been calculated by Sargent [10] for convenient intervals, as presented by Duffie and Beckman [9]. If the sun is assumed to be a blackbody at 5777 K, the fraction of energy between zero and the red edge of the visible spectrum $\lambda T = 0.78 \mu$m $\times$ 5777 K $= 4506\,\mu$mK is 56 %.

[h]

We performed absorption spectrometry in order to determine the optical properties of materials used as well as the usable part of the solar spectrum for electron-hole generation. The Airmass 1.5 solar spectrum is shown in Fig. 1.1. Superimposed are the absorption spectra for P3HT, PCBM, and for the P3HT:PCBM blend in a 1:3 mass ratio composition. For P3HT, the absorption edge is at about 0.68 μm. The fraction of energy in the zero to λT range is therefore about 46 %. In the case of [6,6]-phenyl-C61 butyric acid methyl ester (PCBM), a methano-fullerene electron acceptor, there is no appreciable absorption after 0.55 μm, and the fraction capable of generating electron-hole pairs is therefore about 32 %. Hence, it is not expected that the energy conversion efficiency of the best P3HT:PCBM based solar cell exceeds the fraction of energy of the photons carried by the photons whose energy is larger than the required to create electron-hole pairs in the two materials. The limiting efficiency of such solar cells, only based on radiation that can not be absorbed is therefore about 46 %. Note that such a value would be reached only if the two materials absorbed like black
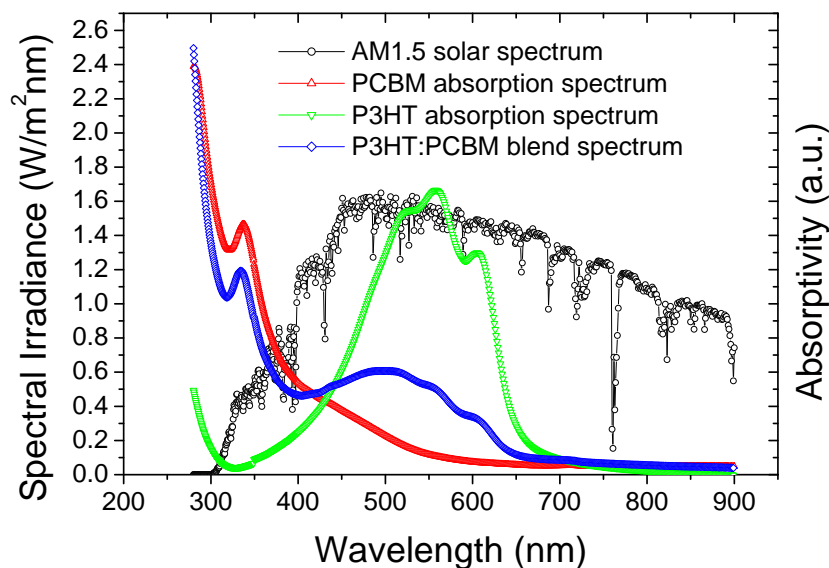
Figure 1.1: *Comparison of the absorption spectra of the active components with the AM1.5 solar spectrum. The absorption spectrum of the P3HT:PCBM blend is a superposition of the individual spectra of P3HT, and of PCBM.*

bodies, where the absorptance is 100 % independent of wavelength, and if every absorbed photon generated an electron hole pair that is collected. This is obviously not the case.

It may happen that some of those photons with the potential to generate electron - hole pairs are reflected by the surface (reflection losses), and due to the small thickness of the cell some are transmitted (transmission losses) without being absorbed. Selection of materials is therefore a fundamental step in the development of solar cells. The synthesis of solution processable conjugated polymers with different bandgaps provides a wide potential of candidate materials for organic solar cells.

1.3.3 Separation of electrons from holes

It is not sufficient to just create electron-hole pairs, i.e., an electron moving from valence to conduction band, since these will recombine radiatively at the first possible opportunity. It is necessary to move the electron away from the hole and to ensure that the two do not recombine. For this to happen, some mechanism must provide a force equal to or greater than the Coulombic attraction force between the electron and the hole, such that it will be preferable for the electron to stay away from the hole, or even to move away from it. If such a force is non-existent, the electron and hole will recombine radiatively, emitting bandgap energy that it had absorbed. Such emission may be observed as photoluminescence. In polymers, the formed electron-hole pair bound by Coulombic forces is called an exciton, and may be split at defects or interfaces with other materials. For example, almost complete quenching of photoluminescence was observed on mixing P3HT and PCBM, suggesting an effective electron transfer from P3HT to PCBM. The idea of bulk heterojunction solar cells is to create as many exciton splitting interfaces as possible within the bulk of the absorber materials.

1.3.4 Maintenance of the electron-hole separated state

Once separated the solar cell configuration must ensure that the electron and hole remain separated. This may be achieved by creating paths that selectively transport holes and block electrons, or vice versa, or both. In a single layer device, negative electrode materials that have work functions close to the conduction band, and positive electrode materials with workfunctions close to the valence band energy is one option, while a two layered device with different types of conductivity (eg. p and n), is another option. In the latter, the negative and positive electrodes could have the same workfunction.

1.3.5 Transport to electrodes

The separated electrons must be transported to one electrode, and the holes to another electrode, where their lifetime should be long. This creates a voltage that is measurable on an illuminated solar cell. The generation rate should be greater than the recombination rate in order to observe the photovoltaic effect.

The maximum voltage is determined by the difference in potential of the valence (or transport level for holes) and conducting (transport level for electrons) bands, i.e., when all possible valence electrons have been excited to the conduction band. Barriers at the electrode/absorber interfaces also play a critical role on the collection of the generated charges. Big potential barriers limit charge collection. Ideally zero barrier is the best. Electrode materials must form ohmic contacts with the polymer. The electron collecting electrode must form an ohmic contact with the conduction band (CB), while the hole collecting material must form an ohmic contact with the valence band (VB). Best electrodes are therefore those whose workfunctions are aligned to the VB and CB, respectively.

The natural resistance to electron flow in a cell decreases cell efficiency. These losses predominantly occur in three places: in the bulk of the primary solar cell material, in the thin top layer typical of many devices, and at the interface between the cell and the electrical contacts leading to an external circuit.

Like in any battery, the recombination path through the cell should be difficult as compared to the short circuiting of the two electrodes. This way it is possible to let a current flow through an external circuit, in order to try and destroy the non-equilibrium state created.

1.4 Scope

The second chapter briefly reviews, and introduces into the thesis, concepts related to solar cells in general, and to organic solar cells in particular. The accepted model of the operation of p-n junction solar cells is discussed bringing out the uncertainties related to that model, and hence emphasizing the need for a systematic study of the operation of organic solar cells. The subject of metal - semiconductor interfaces is treated with a view of understanding current limiting mechanisms. The models that describe charge injection and transport in single and double carrier devices (the Richardson Schottky thermionic emission, Fowler-Nordheim field emission, and space charge limited currents (SCLC) models) are briefly summarized.

The properties of the materials used (structures and mechanisms of degradation), and the methods used in preparing devices, measuring and analysis of data, are discussed in chapter 3, highlighting positive and negative aspects, where possible. The materials used included the solvents (Acetone, Isopropanol, Chloroform, Toluene, and Chlorobenzene), polymers and electrode materials (ITO, PEDOT-PSS, Poly(3-hexylthiophene), PCBM, Aluminium, and Gold). The methods used in

the project included substrate cleaning and electrode patterning; ultra-sonication, plasma etching, spin coating, thermal evaporation in vacuum, dark, and illuminated temperature dependent current-voltage (*J(V)*) measurements; external quantum efficiency measurements; absorption spectrometry; and surface profiling with an atomic force microscope. These are described in the second part of chapter 3.

We make an in depth study of charge injection and transport theories, explore their strengths and weaknesses, and combine them in order to interprete *J(V)* characteristics of metal/polymer/metal sandwich devices. The explanations are centred on the studies done for ITO/P3HT/Al (chapter 4) and ITO/PEDOT:PSS/P3HT/Al (chapter 5) devices, with the vision of simplifying the interpretation of *J(V)* data for one component diodes, and latter for the hetero-junction solar cell. Some of the determined parameters include charge injection mechanisms, transport mechanisms, transition from injection limited to bulk limited conduction and vice versa, charge carrier density, charge carrier mobility, variation with temperature, variation with field strength, contribution of tunneling currents, contribution of thermionic currents, calculation of effective interface barriers, trap density in the bulk, activation energy and effects of thermal annealing, as well as effects of illumination on the *J(V)* characteristics.

The experiments to study charge injection and transport in electrode/Polymer/electrode devices, where Polymer is either PCBM; or the P3HT:PCBM blend, and electrodes: ITO; PEDOT:PSS; Au and Al, are described in chapter 6.

Chapter 7 looks at the performance, and improvement of efficiency of polymer-fullerene solar cells based on Poly(3-hexylthiophene). We discuss possible manifestations of the studies described in chapters 4, 5 and 6, in a solar cell based on P3HT. Dark characteristics and illuminated temperature dependent *J(V)*characteristics are presented, as well as external quantum effieciency curves, in a bid to extract the efficiency limiting mechanisms. Effects of heat treatment on morphology and performance, as well as effects of donor:acceptor ratio, are discussed. In the third section a model of an ideal organic solar cell based on: origin and limit of V_{oc}, origin and limit of short circuit current, and limit of Fill Factor is proposed.

Chapter 8 describes the experiments carried out to establish why the efficiency of P3HT:PCBM solar cells improves after a thermal annealing step. Chapter 9 gives the main conclusions and recommendations.

Although each chapter is written in such a way that it can be read as a complete unit, it is more informative to read them in the order presented here because some of the conclusions reached in preceding chapters may be used without much elaboration in subsequent chapters.

1.5 Main ideas

Below are some of the main ideas developed during the course of this research.

(a) We proposed that the total current in electrode/semiconductor/metal structures is comprised of the sum of the tunneling and the thermionic emission currents, and identified the corresponding regions in Fowler - Nordheim plots. We also showed that there is no defined boundary between the two effects but rather that the measured currents are a superposition of the two, with one dominating the *J(V)* characteristics under given conditions.

(b) The exponential trap distribution model has been briefly described, and an expression for the calculation of the total trap density was deduced, clarifying the limiting values of a pre-factor that defines the validity of the model. The deduced expression yielded reasonable agreement with our

experimental *J(V)* data for ITO/PEDOT:PSS/P3HT/Al devices. The total deep hole trap density was estimated to be 5×10^{16} cm^{-3}, and the activation, energy at absolute zero temperature, was obtained to be 54 meV. A hole mobility of 3 x10^{-5} cm^2/Vs, at 304 K was also estimated under trap-free space charge conditions.

(c) We have shown that thermal annealing of ITO/P3HT/Al devices occurs in two stages, the first leading to a reduction in the conductivity due to dedoping of impurities like oxygen, remnant solvent and water vapour, and the second stage leading to an increase in conductivity, which we attribute to stronger interchain interaction resulting from re-ordering and densification of the polymer chains.

(d) We concluded that the optimum donor acceptor ratio by molecular numbers is 6 P3HT monomer units to one PCBM molecule. This ratio ensures the maximal photo-induced electron transfer from P3HT to PCBM. Annealing of the blend devices reduces traps in the blend, concentrates PCBM into islands, thereby conducing to the optimum 6:1 ratio, and hence the efficiency of the solar cells increases. The pure PCBM islands are regarded as dead parts of the cell.

(e) We concluded that P3HT/PCBM heterojunctions provide the exciton splitting interfaces, while the PEDOT:PSS/P3HT:PCBM interface provides the charge separating interface in the bulk hetero-junction solar cells. Considering that PEDOT:PSS is p type material, the P3HT:PCBM blend may be considered to play the role of an n type material, and the p-n junction theory may be used to describe some of the features of the developed solar cell.

2 Theoretical Review

We briefly review, and introduce concepts related to solar cells in general, and to organic solar cells in particular. The subject of metal - semiconductor interfaces is treated with a view of understanding current limiting mechanisms. The models that describe charge injection and transport in single and double carrier devices are briefly summarized.

2.1 Semiconductor theory

A conductor may be described as a substance in which the free electron density is of the same order as the density of atoms, while an insulator is a substance in which the density of free electrons is negligible when compared to atomic density. In insulators, the ratio of free electrons to atoms per unit volume is less than 10^{-20}. Semiconductors are defined for ratios greater than this. Metallic conductivity is typically between 10^6 and 10^4 (ohm.cm)$^{-1}$ while typical insulators have conductivities less than 10^{-10} (ohm.cm)$^{-1}$. Some solids with conductivities between 10^4 and 10^{-10} (ohm.cm)$^{-1}$ are classified as semiconductors. Insulators and semiconductors belong to the same class of materials - a class in which electrons are not free to move from one atom to another; their difference is one of degree.

All crystals in which the covalent bond is operative exhibit intrinsic semi-conductivity to a greater or lesser degree, but in many crystals the energy required to free an electron is so large that at room temperatures only a very few holes and electrons exist per unit volume and the conductivity is negligible. Extremely small percentages of certain impurities, the atoms of which replace atoms in the parent substance in the lattice, can give rise to a similar type of conductivity. In connection with impurity semiconduction, there is always a degree of intrinsic semiconductivity present. For that reason, the conductivity is never wholly n or p type. Both holes and electrons are always present. We speak of the major part of the current as the majority carriers and of the minor part as the minority carriers.

The most striking difference between metals and semiconductors is that, in the former, the number of carriers is large and constant, whereas in the latter the number is smaller and variable. This variable characteristic suggests that, in semiconductors, the number of carriers, and hence conductivity may be controlled. This control may be effected by control of impurity content, but the carrier density may also be varied for a material of fixed impurity content. The ability to control the carrier density in semiconductors is the main reason for their great technological importance.

A semiconductor doped with impurities, which are ionized (meaning that the impurity atoms either have donated or accepted an electron), will contain free carriers. Shallow impurities are impurities, which require little energy - typically around the thermal energy, $k_B T$, or less - to ionize. Deep impurities require energies much larger than the thermal energy to ionize so that only a fraction of the impurities present in the semiconductor contribute to free carriers. Deep impurities, which are more than five times the thermal energy away from either band edge, are very unlikely to ionize. Such impurities can be effective recombination centers, in which electrons and holes fall and annihilate each other. Such deep impurities are also called traps. Ionized donors provide free electrons in a semiconductor, which is then called n-type, while ionized acceptors provide free holes in a semiconductor,

Distance between centres of atoms
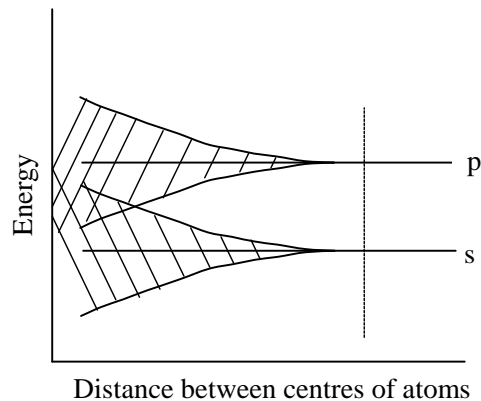
Figure 2.1: *The broadening of energy levels occurs when atoms of an element are brought into close proximity as in a solid.*

which we refer to as being a p-type semiconductor.

2.1.1 Charge carrier mobility

Mobility is measured in (cm/sec) per (volt/cm); i.e. the average velocity of a carrier in a field of 1 Volt/cm. For a material exhibiting little intrinsic conductivity, and having effectively only one type of impurity, the mobility is very high. In absolute terms mobility varies enormously from one semiconductor to another. The outstanding case of a material having a high carrier mobility which can be used is indium antimonide. The electron mobility in this substance may be as high as 65000 cm^2/Vs, compared with a typical value for silicon of 100, and for Polythiophene of 0.1 to 10^{-5} in the same units.

The concept of mobility is very important because it provides us with information on how fast a charge carrier will move per unit applied field. Achievable fields for a given solar cell maybe limited by the energetics of the materials employed and dopant concentration, but the current that can be collected will depend strongly on how fast the charge carriers move under the influence of the generated external voltage. Electric current measures the number of charge carriers that cross a unit cross sectional area per unit time. Area of a solid state device may be considered constant, so mobility becomes the important comparison parameter.

2.1.2 The energy gap

The quantum physics picture of the metallic conductor stresses the importance of energy levels and energy bands. In the case of a simple metal such as zinc in the gaseous state, the two valency electrons are in the 4s state, and an energy diagram of the s and p levels would look like the part to the right of the dotted vertical line of Fig. 2.1 .

For low temperature the atoms are closer together, and the simple s and p levels split up into bands which overlap. In the metallic crystal the distances are such that the overlap is considerable. The 4s electrons can now pass to the unfilled band represented by the expansion of the p level. In fact,

the atoms have become so closely interknit that the individuality of the discrete s and p levels has disappeared. Very little energy is sufficient to move an electron in the metal into the unfilled band.

In a semiconductor the two bands (the filled band and unfilled band or conduction band) do not overlap, but they are separated by such a small gap that the thermal energies due to ordinary temperatures are of the same order of magnitude. An insulator would have an energy gap greater that 7 eV. In a semiconductor thermal energy can raise electrons from the filled to the conduction band.

2.1.3 Junction theory, Fermi level

If there happens to be an allowed level with energy $E = E_F$ it is equally likely to be occupied or to be empty. In any case, all the levels with $E > E_F$ are more likely to be empty, than occupied and all levels with $E < E_F$ are more likey to be occupied than empty. The energy corresponding to E_F is called the Fermi level. The Fermi level is related to the thermodynamic potential, and so is constant for a system made up of different "phases", e.g., two different semiconductors in contact. If two materials have different Fermi levels, on bringing them into intimate contact, the difference in Fermi levels creates a potential difference which will cause electrons to move from one material to the other, until the Fermi levels align.

2.1.4 The p-n junction diode

In a p-doped material, the Fermi level is close to the valence band, i.e. below the midgap position, while in an n-doped material the Fermi level is close to the valence band (above midgap). On making a p-n homojunction the Fermi levels will align, and be at the same potential, so that in equilibrium no net movement of charge is possible. The Fermi level alignment results in a shift of the valence and conduction bands of the p and n materials by a step equal to the difference in potential that was originally present before contact was established. Any departure from equilibrium due to injection of charge by applied field, or due to absorption of light, or to temperature change will split the Fermi level into quasi Fermi levels for holes and electrons in p and n materials, respectively. The potential gradients in the quasi Fermi levels will cause a drift of charge carriers towards opposite electrodes respectively, in a bid to restore equilibrium.

2.1.5 The p-n junction solar cell - principles of operation

Junction formation and built-in potential

When p and n materials are brought into intimate contact, the conduction electrons on the n-side diffuse to the p-side of the junction, and the valence holes diffuse to the n-side of the junction. When an electron leaves the n-side for the p-side, it leaves behind a positive donor ion on the n-side right at the junction. Similarly, when a hole leaves the p-side for the n-side, it leaves behind a negative acceptor ion on the p-side. As a result of Gauss's law, an electric field that originates on the positive ions and terminates on the negative ions is created across the junction. However, the number of positive ions on the n-side must be equal to the number of negative ions on the p-side.

The electric field at the junction gives rise to a drift current in the direction of the field. Holes will travel in the direction of the field and electrons will travel in the opposite direction. For both electrons and holes, the drift component of the current is opposite the diffusion component. From Kirchhoff's law, the drift and diffusion components of each charge carrier must be equal since there is no net current flow across the junction. This phenomenon is known as the law of detailed balance.

By setting the sum of the electron diffusion current and the electron drift current equal to zero and recalling from electromagnetic field theory that

$$E = -\frac{dV}{dx},$$
(2.1)

it is possible to solve for the potential difference across the junction in terms of the impurity concentrations on either side of the junction. Proceeding with this operation yields:

$$-q\mu_n n \frac{dV}{dx} + qD_n \frac{dn}{dx} = 0,$$
(2.2)

that can be written as:

$$dV = -\frac{D_n}{\mu_n} \frac{dn}{n}.$$
(2.3)

Finally recognising the Einstein relationship,

$$\frac{D_n}{\mu_n} = \frac{k_B T}{q}.$$
(2.4)

and integrating both sides from the n-side of the junction to the p-side of the junction yields the magnitude of the built in voltage across the junction, V_j, as:

$$V_j = \frac{k_B T}{q} ln \left(\frac{n_{no}}{n_{po}} \right).$$
(2.5)

It is now possible to express the built-in potential in terms of the impurity concentrations on either side of the junction by recognising that $n_{no} \approx N_D$ and $n_{po} \approx n_i^2/N_A$. Substituting these values in Eq. (2.5) yields:

$$V_j = \frac{k_B T}{q} ln \left(\frac{N_A N_D}{n_i^2} \right).$$
(2.6)

Thus the built in voltage is dependent on the impurity conentrations on either side of the junction. We add that the built in voltage is also dependent on the energetic levels of the dopant species.

The illuminated pn junction

If an electron - hole pair is generated within the junction, both charge carriers will be acted upon by the built-in electric field. Since the field is directed from the n-side of the junction to the p-side of the junction, the field will cause electrons to be swept quickly towards the n-side and holes to be swept towards the p-side. Once out of the junction region, the optically generated carriers become part of the majority carriers of the respective regions with the result that excess concentrations of the majority carriers appear at the edges of the junction. These excess majority carriers then diffuse away from the junction, since the concentration of majority carriers has been enhanced only near the junction.

The addition of excess majority charge carriers to each side of the junction results in either a voltage at the external terminals of the material, or a flow of current in the external circuit or both. If an external wire is connected between the n-side and the p-side of the material, a current will flow in

the external circuit. This current will be proportional to the number of electron-hole pairs generated in the junction region.

If an electron hole pair (EHP) is generated outside the junction region, but close to the junction, it is possible that due to random thermal motion, either the electron or the hole, or both, will end up moving into the junction region. Suppose that an EHP is generated in the n-region, close to the junction, and that the hole, which is the minority carrier in the n-region, manages to reach the junction before it recombines, then it will be swept across the junction to the p-side and the net effect will be as if the EHP had been generated in the junction region, since the electron is already on the n side where it is the majority carrier.

The minority carriers of the optically generated EHPs outside the junction region must not recombine before they reach the junction. If they do, then effectively they are lost from the conduction process. Since the majority carrier is already on the correct side of the junction, the minority carrier must reach the junction in less than a minority carrier lifetime, τ_n or τ_p.

The carriers travel by diffusion once they are created. The minority diffusion length represents the distance, on average, which a minority carrier will travel before it recombines. The diffusion length can be shown to be related to the minority carrier lifetime, τ, and diffusion constant, D by the formula:

$$L_m = \sqrt{D_m \tau_m}.\tag{2.7}$$

where m represents n for electrons and p for holes. It can also be shown that on the average, if an EHP is generated within a minority carrier diffusion length of the junction, that the associated minority carrier will reach the junction.

Hence to maximise the photocurrent it is desirable to maximise the number of photons that will be absorbed either in the junction or within a minority carrier diffusion length of the junction. The minority carriers of the EHPs generated outside this region have a higher probability of recombining before they have a chance to diffuse to the junction. Furthermore, the combined width of the junction and the two diffusion lengths should be several multiples of the reciprocal of the absorption constant, α, and the junction should be relatively close to a diffusion length from the surface of the material upon which the photon impinges, to maximise collection of photons.

When a load is connected to an illuminated solar cell, the current that flows is the net result of two counteracting components of internal current:

(a) The photogenerated current, I_L due to the generation of charge carriers by light.

(b) The diode, or dark current, I_D, due to the recombination of charge carriers, driven by the external voltage. This voltage is the photogenerated voltage necessary to deliver power to the load.

In many practical instances, the two currents may be superimposed linearly [11], and the current in the external circuit can be calculated as the difference between the two components:

$$I = I_L - I_D.\tag{2.8}$$

Only one electron-hole pair is created for each photon absorbed, whatever the energy of that photon. Thus the number of photogenerated pairs is equal to the number of photons absorbed. The photogenerated current may therefore be calculated as:

$$I_L = q A_C \int_{E_G}^{\infty} S(E)\alpha(E,W)dE,\tag{2.9}$$

13

where q is the electronic charge, $\alpha(E,W)$ is the spectral absorbance dependent on energy E, and thickness W, and $S(E)$ is the number of photons of energy E incident on the cell per unit area, and A_C is the area of the illumiated cell. [11] The non absorption losses are inevitable and depend only on the properties of the semiconductor. If transmission and reflection losses are minimised by suitable device design, the maximum photocurrent that can be expected from a solar cell may be obtained by discounting reflection and transmission losses. It then reaches the theoretical maximum of:

$$I_L \leq qA_C \int_{E_G}^{\infty} S(E)dE, \tag{2.10}$$

which depends only on the bandgap and the solar spectrum ($S(E)$). The current therefore decreases as E_G is increased.

Quantum Efficiency

The external quantum efficiency (EQE) of a solar cell is a characteristic of the device that measures the fraction of incident photons that result in actually collected electron hole pairs, under short circuit conditions. It does not take into account the reflected and transmitted photons. EQE therefore relates to the response of a solar cell to the various wavelengths in the spectrum of light shining on the cell. The QE for most solar cells is less than unity because of the effects of recombination, where charge carriers are not able to move into an external circuit. The same mechanisms that affect the collection probability also affect the QE.

The monochromatic external quantum efficiency (EQE_λ) is defined as

$$EQE_\lambda = \frac{I_{sc\lambda}}{qN_{0\lambda}}, \tag{2.11}$$

where $I_{SC\lambda}$ is the short-circuit photocurrent due to incident photons of wavelength λ, q the elementary charge, and $N_{0\lambda}$ is the incident photon flux density at wavelength λ, which can be calculated thus:

$$N_{o\lambda} = \frac{P(light)_\lambda}{P(photon)_\lambda} = \frac{E(light)_\lambda\lambda}{hc}. \tag{2.12}$$

Assuming that each photon absorbed is capable of generating only one electron hole pair, we may estimate the number of photons actually converted to photocurrent. The short circuit current density per wavelength is therefore given by:

$$J_{sc\lambda} = \frac{qE(light)_\lambda\lambda}{hc}EQE_\lambda. \tag{2.13}$$

If the solar cell area is homogeneous, and the incident light intensity homogeneous over the illuminated area, the EQE_λ does not depend on the cell area nor on the intensity of the incident light. From the knowledge of the incident solar spectrum and of the EQE spectrum one can estimate the short circuit current density of the cell. To obtain the EQE of a solar cell for a given range of incident wavelengths, one must integrate Eq. (2.13) and evaluate the limits of wavelengths considered. The AM1.5 solar spectrum gives the intensity (W/m^2) of solar radiation for each wavelength λ, and one can obtain the contribution of each λ to the integral intensity from the spectrum. By considering that the energy of a photon $E_\lambda = hc/\lambda$, one can calculate the number of photons of a given wavelength present in an AM1.5 solar spectrum.

The quantum efficiency can be viewed as the collection probability due to the generation profile of a single wavelength, integrated over the device thickness and normalized to the number of incident photons. As a function of external quantum efficiency, the photocurrent of a given solar cell may be calculated thus:

$$I_L = qA_C \int_{E_G}^{\infty} S(E) \cdot (EQE_\lambda) \cdot E\,dE, \tag{2.14}$$

Internal Quantum Efficiency refers to the efficiency with which light not transmitted through or reflected away from the cell can generate charge carriers - specifically electrons and holes - that can generate current. By measuring the transmission and reflection of a solar device, the external QE curve can be corrected to obtain the internal QE curve.

Dark current

Based on the Shockley ideal diode equation, the dark current may be approximated by a single exponential of the type:

$$I_D = I_0 \left[exp\frac{qV}{mkT} - 1 \right], \tag{2.15}$$

with $1 < m < 2$. At low voltages $m \rightarrow 2$, corresponding to recombination behaviour in the space charge region, whereas at high voltages $m \rightarrow 1$, corresponding to recombination dominated by diffusion in the quasi neutral regions. However, for polymer based and other solar cells, typical values of $m > 2$ have been observed at low bias voltages. Apart from current leakages that can be modelled as a parallel resistance, different causes have been suggested such as the tunnel effect, breakdown by microplasmas, leaks along surface channels, etc.

Current-Voltage Characteristics

Current-voltage (*I(V)*) curves of a solar cell are obtained by exposing the cell to a constant level of light, while maintaining a constant cell temperature, varying the resistance of the load, and measuring the voltage and current that is produced. Alternatively, a variable voltage is supplied to the solar cell, and the current through, and voltage across, the cell are measured.

The current- voltage characteristics of an illuminated solar cell follows Eq. (2.8), which becomes:

$$I = I_L - I_0 \left[exp\frac{qV}{mkT} - 1 \right]. \tag{2.16}$$

On an *I(V)* plot, the vertical axis refers to current and the horizontal axis refers to voltage. The actual *I(V)* curve typically passes through two significant points: The short-circuit current (I_{sc}) is the current produced when the positive and negative terminals of the cell are short-circuited, and the voltage between the terminals is zero, which corresponds to a load resistance of zero. The open-circuit voltage (V_{oc}) is the voltage across the positive and negative terminals under open-circuit conditions, and the current is zero, which corresponds to a load resistance of infinity. Its value is such that the photocurrent is completely cancelled by the bias current, i.e., $I_L = I_D(V_{oc})$ under open circuit conditions, hence:

$$V_{oc} = m\frac{k_B T}{q} ln \left[\frac{I_L}{I_0} - 1 \right]. \tag{2.17}$$

The cell may be operated over a wide range of voltages and currents. By varying the load resistance from zero (a short circuit) to infinity (an open circuit), we can determine the highest efficiency as the point where the cell delivers maximum power. Since power is the product of voltage times current, therefore, on the *I(V)* curve, the maximum-power point (mpp) occurs where the product of current times voltage is a maximum. No power is produced at the short-circuit current with no voltage, or at open-circuit voltage with no current. So we expect to find maximum power generated somewhere between these two points. Maximum power is generated at only one place on the power curve, at about the "knee" of the curve. This point represents the maximum efficiency of the solar device in converting sunlight into electricity.

The fill factor measures the "squareness" of the *I(V)* curve and describes the degree to which the voltage at the maximum power point (V_{mpp}) matches V_{oc} and that the current at the maximum power point (I_{mpp}) matches I_{sc}. The higher the fill factor's percentage or match, the "squarer" the curve.

2.2 Polymer Semiconductors

2.2.1 Introduction

Polymeric photovoltaics present the possibility of producing coatings that function as sunlight-harvesting paints on roofs or even as an integral part of fabrics to produce electricity from sunlight. Since the first report of metallic conductivities in 'doped' poly- acetylene in 1977 [12], the science of electrically conducting polymers has advanced very rapidly. Electronically conducting materials based on conjugated polymers have been applied in diverse items such as sensors, biomaterials, light-emitting diodes, polymer actuators, and corrosion protection agents. More recently, as high-purity polymers have become available, a range of semiconductor devices have been investigated; these include transistors [13], [14], [15], [16], [8], photodiodes [17] and LEDs [18], [19]. The potential for commercialization is perceived to be high for these semiconductor devices because they are seen to compete in application areas where the market can bear the costs of development [20]. In particular, polymer LEDs now show attractive device characteristics, including efficient light generation, and there are several development programmes now set up to establish procedures for manufacture. The principal interest in the use of polymers lies in the scope for low-cost manufacturing, using solution-processing of film-forming polymers.

In a poly conjugated system the π orbitals are assumed to overlap, and form a valence and a conduction band as predicted by band theory. If all the bond lengths were equal, i.e. delocalisation led to each bond having equal partial bond character, then the bands would overlap and the polymer would behave like a quasi-one dimensional metal having good conductive properties. Experimental evidence does not substantiate this and reference to the physics of a mono-atomic one dimensional metal, with half filled conduction band has shown that this is an unstable system and will undergo lattice distortion by alternative compression and extension of the chain. This leads to alternating atom pairs with long and short interatomic distances found along the chain. The effect is embodied in the Peierls's theorem which states that a one dimensional metal will be unstable, and that an energy gap will form at the Fermi level because of this lattice distortion so that the material becomes an insulator or a semiconductor. This break in the continuity of the energy bands is caused by the use of elastic energy during lattice distortion which is compensated by a lowering of the electronic energy and formation of a band gap. Peierls distortion leads to formation of an energy gap and production of semiconductor (or insulator) rather than a conductor.

Conjugated polymers have a framework of alternating single and double carbon-carbon (some-

times carbon-nitrogen) bonds. Single bonds are referred to as σ-bonds, and double bonds contain a σ-bond and a π-bond. All conjugated polymers have a σ-bond backbone of overlapping sp^2 hybrid orbitals. The remaining out-of-plane p$_z$ orbitals on the carbon (or nitrogen) atoms overlap with neighboring p$_z$ orbitals to give π-bonds.

Although the chemical structures of these materials are represented by alternating single and double bonds, in reality, the electrons that constitute the π-bonds are delocalized over the entire molecule. For this reason, polyaniline (PAn) and poly(N-vinylcarbazole) (PVCZ) are considered to be conjugated polymers, with the nitrogen p$_z$ orbital assisting the delocalization of the π-electrons. In some conjugated polymers such as polyacetylene (PA) and PAn, delocalization results in a single (degenerate) ground state, whereas in other polymers the alternating single and double bonds lead to electronic structures of varying energy levels [21].

The behavior of conjugated polymers is dramatically altered with chemical doping. Generally, polymers such as polypyrrole (PPy) are partially oxidized to produce p-doped materials. p-doped polymers have wide application - for example, electrochromic devices, rechargeable batteries, capacitors, membranes, charge dissipation, and electromagnetic shielding.

Conducting polymers also act as semiconductors, and their electronic properties appear to be analogous to those of inorganic semiconductors. The characteristics of the π-bonds are the source of the semiconducting properties of these polymers. First, the π-bonds are delocalized over the entire molecule; and then, the quantum mechanical overlap of p$_z$ orbitals actually produces two orbitals, a bonding (π) orbital and an antibonding (π*) orbital. The lower energy π-orbitals produce the valence band, and the higher energy π*-orbitals form the conduction band. The difference in energy between the two levels produces the band gap that determines the optical properties of the material. Most semiconducting polymers have band gaps that lie in the range 1.5 - 3 eV, which makes them ideally suited as optoelectronic devices working in the optical light range.

The charge conduction mechanism appears to be more complex for conducting polymers than for inorganic semiconductors. Although the action of an incident photon on a conducting polymer excites an electron from the valence band into the conduction band, the resulting electron and hole are bound, and their motion through the material is coupled. These coupled moieties are known as excitons and are responsible for many of the electronic properties found in the most common and efficient polymer-based electronic devices.

In conventional semiconductors, the excited electron and the resulting hole migrate freely to opposite electrodes, where they can do useful work in an electrical device. In a conducting polymer, however, the electron and hole that are generated by the incident photon are bound into an exciton. However, the bound exciton can be split at interfaces. The simplest interface is created at the junction between the electrode and the conducting polymer.

Unfortunately, the exciton-splitting process that occurs at a conducting polymer-electrode interface is not very efficient and is one of the causes of the low quality of early polymer photovoltaics. Another cause of the very low efficiencies of early devices is the effect of impurities, such as oxygen, which act as traps to the migrating excitons.

Attempts to improve the efficiency of the exciton-splitting process led to the development of new conducting polymer species that contained electron-donating and electron-accepting species. By creating interfaces among conducting polymer molecules of differing electron affinities, it is possible to enhance the probability of electron transfer between molecules. This process (photoexcited charge transfer) causes the bound charges to separate, and the junction formed at the donor - acceptor interface is analogous to a semiconductor heterojunction.

These heterojunctions work very well at separating excitons that arrive at the junction. Unfor-

tunately, the lifetime of excitons is short, and only excitons that are formed within $\sim$10 nm of the junction will ever reach it. This short exciton range clearly limits the efficiency of these photovoltaic devices. In an attempt to develop a more efficient photovoltaic structure, interpenetrating networks of electron-accepting and electron-donating polymers have been produced [22]. With these materials, the number of heterojunctions within the polymer blend is greatly increased, and thus the probability that an exciton will encounter a junction and be split.

Under open-circuit conditions, holes are collected at the high work function electrode, and electrons are collected at the low work function electrode. Indeed, the V_{oc} generated by single layer devices depends upon the work function difference between the two electrodes. Although these polymer photovoltaic devices are currently much less efficient than their silicon counterparts, they do produce much higher open-circuit voltages. By using calcium anodes (which need to be capped to prevent oxidation in the atmosphere) and an ITO cathode, Grandstrom *et al.* obtained open-circuit voltages >2 V. [23] Silicon-based solar devices, on the other hand, have open-circuit voltages that are <1 V. The higher open-circuit voltages produced by the polymer-based devices mean that, compared with silicon cells, fewer polymer-based cells need to be cascaded together to obtain the same net output voltage.

The level of oxidation in the inherently conducting polymer has a dramatic effect on the photovoltaic efficiency. Highly oxidized materials are the most conducting, but they are less photoefficient (fewer excitons generated per photon absorbed). Fully reduced materials are highly resistive but the most photoefficient. [21]

2.2.2 Doping of polymers

Band theory is not entirely suitable for the description of electronic conduction in polymers, because the atoms are covalently bonded to one another, forming polymeric chains that experience weak intermolecular interactions. Thus macroscopic conduction will require electron movement, not only along chains but also from one chain to another.

Polymers have the electronic profiles of either insulators or semiconductors; thus the band gap in a fully saturated chain such as polyethylene is 5 eV and decreases to about 1.5 eV in the conjugated system polyacetylene. Conducting polymers can be prepared either by oxidising or reducing the polymer using a suitable reagent. The band theory model would explain the increased conductivity as either removal of electrons from the valence band by the oxidising agent, leaving it with a positive charge, or donation of an electron to the empty conduction band by a reducing agent. These processes are called p-type and n-type doping respectively.

While the addition of a donor or acceptor molecule to the polymer is called "doping", the reaction which takes place is actually a redox reaction and is unlike the doping of Si or Ge in semiconductor terminology where there is a substitution of an atom in the lattice. Although the terminology in common use is retained here, it should be noted that the doping of conductive polymers involves the formation of a polymer salt, and that this can be effected either by immersing the polymer in a solution of the reagent, or by electrochemical methods.

The reactions can be represented in the generalised case for oxidation by:

$$P_n \rightleftharpoons \frac{Ox/A^-}{Red} \rightleftharpoons \left[P_n^+ A^- \right] \rightleftharpoons \frac{Ox/A^-}{Red} \rightleftharpoons \left[P_n^{2+} 2A^- \right], \qquad (2.18)$$
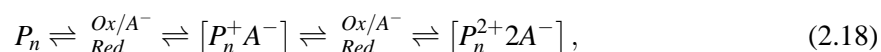
where P_n represents a section of a polymer chain. The first step is the formation of a cation (or anion) radical, which is called a polaron. This step may then be followed a second electron transfer
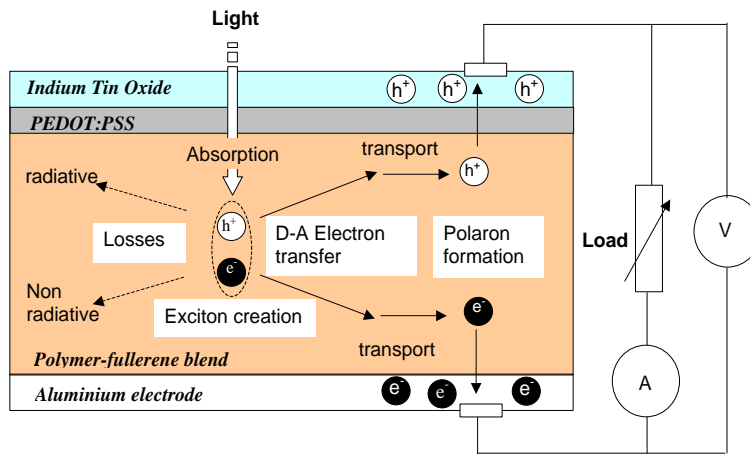
Figure 2.2: *Simplified diagram showing the photovoltaic effect in a heterojunction solar cell based on conjugated organic absorber material*

with the formation of a dication (or dianion) known as a bipolaron. Alternatively, after the first redox reaction, charge transfer complexes may form between charged and neutral segments of the polymer when possible, as represented in Eq. (2.19).

$$P_n^+ A^- + P_m \rightarrow \left[(P_n P_m)^+ A^- \right]. \tag{2.19}$$

2.2.3 Conjugated Polymer solar cells

A simplified diagram showing the photovoltaic effect in a solar cell based on conjugated organic polymer absorber material is shown in Fig. 2.2.

The steps involved in the generation of the photovoltaic effect are: absorption of photon; exciton creation; exciton diffusion; electron transfer to charge transfer complex; electron - hole separation in built-in field; carrier transport to electrodes; electron transfer at electrodes; and electric power extraction. It is in these areas that there is still is room for improvement.

The efficiency of solar cells depends on their capability for the absorption of photons, charge carrier generation, separation and transport to the electrodes. Interpenetrating conjugated polymer-fullerene (donor-acceptor) networks, also referred to as bulk heterojunctions, are a very promising approach for the improvement of efficiency of polymer solar cells. Photovoltaic devices based on these interpenetrating networks provide increased charge exciton splitting interfaces, as compared to bi-layer photovoltaic devices.

The general scheme of the charge carrier generation processes in non-degenerate conjugated polymers (without acceptor) can been described as follows: The mobile charge carriers responsible for the photocurrent are produced as a result of the dissociation of primarily generated singlet excitons due to inter-chain interaction, presence of oxygen [24], [25], [26], or impurities. Nevertheless, the charge carrier generation yield remains low, since other competitive processes, for example, photolumines-

cence and non-radiative recombination also occur. The carrier generation yield can be enhanced by the presence of a strong acceptor species, such as e.g. C_{60} molecule. [22] The process of charge separation in polymer/fullerene composites is ultra fast, and can occur within 40 fs in PPV/PCBM composites [27], whereas the electron back transfer is much slower. [22] This results in effective formation of a metastable charge-separated state. The photo-induced charge transfer is dependent upon the electronic overlap of the donor (D) - acceptor (A) pair of molecules. A simple scheme for the charge electron transfer mechanism is as follows: First the donor is excited, the excitation is delocalised on the D-A complex before charge transfer is initiated, leading to an ion radical pair and finally charge separation can be stabilised possibly by carrier delocalisation on the D^+ (or A^-) species by structural relaxation. [22]

$$D^* + A \rightarrow (D - A)^* \rightarrow (D^{+\bullet} - A^{-\bullet\cdot}) \rightarrow D^{+\cdot} - A^{-\bullet\cdot} \qquad (2.20)$$
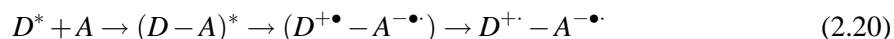
Electron transfer will only take place if the condition: I_D^* - A_A - $U_c < 0$ is satisfied locally, where I_D^* is the ionisation potential of the excited state of the donor, A_A is the electron affinity of the acceptor, and U_c is the Coulomb energy of the separated radicals (including polarisation effects). Stabilisation of the charge separation can be enabled by carrier delocalisation on the donor or acceptor species and by structural relaxation. We add that the presence of a highly polar environment due to an electric field might assist this delocalisation and facilitate general drift according to a Coulombic type interaction. Such a "field" may result from the use of carefully selected electrode materials of different work functions. This selection is a very important step in the design of polymer-fullerene solar cells. The properly chosen electrodes will selectively extract one type of charge carrier and block the other. Further, the accumulation of charges near the electrodes provides the voltage of the solar cell, while current will depend principally on the mobility of holes within the polymer and electrons within percolated fullerene networks.

The mechanism of charge transport has been proposed as follows: A polaronic type radical cation is created due to the positive charge in the organic molecular material, and variable range hopping of this charge between adjacent polymer chains, or conjugated segments, generates the overall charge transport. [28], [29], [30] Many results such as those on the structure dependent conductivity and on field effect transport between metal islands strongly support the model of hopping transport. In a similar way, it is assumed that the electrons are transported through the fullerene to the electrodes via a hopping mechanism. The energetic picture of an ideal polymer/fullerene heterojunction solar cell, with the necessary electronic overlap, where there are no barriers at the electrode interfaces is proposed in Fig. 2.3.

For the estimation of the limiting values of power conversion efficiency, η, open-circuit voltage, V_{oc}, short-circuit current, I_{sc}, and fill factor, FF, we propose the consideration of such a model. If that is the case, then highest purity grade of materials should be assumed.

We note that in practice, even if all workfunctions (Fermi levels) were matched exactly to the highest occupied molecular orbital (HOMO) or lowest unoccupied molecular orbital (LUMO) levels, there exists a finite probability of having potential barriers at all the junctions possibly due to surface states, impurities adsorbed during junction formation and possible chemical reactions between the materials contacted. In principle, these junctions operate like diodes. Further it is very difficult to find compatible materials with exact match of the necessary energy levels. For efficient charge collection from the absorber layer to an external circuit, both the positive and negative electrodes must form ohmic contacts with the donor and acceptor networks, respectively. If this is not the case, charge collection would be limited depending on the nature of potential barriers built up at the contacts.
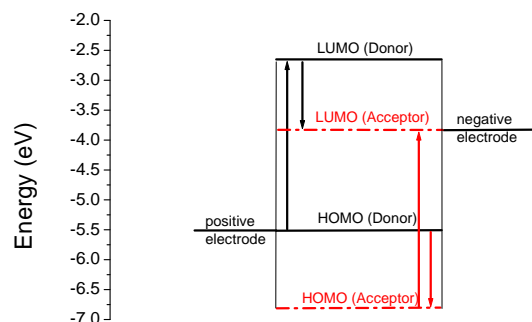
Figure 2.3: *Operation principle of an ideal polymer-fullerene heterojunction organic solar cell: Photons with energy $h\nu \geq E_{LUMO(D)} - E_{HOMO(D)}$ excite electrons into LUMO(D) which are then transferred to LUMO(A) from which they can be collected by the negative electrode with workfunction equal to LUMO(A). Holes are collected by the positive electrode with workfunction equal to HOMO(D). The red arrows indicate a complementary photo-induced electron transfer from D to A.*

Analysis of the charge injection capability of an electrode into a polymer can yield conclusive results of whether a contact is ohmic or not.

2.3 Metal - Semiconductor Interfaces

2.3.1 Introduction

The performance of organic-based electronic and opto-electronic devices depends in a very direct way on the electronic structure of metal/organic interfaces and the charge carrier injection efficiency at these interfaces. Up to a few years ago, a widespread misconception was the assumption of a linear relationship between the work function of the electrode material and the charge injection barrier to the organic material. From 1997 on, a considerable amount of work done by several groups [31] [32] [33] [34] started to dispel this notion by demonstrating the existence of large dipole barriers at metal/organic interfaces. The origin of these dipoles has since been traced to various mechanisms, such as charge transfer with [35] and without [32] interface chemistry, or modification of the metal substrate work function by the organic molecules. [31]

Koch *et al* [36] have shown that hole injection from PEDOT:PSS contacts into organic materials (α-NPD and pentacene) is much more efficient than from Au contacts, albeit the similar work function of both electrode surfaces. This is due to the significantly lower hole injection barriers between the molecular materials and the conducting polymer.

In a theoretical description of bulk transport, the equations of space charge limited currents (SCLC) in insulators without or with traps (at a single level or at a distribution of energy) [37] can successfully be applied to conjugated polymers. [38] Similarly, basic principles of inorganic semiconductors have been applied to explain the injection process in PLEDs as a combination of tunneling, thermionic emission, and interface recombination current and have been proven to be in agreement with experimental data. [39] Within the framework of these models the spatial distribution of the internal

electric field and carrier densities has been calculated, yielding a uniform distribution of electric field and charge in devices with high barriers, and the accumulation of space charge expected near the injecting electrode in low barrier devices. [40], [41]

2.3.2 Contacts

An electrical contact is generally referred to as a contact between a metal and a non metallic material which maybe an insulator or a semiconductor, and its function is either to enable or to block carrier injection. This type of contact has an interesting peculiarity: Semiconductors can be characterised by the presence of both electrons and holes, while metals have only electrons as current carriers. Passage of electric current through a device depends on the charge carrier injection mechanism as well as the transport mechanism within the bulk.

In modeling the current in metal/polymer/metal structures two basic processes have to be considered. First, the injection of charge carrier from the electrode into the polymer and vice versa, and second, the transport of charge in the bulk of the film. Depending on the specific experimental situation (external bias, temperature, electrode workfunction, transport and trapping levels of the polymer, trap density, etc.) one of the two processes may have a significantly lower rate, which means that this process dominates the current characteristic of the sample. The current is then assigned as either injection limited or bulk transport limited. The transition between injection limited and bulk limited conduction is bias and temperature dependent. The two most important parameters that have an influence whether the current is injection limited or transport limited are the externally applied electric field and the height of the injection barrier, i.e., the difference between the electrode workfunction and the corresponding transport levels of the polymer. [42] Meanwhile, it has been established that for barrier heights less than 0.2 eV charge injection is quasi unhindered and the current is solely limited by SCLC in the bulk of the film. For barriers higher than 0.2 eV a decreasing injection rate has more and more influence on the charge balance and for barriers greater than 0.5 eV and moderate biases the current becomes injection limited. [40]

A better knowledge and control of the effects determining the efficiency of charge carrier injection from a metal contact is important for a better theoretical understanding as well as for optimising device performance. Kiy *et al* [43] have shown that the steep current increase in the *I(V)* curves can be determined both by injection barriers or by trap filling processes with charge diffusion from ohmic contacts, depending on the purity of the materials and on the characterisation environment.

2.3.3 Carrier generation in the bulk

Excluding the impact ionisation process, which may lead to the destructive breakdown of the material specimen, the following mechanisms are, in general responsible for carrier generation which in turn determines the dark or photoconductivity of the material.

• *Injection of carriers from the electrodes:* Electrons injected from the cathode and holes from the anode may result in space charge conduction. The injection may be thermionic, quantum mechanical tunneling, or both, or via surface states. Electrons may be emitted from illuminated electrodes into a solid specimen, and this is generally referred to as the photoemission from electrodes and may result in increase in photoconductivity, in the same manner as the contribution of carrier injection from electrodes to the dark electric conductivity.

• *Intrinsic excitation:*

Electrons and holes may be generated by thermal or photo- excitation from the valence to the conduction band in organic semiconductors, as in inorganic semiconductors. Intrinsic photogeneration may be summarised as:

(i) one quantum processes: (a) Direct ionisation - absorbed photons create directly free electron-hole pairs without intermediate steps which involve excitons. (b) Indirect ionisation - the absorption of a quantum produces an exciton, and the carriers are then generated through a reaction of the exciton with or without a defect. The exciton may move between neighbours in a similar way to a charge transfer process, and during the transfer the thermal or field dissociation of the exciton to form free carriers may occur.

(ii) Two quantum processes: two photons, or two excitons, or one photon and one exciton are involved in a single interaction process. The most probable mechanism for charge carrier generation in the bulk of molecular crystals is the collision of two singlet excitons.

(iii) Multi quantum processes: More than two quanta (each of which can either be a photon or an exciton) are involved in a single interaction process.

- *Extrinsic excitation:* The collision of excitons with impurities or surfaces will generate carriers.

- *Field assisted generation:* The electric field may separate generated carriers before geminate recombination due to mutual Coulombic interaction. The electric field may also modify the potential barrier profile of a trap to make it easy for the trapped carrier to be liberated from the trap (Poole-Frenkel effect). Although avalanche ionisation under a high field is unlikely to occur in a low mobility molecular crystal even at its breakdown strength, the mutual enhancement between the electric and thermal conduction processes may cause a rapid increase in the production of thermally generated carriers.

2.3.4 Charge carrier injection processes

To be injected into the polymer, the charge carriers must overcome the potential barrier at the metal/polymer interface. As is the case for small barriers or at high temperatures, a large number of charge carriers will have energies large enough to cross the interface barrier in the classical way - denoted thermionic emission [44]. But when the temperature decreases or when the potential barrier height presents a large value, a reduced number of charge carriers has energies larger than the potential barrier height, and the thermionic emission becomes insignificant. The injection then can only occur via quantum mechanical tunneling through the potential barrier. The charge carriers tunnel from the metal to the empty states at the lowest unoccupied molecular orbital (LUMO) or at the highest occupied molecular orbital (HOMO) level in the polymer. Alternatively, if the polymer layer contains a high concentration of impurities, the tunneling may occur from the metal to empty localized states in the polymer layer, constituting a hopping-type process [45]. It is the smallest barrier at each interface which always dominates the injection. [38]

In the absence of either surface states that may pin the Fermi level at the interface between a dielectric and the electrode or a depletion layer due to impurity doping, the energy barriers that control hole and electron injection are $\Delta E = I - \varphi_{anode}$ and $\Delta E = \varphi_{cathode} - A$, where φ is the workfunction of the electrode and I and A are the ionisation energy and electron affinity of the organic dielectric, respectively, and indicate at which energies hole and electron transport proceeds or, equivalently, where the highest occupied and lowest unoccupied molecular orbitals are located energetically. Depending on the magnitude of ΔE a measured current can either be injection limited or transport limited (space charge limited). The SCLC case requires one of the electrodes to be ohmic, i.e., it must be able to supply more charge carriers per unit time than the sample can transport. Under these conditions, the

electric field at the injecting contact vanishes. This requires the injection barrier to be small enough to guarantee efficient injection without assistance of an electric field. The SCL current is the maximum currrent a sample can sustain at a given electric field unless the exit contact is able to inject an amount of opposite carriers sufficient to compensate for the internal space charge.

2.3.5 Thermionic emission

Thermionic emission postulates that only electrons with energies greater than the conduction band energy at the metal semiconductor interface contribute to the current.

The essential assumption of the RS model of thermionic emission is that an electron from the metal can be injected into the polymer, once it has acquired a thermal energy sufficient to cross the potential maximum that results from the superposition of the external and the image charge potential. This model usually is valid at lower fields and higher temperatures. At higher fields, the metal work function for thermionic emission is reduced, thus lowering the Schottky barrier height (image force lowering). The Schottky equation, taking into account image force lowering, may be written as: [46] [47] [48]

$$J = A^* T^2 exp\left(-\frac{\phi_B}{k_B T}\right) exp\left[\left(\frac{q^3 V}{4\pi\varepsilon_0\varepsilon_r d}\right)^{1/2} / k_B T\right].$$

(2.21)

where ϕ_B, d, ε_0 and ε_r are the interface potential barrier height, film thickness, vacuum permittivity and optical dielectric constant, respectively. k_B is Boltzmann's constant, q the elementary electronic charge, T the absolute temperature, and the applied voltage V is positive for forward bias and negative for reverse bias. A^* is the Richardson-Schottky constant ($A^*=4\pi qm^*k_B{}^2/h^3 = 120$ A/cm^{2}K), for free electrons, where the effective carrier mass m^* equals that of the free electron, otherwise it depends on the anisotropy of the material [49]; h is Planck's constant.

2.3.6 The tunneling (field emission) current

Field emission is the quantum mechanical tunnnelling of electrons through a potential barrier from a metal to a semiconductor or an insulator under an intense electric field. The Fowler-Nordheim formulation of tunneling through a triangular barrier [50] has been applied successfully to analyse $J(V)$ curves for ITO/BDMOS-PPV/Al [51] devices, organic double layer light emitting diodes [52], Mg/Alq3/Mg devices [43] , PPV [53] , [54] , and in MEH-PPV [55] devices, among many others. In the following section the basis of the FN theory is described.

Tunneling is a quantum mechanical process without a classical analogue. An electron (or other quantum mechanical particle) incident upon a potential barrier whose height is larger than the kinetic energy of the electron will penetrate (tunnel) a certain distance into the barrier. This is most visualised by considering the one dimensional Schroedinger equation for the wave function of such an electron:

$$-\frac{\hbar^2}{2m}\frac{\partial^2\psi}{\partial x^2} + V(x)\psi = E\psi$$

(2.22)

If $V(x)$ varies relatively slowly with distance, x, the solution of equation (2.22) can be approximated by:

$$\psi = \psi_0 exp\left[\pm i\frac{\sqrt{2m}}{\hbar}\sqrt{E - V(x)}\right],$$

(2.23)
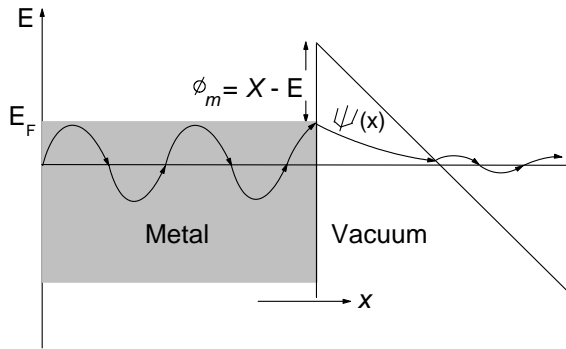
Figure 2.4: *Illustration of the tunneling phenomenon*

where ψ_0 is a constant, x is distance into the barrier, and i is the imaginary factor $i=\sqrt{-1}$. The non-classical case is the one where the electron energy E is smaller than the potential $V(x)$. Then ψ is no longer an oscillating wave but it is real and decays exponentially with distance into the barrier. The penetration probability into the barrier is equal to the ratio of the probability density $|\psi(x)|^2$ at the exit from the barrier to its value at the entrance. Equation (2.23) shows that this probability is exponentially dependent on barrier height and thickness. The tunneling takes place at a constant electron energy as there is no scattering involved.

A more accurate solution of equation (2.22) which adequately describes many real situations may be calculated by the Wentzel, Kramers, Brillouin (WKB) approximation. The tunneling probability through a barrier then becomes

$$P \approx exp\left[-2\int_{x1}^{x2}\sqrt{\frac{2m}{\hbar}}\sqrt{V(x)-E}dx\right] \tag{2.24}$$

Tunneling can occur in many physical situations. The simplest case is that of field emission. This is the emission of electrons from a solid by the application of very high fields. The energy diagram of such a system is as shown in Fig. 2.4.

The electrons in a metal surrounded by vacuum may be regarded as an ensemble of quasi free electrons held in a potential well by the positive charges of the metal ions. The depth of the well is called the electron affinity χ. The potential well is filled with electrons up to the Fermi level (E_F) and consequently electrons at this level 'see' a barrier (workfunction) surrounding them. They can tunnel a short distance into the walls of the potential well, but can not escape from it.

If a high positive field F is applied to the metal (e.g., by applying a potential difference between the metal under consideration and an adjacent piece of metal), the potential energy distribution is that shown in Fig. 2.4.

There now exists a barrier through which, under appropriate conditions, the electrons may tunnel.

The maximum height of the barrier is ϕ_M, and its width is approximately ϕ_M/F so that the current becomes

$$I \propto P \approx exp\left[-\frac{4\sqrt{2m}\phi^{3/2}}{3\hbar F}\right],\tag{2.25}$$

if ϕ_M is given in eV and F in V/cm. Since ϕ_M generally has a value between 2 and 5 eV, an electric field of the order of 10^7 V/cm is required before appreciable numbers of electrons will be emitted into vacuum.

Fig. 2.4 is a somewhat simplified picture of an actual metal-vacuum interface. An electron outside the metal experiences a polarisation force towards the metal, the so called image force. While this is not a true potential, it may nevertheless be included in the potential energy diagram as a rounding off of the band well edge (Schottky effect). When the field is applied, the barrier is lowered so the tunneling probability increases. Particularly at high fields this causes a departure from the simple current relationship described above. If these effects are included in the calculation, good agreement can be obtained with experimental results.

Current flow at a metal/semiconductor interface may be treated in the same way as that at a metal vacuum boundary. The potential barrier is now given by the energetic distance from the metal Fermi level to the bottom of the insulator conduction band, which is usually smaller than the workfunction. Also the dielectric constant of the insulator must be taken into account (e.g., in the image force). These modifications do not change the basic current-voltage relationship, Eq. (2.25).

The Fowler - Nordheim (FN) model for tunneling injection (field emission) ignores image charge effects and invokes tunneling of electrons from the metal through a triangular barrier into unbound continuum states. It predicts that when field emission dominates, the *J(V)* characteristics are described by

$$J = AF^2 exp\left(-\frac{8\pi\sqrt{2m^*}\phi_B^{3/2}}{3hqF}\right).\tag{2.26}$$

where m^* is the effective charge carrier mass, F the applied electric field, and A [in A/V^2] a rate coefficient that contains a tunneling prefactor and the rate of current back-flow [56]. It can be deduced from the treatment by Kao and Huang [46] that A is given by

$$A = \frac{q^3}{8\pi h\phi_B}.\tag{2.27}$$

Equation (2.26) can also be written as

$$J = AF^2 exp\left(\frac{-\kappa}{F}\right),\tag{2.28}$$

where

$$\kappa = \frac{8\pi\sqrt{2m^*}\phi_B^{3/2}}{3hqF} = constant.\tag{2.29}$$

If the value of κ is known, then the barrier height between the electrode and the film may be estimated from Eq. (2.29) as

$$\phi_B = \left(\frac{3\kappa q h}{8\pi\sqrt{2m^*}}\right)^{3/2}. \tag{2.30}$$

There may be localised electronic states in the barrier region, either due to impurities in the insulator region or due to adsorbed molecules at the metal-insulator or metal-vacuum interfaces. An electron in the metal at the energy of the impurity state will have a higher probability of tunneling to the impurity state and from there to the other side of the barrier than the probability of tunneling directly through the barrier. This means that when the voltage raises the Fermi level in the metal to the energy of impurity states in the barrier, there will be a sudden increase in current. The current voltage characteristic can then be used to study the distribution of impurity states.

When a potential difference is applied, one tunneling direction is favoured and net current flows. For small potential differences (much less than the barrier heights) the tunneling probability does not vary with applied field and the current flowing will be proportional to the difference in number of electrons available on the two sides of the barrier at the same energies.

2.3.7 Charge transport mechanisms

The structure of the material, - crystalline, amorphous, disordered, etc.- determines the charge transport mechanisms. The current is injection limited when the bulk is able to sweep away and transport all the injected charge thereby avoiding any accumulation of injected charge near the injection electrode. It is transport limited when the injection rate is higher than the transport rate. In this case the material cannot transport immediately all the injected charge. As a result, charge accumulates near the injecting electrode and builds up a field that impedes further injection. Such charge is referred to as space charge and the current obtained, Space Charge Limited Current (SCLC).

An ohmic contact is defined as an infinite reservoir of charge that is able to sustain a steady state SCLC in a device. With ohmic contacts, the current-voltage relation is often linear at low bias up to a certain value since the electrical field due to the injected carriers is negligible compared to that due to the applied bias. The slope of a log-log plot between current *I* (or current density *J*), and voltage *V* at low voltages is then equal to 1, and the behavior is described by Ohm's law, equation (2.31) [57]:

$$J_{ohm} = q n \mu \frac{V}{d}, \tag{2.31}$$

where q is the electronic charge, n the charge carrier density, μ the carrier mobility, V the applied voltage and d the thickness of the sample. This condition breaks down at the space charge limit when the injected carrier density becomes so large that the field due to the carriers themselves dominates over that of the applied bias and then becomes space charge limited. SCLC occurs when the transit time of any excess injected carrier is less than the bulk dielectric relaxation time. Under these circumstances, the trap free space charge limited current (TFSCLC) takes the simple form of Child's law [see Eq. (2.32)]. This behavior is characterized by a strict quadratic dependence of current on voltage (slope 2 in a logJ-logV plot). (Note that this does not necessarily imply the absence of traps in the material, but rather that they are all filled) [58].

$$J_{TFSCL} = \frac{9}{8}\varepsilon_0\varepsilon_r\frac{V^2}{d^3}. \tag{2.32}$$

Here, ε_r and ε_0 are relative permittivity and permittivity of free space, respectively. Space charge limited currents in a device can occur if at least one contact [30] is able to inject locally higher carrier densities than the material has in thermal equilibrium without carrier injection. An emission limited contact is one which falls short of an ohmic contact's ability to supply charge. The emission limitation can range from totally blocking to finite injecting [59].

In practice, the field dependence of the current is often insufficient to distinguish trap-limited SCLC from injection limited conduction. In that case, the predicted dependence of the SCLC on sample thickness provides an unequivocal criterion. Injection limited *J(F)* curves donot depend on sample thickness while SCL currents do.

When optical excitation is inhomogeneous along the electric field, diffusion and drift act in parallel on the excess carriers. At low electric field, both carriers move in a coupled way so as to preserve local neutrality: this is known ambipolar type of motion. Under high electric field, diffusion is negligible and unipolar carrier motion may appear.

2.4 Summary

Semiconductor theory has been described basing on the doping, which result in n and p type materials respectively. The pn junction formation and opto-electrical response has also been described. Further, polymer solar cells have also been introduced. Charge injection and transport mechanisms have been introduced, and these will be explored further in chapter 4, where an expression is derived, for employment in the interpretation of current-voltage curves of electrode/semiconductor/electrode devices.

3 Materials and methods

In this chapter we list the properties of the materials studied, and highlight the methods used in preparing devices, measuring and analysis of data.

3.1 Materials

3.1.1 Indium Tin Oxide (ITO)

Indium oxide doped with tin oxide, ITO, is used to make transparent conductive coatings. Thin film layers can be deposited by electron-beam evaporation or sputtering. It is one of the few metal oxides that combine technologically interesting properties such as high transparency in the visible range, good electrical conductivity and excellent substrate adherence. Because of its transparency, high conductivity, and efficiency as a hole injector into organic materials, indium tin oxide - ITO has been widely used as the anode contact for organic light emitting devices - OLEDs. Typical applications of ITO-coated substrates include touch panel contacts, electrodes for LCD and electrochromic displays, energy conserving architectural windows, defogging aircraft and automobile windows, heat-reflecting coatings to increase light bulb efficiency, gas sensors, antistatic window coatings, wear resistant layers on glass, etc.

The optical and electronic properties of ITO films are highly dependent on the deposition parameters and the starting composition of evaporation material used. [60] The deposited film layer must contain a high density of charge carriers for it to conduct. These carriers are free electron and oxygen vacancies, and an excessive population gives rise to absorption. High conductivity (or low sheet resistance) is balanced against high transmission in the visible region. Sheet resistance can be less than 10 Ohms/sq. with a visible transmission of >80 %. To obtain transmission near 90%, sheet resistance must be >100 Ohms/sq. ITO films behave as metals to long wavelength light because they have a plasma wavelength above 1 μm. At longer wavelengths, the film becomes reflecting, and the IR reflectance is related to the sheet resistance of the film; sheet resistance must be <30 Ohms/sq. to obtain IR reflectance >80 %.

The deposition parameters play interdependent roles in the optimization of film properties. Principal among the deposition parameters are partial pressure of oxygen, substrate temperature, rate of deposition and material composition. Some processes require post deposition baking at 300-500° C in air to oxidize residual fractionated metal component and improve conductivity. For sputter processes, a high energy plasma can be substituted for a high substrate temperature.

Since the organic thin film is in direct contact with the ITO, the surface properties of the ITO are expected to directly affect the characteristics of the device. Abnormal device behaviors such as shorting, unstable I - V characteristics, and damage on the surface of the top cathode contact after continuous operation of the device have been observed in OLEDs built on bare cleaned ITO surfaces. [61] [62] [63] Furthermore, as-grown ITO contacts have been found to be less efficient for hole injection than low work function metal cathodes for electron injection, resulting in hole-limited devices. The mitigation of these problems has so far involved changing the properties of the organic materials or introducing an intermediate stabilization layer with proper carrier injection/transport characteristics between the ITO and the active luminescent layers. The alternative of modifying the
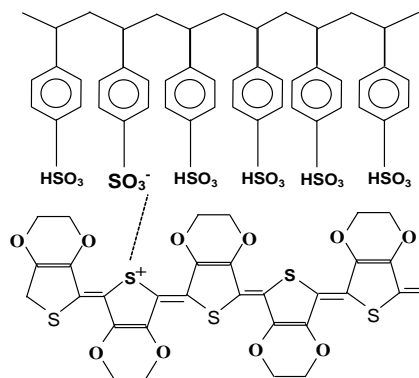
Figure 3.1: *Formula of Poly(3,4-ethylenedioxythiophene), PEDOT (bottom) - polysytrenesulphonate, PSS (top)- PEDOT:PSS*

ITO itself, however, has not been extensively investigated. Wu *et al.* [64] have reported that an oxygen plasma treatment is an effective way to modify the surface of ITO. They have shown that, without degrading the bulk properties of ITO (sheet resistance and transmittance), the chemical composition of ITO surface layers could be substantially modified by treatment in plasmas of different gases. As a result, the OLED device characteristics can be dramatically improved. The oxygen plasma was found to be the most effective in preparing the ITO surface for high performance OLEDs.

ITO is generally considered as a heavily doped and degenerate n-type indium oxide with both Sn dopants and oxygen vacancies contributing to its conduction. [65] The enhancement of hole injection may be due to an increase in the work function of the ITO as the surface Sn:In ratio is decreased and the oxygen concentration is increased. Ultra-violet photoemission spectroscopy measurments on the oxygen plasma-treated ITO surfaces show an increase in the work function of 100 - 300 meV with regard to the cleaned as-grown ITO surfaces. The removal of the organic residue from the ITO surface could therefore also be partially responsible for the device improvement.

3.1.2 Poly(3,4-ethylenedioxythiophene)-polysytrenesulphonate (PEDOT:PSS)

PEDOT is a conjugated polymer that is positively doped [66] and neutralised with the PSS polyanion. An H^+ disassociates from the PSS and dopes the PEDOT polymer backbone. Oxidation (further p-doping) of PEDOT:PSS results in an absorption spectra in the NIR-region due to more free charge carriers, i.e. bi-polarons, and the initial sky-blue coloured polymer turns to a more transparent and uncoloured state. PEDOT:PSS absorbs strongly in the red/orange wavelength region upon reduction, therefore, it appears as a dark blue colour to the human eye in its reduced state. The reduced form of PEDOT:PSS shows very low electronic conductivity, while the pristine (semi-oxidized) form of PEDOT:PSS acts as a one-dimensional synthetic metal with high electronic conductivity.

Poly(3,4-ethylenedioxythiophene) doped with poly(styrenesulfonic acid) (PEDOT:PSS) is commonly used as buffer layer between indium tin oxide anode and the emitting layer in organic light emitting diodes, where the PEDOT:PSS layer forms effectively the anode in this device set-up. [67] PEDOT:PSS has been commercialised by H. C. Starck under the trade mark of Baytron P. The formula of PEDOT:PSS is represented in Fig. 3.1.
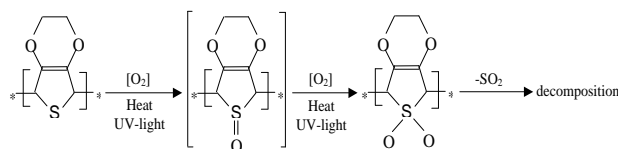
Figure 3.2: *Proposed chemical mechanism of degradation of PEDOT:PSS:- Diels-Alder-Reaction /SO$_2$ extrusion.*

PEDOT undergoes an electrochemical half-reaction as follows:

$$PEDOT^{+1} + PSS^- + M^+ + e^- \rightleftharpoons PEDOT^0 + M + PSS^- \tag{3.1}$$

Where M$^+$ is a cation (sodium, hydrogen, etc.) and PSS is a passive counter-ion (that originally doped PEDOT). PEDOT^{+1} is a sky blue material that is highly conductive ($\approx$200 S/cm), while PEDOT^0 is a dark blue material with a relatively low conductivity (estimated at $\approx 10^{-5}$ S/cm by Johansson *et al.* [68]). The color change, known as electrochromism makes PEDOT useful in display cells. The conductivity change makes the material suitable for sensors and transistors. [69]

PEDOT is not intrinsically conductive; the π- conjugated carbon chain does not conduct. However, when doped with PSS it becomes a p-type semi conductor. When an electric field penetrates a PEDOT:PSS layer, the positively charged H$^+$ ions are forced to the extremes of the polymer. This essentially depletes the polymer of its dopant. Without the H$^+$ dopant, PEDOT is not conductive.

Thermal degradation of PEDOT:PSS depends on temperature (decomposition starts at about 225 to 230°C), UV light, and oxygen. One proposed path of degradation is shown in Fig. 3.2. [70]

Polar compounds, especially acidic solvents like N-Methylpyrrolidone, N,N-Dimethylformamide, N,N-diethylacetamide, and low volatile alcohols like ethylene glycole, glycerine, sorbitol, partly re-dissolve PEDOT groups, rearrange morphology, decrease resistances between PEDOT:PSS particles and increase film conductivity (during drying).

3.1.3 ITO/PEDOT:PSS interface

In the field of OLEDs, the stability of the ITO/organic interfaces determines to a great extent many of the device properties. [71] [72] [73] [74] [69] [75] [76] In single-layer OLEDs, the oxidation of the organic emitting layer by oxygen diffusing out of the ITO, the presence of electric shorts due to the rough ITO surface, and the unbalanced electron - hole injection, limit the device life-time. [77] [78] [79] To get around these problems, a PEDOT:PSS layer is introduced between ITO and the emissive layer. Because ultrathin layers of PEDOT:PSS are essentially transparent to visible light, this additional layer does not readily diminish the light output and instead leads to a
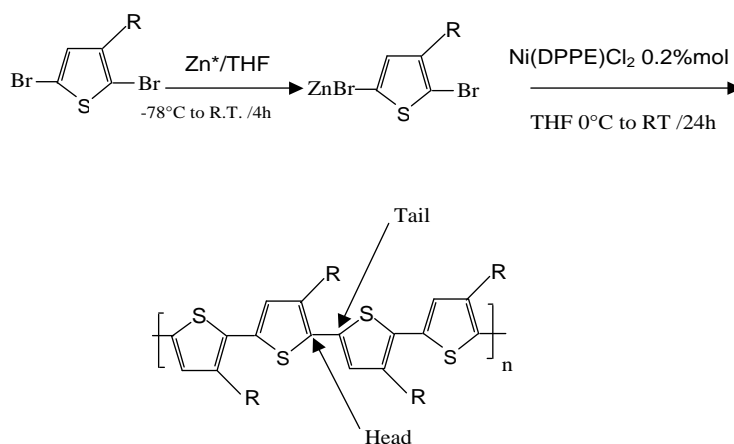
Figure 3.3: *Rieke's regio-controlled synthesis of poly(3-hexylthiophene). The polymer is prepared by the regiocontrolled zinc mediated method of Rieke.*

significant improvement of the lifetime and luminous efficiency and a reduction in the operating voltage. [78] [80] [81] [82] [79] [83] The beneficial effects of PEDOT:PSS arise from the smoothing of the ITO surface and the reduction of the hole-injection barrier due to the high energy of the occupied electronic levels of PEDOT in comparison with that of ITO. [84] [74] The released protons in the emulsion are susceptible to react with ITO during the coating step. [85] The hole-injecting layer PEDOT:PSS may undergo interfacial chemistry with ITO. [75] [76] [86] [77]

PEDOT:PSS is a stable emulsion in water, thus easy to spin-coat on ITO. In PSS, all the sulfonate groups are not involved in the neutralization of the doping charges, most of them are sulfonic acid groups. To build up polymer light emitting diodes (pLEDs) with a PEDOT:PSS layer, the precusor-PPV route cannot be used since the high temperature required would destroy PEDOT:PSS. Hence, a soluble emissive polymer like O-C1-C10-PPV or P3HT can be spin-coated on top of the PEDOT:PSS layer.

In multi-layer pLEDs using PEDOT:PSS as hole injecting layer, the ITO/PEDOT:PSS interface is not stable and very sensitive to air. The hydroscopic nature of PSS plays an important role. Upon exposure to air, water is absorbed by the PEDOT-PSS film and an aqueous acid environment is formed due to the reaction

$$H_2O + PSS(SO_3H).H_3O^+ + PSS(SO_3^-). \tag{3.2}$$
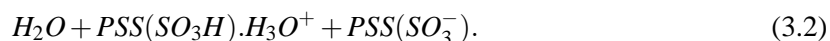
This will facilitate etching of the ITO and transport of the etch products throughout the PEDOT:PSS film. However, the good news for the pLEDs is that indium is not diffusing in the emissive polymer, thus avoiding the formation of quenching sites. [77]

3.1.4 Poly (3-hexylthiophene 2,5 diyl) (P3HT)

For all our experiments we used regioregular head-to-tail P3HT purchased from Rieke Inc., or from Aldrich - Germany. Regioregularity denotes the percentage of sterio-regular head-to-tail (HT) attachments of the alkyl side chains to the three-position of the thiophene rings. The HT regio-specific polymers have improved conductivities, [87] mobilities, [8] optical non-linearity and magnetic properties over the regiorandom HH (head to head) polymers, due to their ability to form supramolecular self-assembled regions when in the solid state. There are several different synthetic routes used to prepare the regioregular HT P3HT, but the two that produce the greatest percentage (98%) of RR HT P3HT are the McCullough method [88] and Rieke method. [89] It is the HT P3HT prepared by the Riecke method that is commercially available from the Aldrich Chemical Co.

M. M. Erwin *et al* [90] showed by Rutherford backscattering spectroscopy that in their 98% rr HT P3HT purchased from Aldrich chemical Co. residual synthetic impurities, Zn and Br were present. These impurities were also shown to affect the optical properties both in solution absorption and emission and also affect the solid state absorption. The Zn and Br can be removed during the methanol phase of Soxhlet extraction.

3.1.5 [6,6]-phenyl-C61 butyric acid methyl ester (PCBM)

The characterization of C_{60} as an electron acceptor capable of accepting as many as six electrons [91] candidates it as the acceptor in blends where conjugated polymers are good photoexcited electron donors.

C_{60} is a molecule that consists of 60 carbon atoms, arranged as 12 pentagons and 20 hexagons. The C_{60} molecule was discovered by Kroto *et al.* [92], in 1985 - won them the 1996 Nobel prize in chemistry. Solid C_{60} is a molecular crystal in which C_{60} molecules occupy the lattice sites of a face centered cubic (fcc) structure. Initially, C_{60} could only be produced in tiny amounts. So there were only a few kinds of experiments that could be performed on the material. Things changed dramatically in 1990, when Krätschmer *et al.* [93] discovered how to produce pure C_{60} in much larger quantities. While the carbon atoms within each C_{60} molecule are held together by strong covalent bonding, van der Waals interactions are the dominant intermolecular forces in C_{60} crystals. [94] Near the temperature $T_c = 250 - 260$ K, the C_{60} crystal is known to undergo a first order phase transition associated with changes in molecular rotations. Above T_c, C_{60} molecules rotate almost freely and therefore are equivalent, thus resulting in fcc structure. [95] Below T_c, the molecular rotations are partially locked with the five-fold symmetry axes having specific orientations. As a result, the molecules are no longer equivalent, and the fcc structure transforms into a sc lattice composed of four sublattices. [96] This phase transition is also accompanied by a discontinuity in the lattice parameter da (from 14.154 $\mathring{A}$ in the fcc to 14.111 $\mathring{A}$ in the simple cubic (sc) phase. [96]

Consider the ideal C_{60} crystal. It is generally assumed that in this solid the charge carriers can easily move within C_{60} molecules, and the carrier mobility is limited by the carrier jumps between the molecules. The jump probability decreases with increase in intermolecular distance. This probability could also decrease during the phase transition from the rotationally ordered sc to rotationally disordered fcc phase, in which molecular rotation should induce extra carrier scattering. This model was used by Katz *et al.* [97] to explain the observed sharp increase in mobility and in dark conductivity of high quality C_{60} single crystals when temperature is lowered through the transition region.

Introduction of defects into the ideal C_{60} crystal may result in disorder, both in the orientations and in the relative distances between the C_{60} molecules, as well as in the appearance of defect
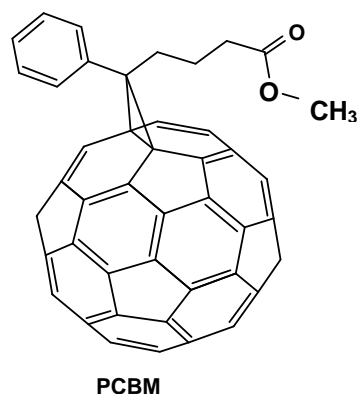
Figure 3.4: *The chemical structure of PCBM.*

levels (charge carrier traps) in the forbidden gap, and ultimately lead to the vanishing of the phase transition. Oxygenation and decrease in crystalline quality result in a smaller discontinuity of the lattice parameter at the phase transition. However changes associated with oxygenation were found to be fully reversible (by heating the oxygenated samples at 150^oC for 2 h).

Reported field effect measurements on thin film evaporated $C_{60} = 8x10^{-6}$ m^2/Vs. [98] For C_{60} single crystals grown from the vapour phase, mobilities of $5x10^{-5}$ m^2/Vs have been measured by time-of flight measurements. [99]

Buckminsterfullerene is a special spherical electron carbon cluster which, unfortunately, is only sparingly soluble in most common solvents. Figure 3.4 shows the chemical structure of PCBM used as the acceptor in PCBM:P3HT solar cells studied in this work. PCBM is a C_{60} based material in which a methyl-ester group is attached to improve the solubility of C_{60} in common organic solvents. A PCBM SCLC electron mobility of $2x10^{-7}m^2$/Vs at room temperature has been reported by Mihailetchi *et al*. [100] They also quote a relative dielectric constant of 3.9 obtained from capacitance -voltage measurements. HOMO = 6.1 eV, LUMO = 3.7 eV, hence Eg = 2.4 eV (intersite distance =3.4 nm).

3.2 Methods

Figure 3.5 shows a block diagram of some of the steps undertaken when preparing the electrode/ polymer/ electrode sandwich devices and solar cells. Solutions were prepared by dissolving the polymer, fullerene, or the polymer-fullerene blend in apropriate solvents, and stirring the solution, in a dark inert atmosphere for at least two hours, using a magnetic stirrer.

The high work function electrode was patterned by etching commercial ITO coated glass substrates in acid. The substrates were cleaned in deionized water, acetone, toluene and isopropanol, respectively, in a hot ultrasonic bath (USB). Ultrasound is a cleaning method which is used in precision mechanical workshops and also for surgical instruments. Ultrasound waves are mechanical waves that are emitted in liquid media and whose intensity decreases in accordance with the square
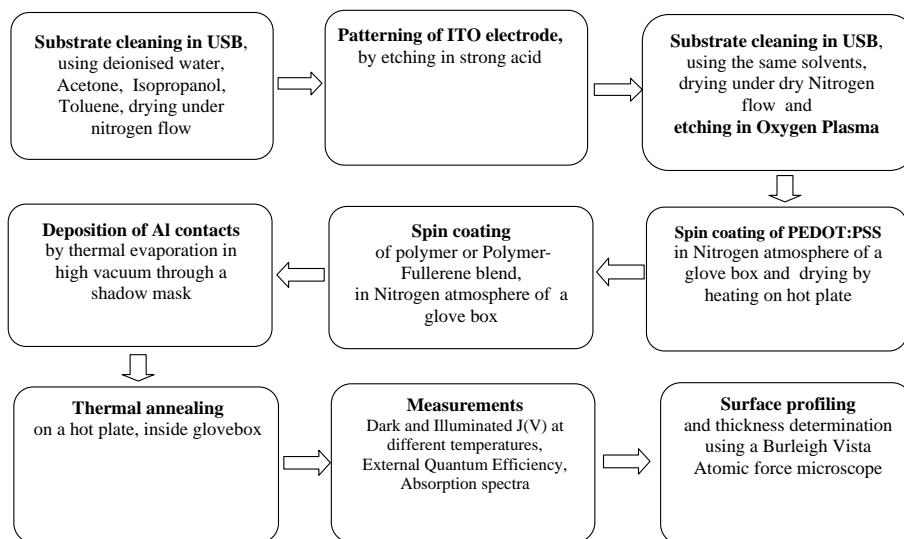
Figure 3.5: *Block diagram showing some of the steps employed in device preparation and characterisation.*

of distance. They are produced by ultrasonic transducers operating with either magnetic or electrical energy (piezoelectric effect). The ultrasound waves are broken on solid objects and walls, thus giving rise to ultrasonic shadowing. The ultrasonic effect is based on cavitation, occurring mainly at the boundary surfaces between water and a solid object. Here cavities are formed containing gas at a negative pressure. When these cavities collide with each other, suction pressures of up to 100 bar are generated and result in the removal of soil particles from solid surfaces. This effect cannot be generated in the case of soft objects, e.g. materials made of rubber, latex and silicon rubber.

The PEDOT:PSS and/or polymer or blend solution was spin-coated onto the patterned ITO substrates in the nitrogen atmosphere of a glove box, O_2 - 2 ppm and H_2O - 0.01 ppm. The metal top electrode (Al) was deposited by thermal evaporation in high vacuum, better than $5x10^{-7}$ mbar, at a rate of between 0.05 and 0.1 nm/s. All devices were stored in nitrogen atmosphere prior to measurement. Dark, temperature dependent, current-voltage characteristics were obtained by utilising a dc current-voltage Source/Monitor Unit (Advantest TR 6143), as a voltage source and current monitor, with the device placed in a liquid - nitrogen - cooled cryostat at high vacuum of better than 10^{-5} mbar in all cases. The temperature range studied was from 100 to 360 K, and the temperature was allowed to stabilize for 3 minutes within $\pm$ 0.01 K before measurement was initiated. The thickness of the devices was then obtained by scrapping off part of the thin polymer film, and using an atomic force microscope (Burleigh Vista -100 Scanning Probe Microscope) to scan the formed step.

3.3 Summary

In this chapter we have given the properties of the polymers, fullerene, and electrodes studied in this project. We have highlighted some of the important properties of ITO, PEDOT:PSS as well as the

properties of their interface. The methods used in the preparation and measurement of the devices are also highlighted in a block diagram.

4 Current limiting mechanisms in ITO/P3HT/Al sandwich devices

We studied the temperature dependent current - voltage characteristics of regioregular poly (3-hexyl thiophene 2.5-diyl) (P3HT) thin films sandwiched between indium tin oxide (ITO) and aluminium (Al) electrodes (ITO/P3HT/Al devices), with the aim of determining the current limiting mechanism(s) in these devices, and the temperature and/or applied electric field range(s) in which these mechanisms are valid. The current-voltage characteristics of the ITO/P3HT/Al devices showed that current flow across the device is limited by hole injection at the Al/P3HT interfaces at temperatures below 240 K, when the device is biased with high potential on Al. Above this temperature, the bulk transport properties control the characteristics. For the reverse bias, the ITO/P3HT contact does not limit the current; instead it is controlled by a space charge that accumulates due to the low charge carrier mobility in the polymer. An expression that provides a criterion to determine the validity of applying either the Richardson-Schottky thermionic emission model or the Fowler-Nordheim field emission model was deduced. It can be employed to determine the electrical field at which the transition from charge injection by thermionic emission to that by field emission for a given temperature and interface potential barrier height takes place. Our experimental data fit to the deduced expression. Theoretical limits of the model are also discussed. By considering the regions of the current-voltage curves where field emission or thermionic emission was applicable, the interface potential barriers were estimated, respectively. Hence, conclusions on whether the current-voltage behavior of the devices was contact limited or bulk limited could be drawn.

4.0.1 Modeling of current in metal/polymer/metal structures

The current - voltage characteristics of metal/polymer/metal devices are controlled by two basic processes: (a) injection of charge carriers from the electrodes into the polymer and vice versa and, (b), transport of charge in the bulk of the film. Steady state current is determined by the less effective mechanism, since this is the one that limits net charge flow depending on specific experimental situation (the externally applied electric field, the height of the injection barrier, i.e., the difference between the electrode work function and the corresponding transport levels of the polymer, and the temperature, etc.). The current is then either injection limited or bulk transport limited.

4.1 Results and discussion

4.1.1 Current - voltage characteristics

An overview of the current density (J) versus voltage (V) characteristics of ITO/P3HT/Al devices, for temperatures ranging from 100 to 360 K, is shown on a linear scale in Fig. 4.1. The asymmetrical nature of the curves is attributed to the difference in the work functions of the electrodes, implying different barriers at each electrode / polymer interface. Figure 4.2 shows double-logarithmic $J(V)$ plots for different temperatures, ranging from 100 up to 360 K in 20 K steps.

Figure 4.2 corresponds to hole injection into the HOMO of P3HT through Al (+ is on Al) and electron injection into the LUMO through ITO (- on ITO). It can be observed that the curves have a slope equal to about 1 at low voltages, suggesting compliance with Ohm's law. It is interesting to
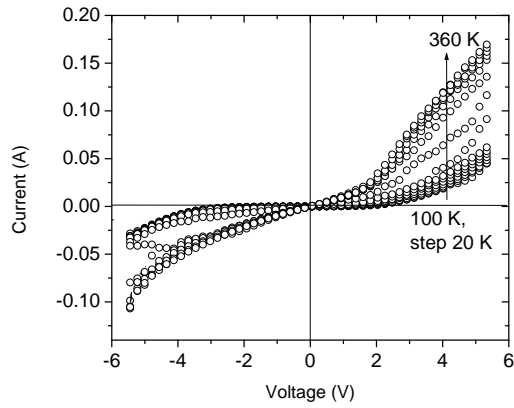
Figure 4.1: *An overview of current-voltage curves for d = 20 nm thick ITO/P3HT/Al devices within the 100 to 360 K temperature range.*
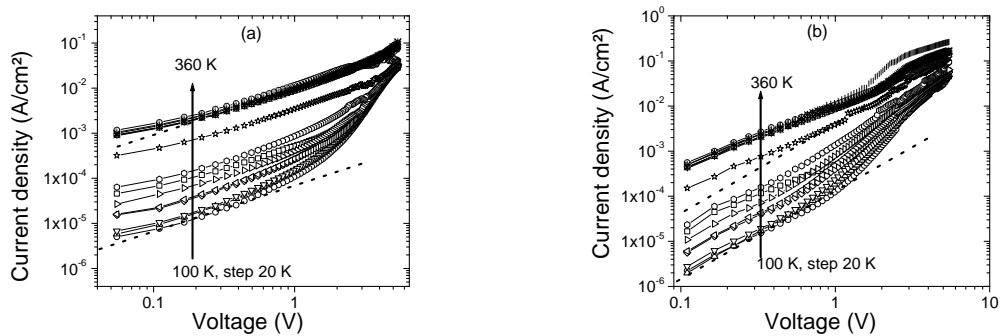
Figure 4.2: J(V) *curves in log-log scale for: (a) hole injection through the Al/P3HT interface (dotted lines correspond to slope 1), (b) through ITO/P3HT interface (dotted lines correspond to slope 2).*

note that the slope then tends to about 4, and each curve approaches this slope at a higher voltage, the higher the temperature is. Since the slope is greater than 2, it might indicate the existence of traps within the bulk of the semiconductor. [30] The limitation of the current by the contact with a relatively high barrier (such as the hole injection through Al/P3HT) is more pronounced at low temperatures. At such temperatures, thermally generated carriers are very few, and at low voltages the injected charge density is small so that the overall behavior is ohmic. As the voltage is increased, the number of injected carriers increases, so that space charge accumulates, tending to limit the current. The number of thermally generated carriers increases with temperature, hence, the current increases with temperature, conforming to semiconductor behavior. Therefore, an even higher voltage has to be applied before the injected charge and the thermally generated charge can become comparable. The super-linearity is, therefore, expected at a higher voltage, when the temperature increases. Super-linear behavior [see Fig. 34.2] suggests that the injected charge overwhelms the transport capabilities of the polymer, hence giving rise to the accumulation of positive charge near the Al hole injecting electrode. The bulk properties start to control the curent-coltage characteristics. When all the curves reach the constant slope line, the *J(V)* curves depend more strongly on the voltage applied rather than temperature. Figure 4.2(b) corresponds to electron injection into the LUMO of P3HT through the Al electrode, and hole injection into the HOMO through the ITO electrode. Below 2 Volts, the slope of the curves measured at low temperatures is approximately 2 (TFSCLC behavior). The bulk controls the current. At higher temperatures, the slope found is between 1 and 2. This means that the thermally generated carrier density exceeds that of the injected charge. The changes in slope with applied voltage seen in Figs. 4.2 (a) and (b) are different due to the different hole injection barrier heights.

4.2 Thermionic emission

At low electrical fields when the slope of ln(*J*) vs. ln(*V*) is about 1, the region is considered as being ohmic. Above the ohmic region, the current - voltage characteristics may be fitted to the Richardson-Schottky (RS) emission model.

Equation (2.21) may be rewritten as

$$ln\left(\frac{J}{T^2}\right) = ln\left(A^*\right) + \left[\left(-\phi_B + \sqrt{\frac{q^3V}{4\pi\varepsilon_0\varepsilon_r d}}\right) \cdot \frac{1}{k_B}\right]\frac{1}{T}. \tag{4.1}$$

According to (4.1), plots of ln(J/T^2) vs 1000/T are straight lines, since all the other parameters are constant, at a given voltage, *V*. The expression in the square brackets of Eq. (4.1) represents the slope of ln(J/T^2) vs. 1000/T and is called activation energy. The effective barrier height between the electrode and the film may be calculated from the slope, thus,

$$\phi_B = \left(-k_B \cdot slope + \sqrt{\frac{q^3V}{4\pi\varepsilon_0\varepsilon_r d}}\right). \tag{4.2}$$

Our experimental data fits well with the RS emission model at high temperatures. As can be noted from Fig. 4.3 (a) and (b), the slopes of ln(J/T^2) vs 1000/T at different voltages tend to straight lines at high temperatures.

This is particularly clear in the case of hole injection through ITO, Fig. 4.3(b), where the straight lines are observed from about 250 K (1000/T = 4) upwards. In the case of Fig. 4.3, i.e., hole
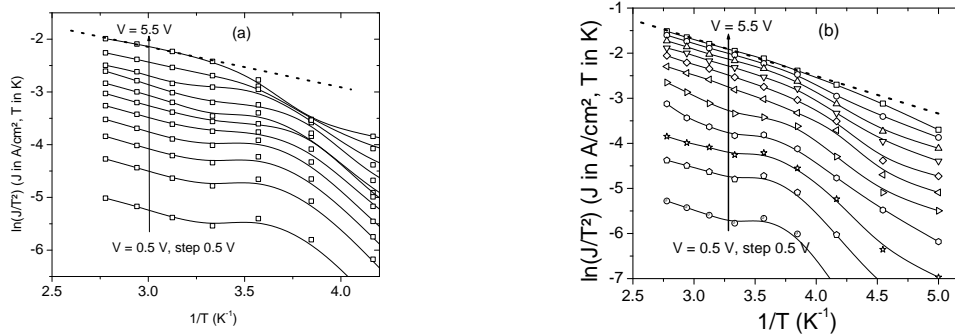
Figure 4.3: *ln(J/T²) vs 1000/T plot for (a) hole injection through the Al/P3HT interface,(b) plot for hole injection through the ITO/P3HT interface. Dotted lines are guides for the eye.*

injection through Al, the straight line behavior seems to be evident above 300 K, but there are too few experimental points to make a reasonable fit. However, the fact that thermionic emission dominated behavior is observed at higher temperatures indicates that a higher hole injection barrier exists at the Al/P3HT interface, since more thermal energy is required before the charge carriers will be able to overcome it. This confirms the difficulty of injection through this barrier as compared to the ITO/P3HT interface as has been observed and mentioned in Section 4.2.1.

The employment of Eq. (4.2) to the fitted straight lines yielded a hole injection barrier equal to 0.44 eV for the ITO/P3HT interface. A larger barrier is expected for hole injection through the Al/P3HT interface. SCLC behavior would be expected for barriers below 0.5 eV.

4.3 Field emission

The equation that relates current density and applied electric field, within the Fowler-Nordheim formulation (Eq. 2.26) may be rewritten thus:

$$ln\left(\frac{J}{F^2}\right) = ln(A) - \kappa\left(\frac{1}{F}\right). \tag{4.3}$$

This is a straight line equation of $ln(J/F^2)$ versus $(1/F)$ with a slope equal to $-\kappa$, and the plot is referred to as the FN plot. The value of κ may, thus, be determined from FN plots. Figure 4.4 show typical FN plots of ITO/P3HT/Al devices for temperatures ranging between 100 and 220 K for (a) - positive, and (b) - negative bias on Al, respectively.

At high applied fields (or low values of 1/F), the FN curves for our devices can be fitted to straight lines. From the slope of the straight part of FN plots, the interface potential barrier height can be computed by using equation (2.30). In Fig. 4.4(a), the curves obtained for different temperatures converge into one common line, at high applied fields. The barrier height for hole injection into the HOMO through the Al/P3HT interface can be, therefore, estimated as 0.85 eV.

In Fig. 4.4(b)), instead, the slopes are temperature dependent. The upper limit of the barrier height for hole injection into the HOMO through the ITO/P3HT interface is 0.47 eV at T=100 K. This indicates that the barrier height, defined as the energy gap between the HOMO of the polymer and the respective electrode work function, slightly varies with temperature in different ways. Note that the
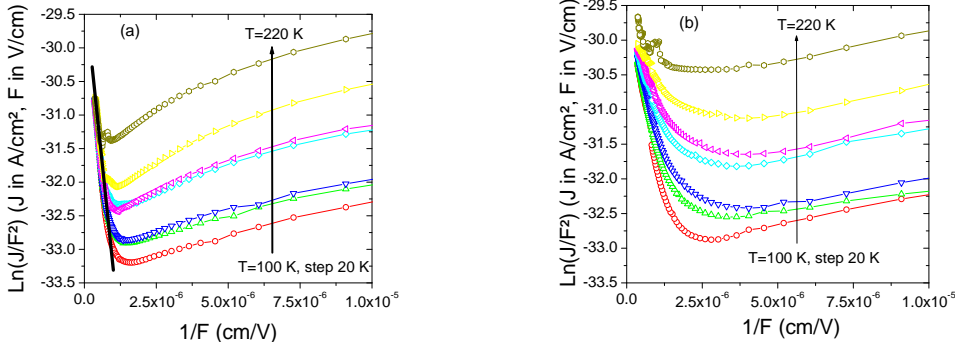
Figure 4.4: *Fowler-Nordheim plots for the tunneling (a) of holes from Al into P3HT, and (b) of holes from ITO into P3HT. Dotted lines indicate the linear parts of the curves.*

variation of band bending in the vicinity of contacts, if present, may be responsible for the latter. The deviation from straight line behavior at lower electric fields is attributed to thermionic emission. Therefore, the injection of holes through the lower barrier (ITO/P3HT) is expected to be more influenced by temperature. We have also calculated the HOMO of the polymer using the procedure suggested by Huemmelgen *et al.* [101], where knowledge of the thickness and the effective mass is not required, but only the work functions of electrode materials and the slopes of the FN curves in reverse and in forward bias, at constant temperature. In this procedure, the ratio of the slopes of the FN curves, from Eq. (2.30), is considered. Such calculations suggest a linear variation of the HOMO from about 5.24 eV at 100 K to about 4.9 eV at 220 K, if the electrode work functions were constant with temperature.

4.4 Transition from field to thermal emission limited characteristics

The concept of tunneling alone, or of thermionic emission alone, does not make much sense within the transition region. The description of this region would call for some kind of a hybrid model. The combined contribution of the two phenomena to the measured current has been described either as field assisted thermionic emission or thermally activated tunneling [49] (see Fig. 4.5).

The increase in electric field implies a stronger barrier lowering (due to image charge), meaning that charge carriers which have a smaller energy can now be emitted over the barrier, and this is denoted as field assisted thermionic emission. On the other hand, since the barrier is considered to be constant in the FN theory, an increase in temperature implies a smaller difference between the energies of the electrons and the top of the barrier, meaning that the barrier to be traversed is now thinner, and the probability of tunneling increases. This is denoted as thermally assisted field emission. Indeed, many studies have been done in other metal/polymer/metal devices, in this respect. For instance, temperature dependent current-voltage measurements on poly-para- phenylene veny-lene (PPV) films revealed a thermally activated behavior at low voltages [53]. The absence of this behavior at higher voltages was attributed to field emission (FN tunneling) at the contacts [102]. However, the theoretical FN expression was not able to quantitatively account for their experimental *J(V)* characteristics. The large deviations were attributed to thermionic emission [103], space charge effects in the bulk of the polymer [104] and band bending effects [105]. It has been demonstrated that at low electric fields and at room temperature the conduction of holes in PPV devices is limited
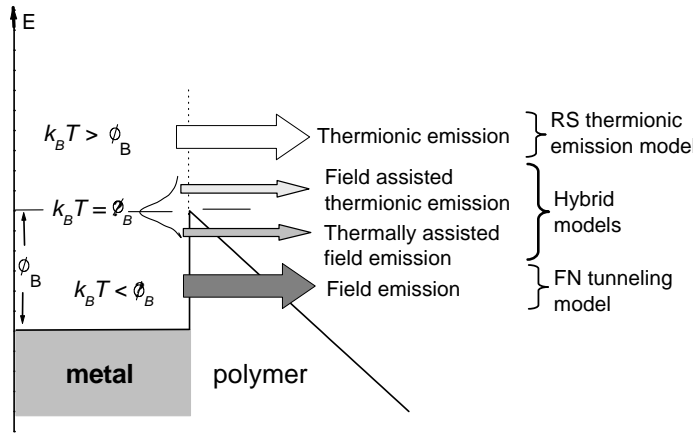
Figure 4.5: *Mechanisms of charge carrier injection through a metal/polymer interface. The energy distribution function is of Maxwell - Boltzmann type.*

by space charge effects in the bulk of the polymer and not by the charge injection from the contact [28]. At high fields, however, the strong field dependence of the current together with its decreased temperature dependence both seem to argue in favor of the tunneling model [29]. The shortcomings of each of the models, RS and FN, considered separately, are the following: At high electric fields, barrier lowering may be comparable to the barrier height itself, and its neglect in tunneling considerations is problematic. Also problematic are the assumptions of a triangular barrier and the existence of a continuum of unbound states into which carriers can tunnel. The application of the RS concept suffers from the neglect of inelastic carrier scattering inside the potential well which is of crucial importance in organic solids where transport is an incoherent process and the mean free path is small. There, clearly, is a need for the harmonization of the two concepts, the classical RS thermionic emission over the barrier and the quantum mechanical FN tunneling through the barrier.

4.4.1 Model

We utilize the expression for the temperature dependent tunneling current through a triangular barrier at metal/polymer interfaces derived in [45], [46], from which we deduce an expression for the minimum electric field that must be applied to a device with a known interface barrier height, at a given temperature T, so that the tunneling contribution equals the thermionic emission contribution to the current. The tunneling current density through the triangular barrier at a metal polymer interface, considering the effect of temperature on the Fermi distribution is given by [45]

$$J(T) = \frac{q^2 \pi k_B T}{h^2} \left(\frac{m^*}{2\phi_B} \right)^{1/2} \cdot F \cdot exp\left(-\frac{8\pi\sqrt{2m^*}\phi_B^{3/2}}{3hqF} \right) \cdot \frac{1}{sin(\beta\pi k_B T)}. \tag{4.4}$$

(see full derivation in Appendix 1), where

$$\beta = \frac{4\pi\sqrt{2m^*}\phi_B^{1/2}}{hqF}.$$

(4.5)

Further, this expression is only applicable if the following condition is satisfied:

$$\beta < \frac{1}{k_BT} - \frac{1}{\phi_B}.$$

(4.6)

Substituting (4.5) in (4.6), we obtain an explicit relationship (4.7) between temperature, applied electric field, and interface barrier height, for the threshold field that must be applied, *F*, for tunneling to dominate the *J(V)* characteristics:

$$F > \frac{2\sqrt{2m^*}k_BT\phi^{3/2}}{q\hbar(\phi_B - k_BT)}.$$

(4.7)

The inequality (4.7) is not defined for $\phi_B = k_BT$, since this would mean that there is no barrier. This is logical considering that the definition of tunneling demands that the energy of the electrons must be smaller than the barrier height, otherwise, for $\phi_B < k_BT$, thermionic emission of electrons across the barrier occurs. In the low-temperature limit, for temperatures such that $k_BT << \phi_B$, the denominator of inequality (4.7) is independent of *T*. This means that for certain interfacial barriers $\phi_{B1} < \phi_{B2}$, a larger field is required to observe the tunneling dominated characteristics. However, as *T* is increased, k_BT approaches ϕ_{B1} first, and the required field becomes so high, overtaking that required for ϕ_{B2}, and then tends to infinity. For ϕ_{B1}, no more tunneling is possible, but for ϕ_{B2} it can still be observed.

The fact that there is no single valued energy for all electrons in a material, but rather distributed energy values about the average energy k_BT according to the Maxwell-Boltzmann statistics, indicates that a portion, exp(-E/k_BT), of the electrons will have energy values larger than *E*. When this portion has crossed over the barrier, we can not distinguish them from those that have tunneled. Another difficulty arises from the fact that there might be no single valued barrier height, but a distribution around ϕ_B, due to the fuzziness in the energy of the polymer band edges caused by disorder [55]. In addition, the evaporated electrodes are not expected to have precisely known values of the work function due to their amorphous structure. The above implies that analysis of either tunneling or thermionic emission makes real sense away from the transition region. The inequality (4.7) has been evaluated for different interface barriers ϕ_B (in eV), where $m = 9.11 \times 10^{-31}$ kg, $k_B = 8.62$ eV/K, T is the absolute temperature, $q = 1.60 \times 10^{-19}$ C, $h = 6.64 \times 10^{-34}$ Js. The result of this evaluation for an interface barrier of 0.025 eV is shown in Fig. 4.6, which shows plots of the minimum electric field, F_z, which must be applied to a metal/semiconductor polymer/metal device, in order for charge carriers to be injected across the barrier through quantum mechanical tunneling, as a function of temperature.

At the field F_z tunneling balances thermionic emission, i.e., for any particular interface potential barrier ϕ_B, at a given temperature *T*, it is necessary to apply an electric field F_z so that the number of electrons injected from the metal into the semiconducting polymer through quantum mechanical tunneling becomes equal to that due to thermionic emission. The vertical dotted line indicates the value of T such that $k_BT = \phi_{B1}$, i.e., the temperature at which the average energy of the charge carriers becomes equal to the potential barrier height. The region to the left of this line indicates the temperatures at which $k_BT < \phi_{B1}$. Charge carriers with such energies can only be injected into the
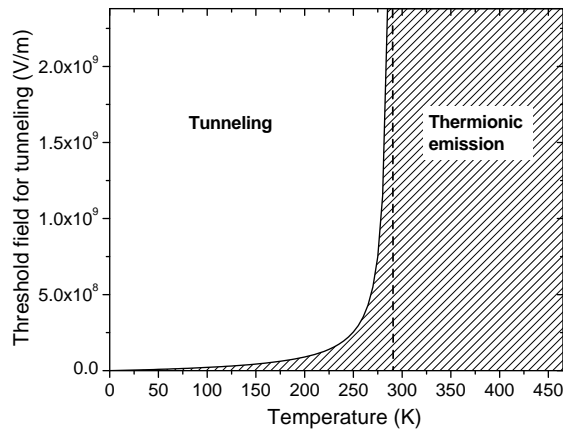
Figure 4.6: *Theoretical curves (inequality (4.7)) showing the boundary between thermionic emission and field emission characteristics for an interface barrier $\phi_{B1}=0.025$ eV. The shaded area corresponds to field and temperature combinations described by thermionic emission. Outside this area, tunneling (field emission) describes the charge injection. The dotted line indicates the temperature at which $k_B T = \phi_{B1}$.*
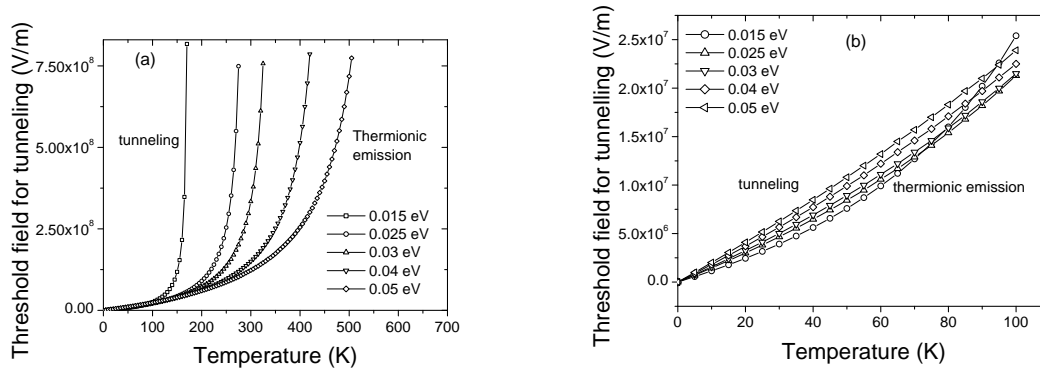
Figure 4.7: *Plots of F vs T (Inequality (4.7)) for various interfacial barriers. (a) Illustrating that the temperature at which thermionic emission dominates the current contribution (for a constant field) increases with the size of interface potential barrier. (b)For very low temperatures, the trend is reversed, since there is practically no thermionic emission, and the temperature at which thermionic emission dominates decreases with increase in potential barrier.*
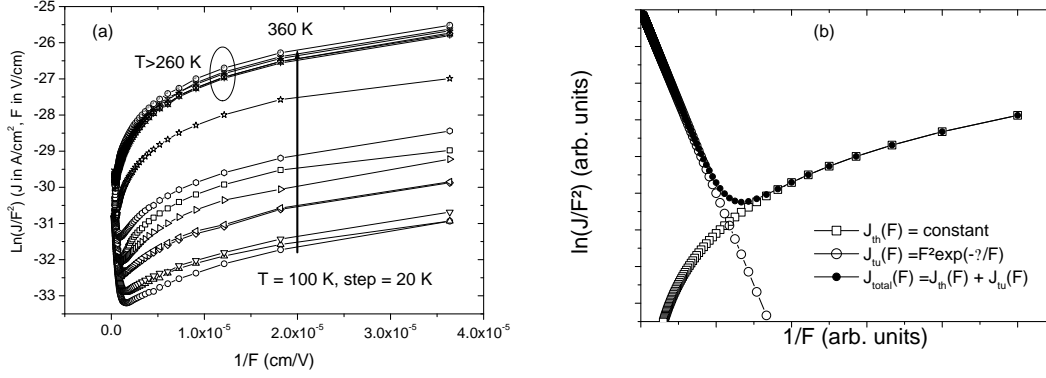
Figure 4.8: *(a) Fowler-Nordheim plots for a reverse biased ITO/P3HT/Al device in the temperature range 100 - 360 K. (b) The proposed superposition of contributions of thermionic Jth(F) (open squares) and tunneling Jtu(F) (open circles) in total current density J(F) (closed circles). In the thermionic term, the potential barrier is considered as field-independent.*

semiconductor by quantum mechanical tunneling. The curve approaches the indicated vertical line asymptotically.

If the applied field is smaller than F_z, the injection is dominated by thermionic emission, otherwise it is dominated by tunneling, provided the temperature is well below the critical value determined by the condition $k_B T = \phi_B$. If T increases, a relatively higher field is required for tunneling to balance thermionic emission. If T is equals values such that $k_B T$ is smaller but comparable to ϕ_B, it becomes important to consider the distribution of energies of charge carriers about $k_B T$ (as mentioned above), and the thermionic emission will dominate. As $k_B T$ approaches to ϕ_B, the electric field F_z tends to infinity, therefore, the definition of tunneling ceases to make sense. Other cases of inequality (4.7) are illustrated in Figs. 4.7.

The above can be summarized as follows: For an interface barrier ϕ_B, any combination of $F > F_z$ and T such that $k_B T < \phi_B$, tunneling dominates the injection at the electrode/metal interface (shaded region). Outside this region, thermionic emission dominates. Below and on the right hand side of the F_z curve, the J(V) characteristics should be independent of tunneling, and the rate of change of the current with applied field is reduced. We should, therefore, expect the bulk properties of the polymer to take over the current limitation, since the electrons do not "see" a barrier. Depending on the mobility of the electrons in the polymer, either ohmic behavior or space charge limitation will be observed.

4.4.2 Comparison with experiment

It has frequently been indicated that the deviation of the FN plot from straight lines at low electrical fields might be due to the contribution of thermionic emission, so most authors truncate their FN curves when the slight curvature starts to appear [45], [101], [102], [106], in order to analyze only the straight line regime, estimate the slope and, hence, the barrier height. In Fig. 4.8(a), we show complete curves obtained for our devices under reverse bias.

Similar shape of curves was obtained also by Kiy et al. [43] for electron tunneling from a magnesium contact into Alq$_3$. As discussed in Section 4.3.3, the slopes are different, yielding a larger barrier for the hole injection through the Al/P3HT interface. The complete plot indicates a straight
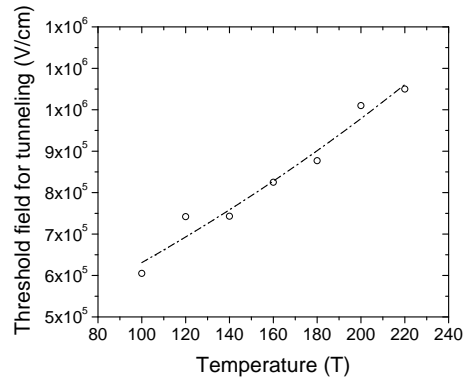
Figure 4.9: *Field at minima of Fowler-Nordheim plots as a function of temperature for ITO/P3HT/Al under reverse bias. The dashed line is a guide for the eye.*

line at high field strength, which curves, reaches a minimum, and then gradually increases for lower applied fields. The contribution of field emission decreases, and the contribution from thermionic emission becomes appreciable and dominates the *J(V)* characteristics thereafter. The overall behavior is schematically represented in Fig. 4.8(b), where the superposition of contributions of both effects, thermionic $J_{th}(F)$ and tunneling $J_{tu}(F)$, results in a minimum.

Note that in the thermionic term the potential barrier is considered as field-independent. At low temperatures, a relatively low electric field strength is required, in order to inject an appreciable number of holes by tunneling, for their density to become comparable to that of those that are injected thermionically. The minimum of the FN plot will shift towards higher applied field strength (to the left in Figs. 4.4, and 4.8) with increase in temperature. The electric field at which the minimum of the FN curves is observed has been obtained from Fig. 4.4 and plotted against temperature, as shown in Fig. 4.9. The trend conforms to inequality (4.7).

If the temperature is high enough, the tunneling regime will not be seen in the FN plot (see Fig. 4.8, *T*>260 K). The *J(V)* behavior becomes nearly temperature independent. As *T* increases beyond $k_B T = \phi_B$, the *J(V)* curves become bunched together (see Fig. 4.8). We may conclude that for any description of the *J(V)* characteristics as contact limited, or bulk limited, it is essential to specify the interface potential barrier, temperature and applied electric field ranges where such limitation would be valid.

4.5 Conclusions

We have shown that the current in ITO/P3HT/Al devices is limited by hole injection at the Al/P3HT contact when the device is reverse biased. The current becomes space charge limited at high voltages when tunneling contributes significantly to the charge injection. The electric field at which the transition from contact limited to space charge limited current takes place increases with temperature. If the current through the device is contact limited, the field of transition from thermionic emission to field emission increases with temperature, tending to infinity when the charge carrier energy is comparable to the interface barrier height. In forward bias, the ITO/P3HT interface supplies a high amount of charge in the polymer semiconductor bulk, and the current is space charge limited in the whole voltage and temperature range studied, suggesting the formation of an ohmic contact for hole

injection at the ITO/P3HT interface. The FN-estimated hole injection barrier heights for Al/P3HT and ITO/P3HT are 0.85 eV and 0.47 eV, respectively.

5 Trap limited hole mobility in semiconducting poly(3-hexylthiophene)

Bulk transport properties of poly(3-hexylthiophene) (P3HT) were studied by analyzing temperature dependent current-voltage characteristics of the polymer thin films sandwiched between Indium Tin Oxide/polysstyrene sulfonate doped Polyethylene dioxy-thiophene (ITO/PEDOT)and aluminium electrodes. It was found that the contacts limit charge injection under reverse bias, but under forward bias the current is limited by space charge that accumulates near the hole injecting electrode (ITO/PEDOT) resulting in a rectification of 10^5. The forward current density obeys a power law of the form $J \sim V^m$, with m>2, described by space charge limited current in the presence of exponentially distributed traps within the band gap. In this chapter we describe the deduction, and discuss the limits, of an expression for the calculation of the total trap density, based on the exponential trap distribution model, which yielded reasonable agreement with our experimental $J(V)$ data. The total deep hole trap density was estimated to be 3.5×10^{16} cm^{-3}, and the activation energy was obtained to be 0.054 eV. Temperature dependent hole mobility in P3HT was also estimated under trap-free space charge conditions, yielding a value of 3×10^{-5} cm^2/Vs, at 304 K.

5.1 Theory

As previously discussed, the dark charge carrier injection depends on the potential barrier at the interface and on the temperature dependent energy of electrons incident on that barrier. Once charge carriers are injected, their transport through the polymer layer towards the adjacent electrode under the influence of the external electric field is determined by the conduction properties of the material itself. For low bias the number of injected carriers is smaller or comparable to the thermally generated intrinsic charge carriers, and the current - voltage characteristics can be described by Ohm's law. The space charge limited current (SCLC) model [46], [57] describes charge transport in a low conductivity material, where the concentration of injected charge may exceed the intrinsic charge concentration, and space charge builds up in the sample. The application of this model provides useful material characteristics such as the trap distribution in the energy band gap, the position of the Fermi energy, and charge carrier mobility.

Investigations have shown that bulk conduction in disordered, and that in undoped, conjugated polymers is also described well by the hopping transport of electrons and holes, taking into account space charge effects and traps of different depths [107]. Current density-Voltage *(J(V))* characteristics of electrode/polymer/electrode devices can often be fitted excellently by the power law $J \sim V^m$ with *m>2*, characteristic of the filling of exponentially distributed traps [108]. Traps may originate from structural defects or due to perturbed molecules in the lattice causing charge of polarization energy in the perturbed regions, which may also tend to lower the bottom edge of the conduction band, or to raise the bottom edge of the valence band. Campbell *et al.* [109] have shown that the SCLC model with field independent mobility, in presence of exponentially distributed traps gives qualitatively the same results as trap free SCLC with a field dependent mobility of the Poole-Frenkel type [110], [30], [111]. In the following section we briefly describe the exponential trap distribution model, and deduce an expression for the calculation of the total trap density, which yielded reasonable agreement with our experimental *J(V)* data.

5.1.1 Exponential distribution of traps

We consider a hole-only device for the following description, and note that the reverse will be equally true for electron only devices. The distribution function for the hole trap density as a function of energy level E above the valence band, and a distance x from the injecting contact for holes can be written as: [46]

$$h(E,x) = n(E)s(x), \tag{5.1}$$

where $n(E)$ and $s(x)$ represent the energy, and spatial distribution functions of traps, respectively. An assumption of uniform spatial trap distribution within the specimen from injecting electrode to collecting electrode implies that the effective thickness of the device, under space charge conditions, remains the thickness itself, and $s(x) = 1$. The specific functional form of the SCLC current density versus voltage, J(V) curve depends on the distribution of charge traps in the band gap.

For traps that are exponentially distributed within the energy band gap, Eq. (5.1) becomes

$$h(E) = n(E) = \frac{N_{vb}}{E_t} exp(-\frac{E}{E_t}), \tag{5.2}$$

which can be written as

$$N(E) = N_{vb} exp(-\frac{E}{E_t}), \tag{5.3}$$

where $N(E)=n(E)E_t$ is the trap density at an energy level E above the valence band edge, and N_{vb} is the trap density at the valence band edge; E_t is the characteristic constant of the distribution, also often expressed as a characteristic temperature T_t, $(E_t = k_B T_t)$, where k_B is Boltzmann's constant. Equation (2) assumes that the maximum number of traps is located at the valence band edge, and decreases exponentially as we go deep into the energy band gap. To extract the physical significance of E_t, we consider the case when the trap energy $E = E_t$, therefore Eq. (5.2) can be simplified as

$$\frac{N(E_t)}{N_{vb}} = \frac{1}{e} = constant. \tag{5.4}$$

Equation (5.4) states that the trap energy level that characterizes the exponential distribution is defined as the energy at which the density of traps has been reduced by *1/e* as compared to the trap density at the valence band edge. The characteristic width of the exponential distribution is therefore set by the energy E_t. At the conduction band edge we expect the density of hole traps to vanish. In Eq. (5.2), $E = E_{cb} >> E_t$, therefore, $N(E_{cb}) \sim 0$, where E_{cb} is the energy level of the conduction band edge. The total density of traps in the distribution is given by $N_{total} = N_{vb} k_B T_t$. [112]

The exponential trap distribution (Eq. (5.3)) implies a power law dependence of current density on the bias voltage given by [46] [57]:

$$J = q^{1-l} \mu_p N_v (\frac{2l+1}{l+1})^{1/l} (\frac{l}{l+1} \frac{\varepsilon \varepsilon_0}{N_{total}})^l \frac{V^{l+1}}{d^{2l+1}}, \tag{5.5}$$

where q is the electronic charge, ε_0 is the permittivity of free space, ε is the dielectric constant of material, μ_p is charge carrier mobility of holes, N_v is the density of states in the valence band, N_{total} is the total density of traps; $l=T_t/T$, T is the measurement temperature in K, d is the sample thickness, $m = l+1$, and $J \sim V^m$ is the power law obtained. After performing some simple algebraic

manipulations we rewrite Eq. (5.5) in its Arrhenius form to bring out the dependence of current density on temperature. Grouping together all the terms with l from Eq. (5.5), we obtain:

$$J = \frac{q\mu_p N_v V}{d} \left[\left(\frac{2l+1}{l+1} \right)^{1/l} \frac{l(2l+1)}{(l+1)^2} \frac{\varepsilon\varepsilon_0 V}{qd^2 N_{total}} \right]^l. \tag{5.6}$$

We can apply the exponential function to a natural logarithm without altering the result, and when we consider that $l = T_t/T$ we obtain that Eq. (5.5) can be written as

$$J = \frac{q\mu_p N_v V}{d} exp \left\{ -\frac{E_t}{k_B T} ln \left[\left(\frac{2l+1}{l+1} \right)^{-1/l} \frac{(l+1)^2}{l(2l+1)} \frac{qd^2 N_{total}}{\varepsilon\varepsilon_0 V} \right] \right\}, \tag{5.7}$$

Therefore, for an exponential distribution of traps, the quasi-Fermi level, which depends on the magnitude of stored charge and hence on the applied voltage is given by

$$E_F(V) = k_B T_t ln \left[f(l) \frac{qd^2 N_{total}}{\varepsilon\varepsilon_0 V} \right], \tag{5.8}$$

with

$$f(l) = \left(\frac{2l+1}{l+1} \right)^{-1/l} \frac{(l+1)^2}{l(2l+1)}, \tag{5.9}$$

E_F is measured from the edge of the valence band for the hole injection, or from the conduction band edge for electron injection.

Kumar *et al.* [113] obtained a similar expression for E_F, which they called activation energy, by rewriting Eq. (5.5) to bring out the Arrhenius dependence of current density on temperature, resulting in that the prefactor with l is equal to 0.5, through some approximation within 4%. Kao and Huang [46] gave an expression for E_F similar to the one in Eq. (5.8), but without the factor raised to the power (-1/l), possibly because they approximated that term to 1. In the analysis, by Tans *et al.* [114], of the power law asymptotes of the J(V) characteristics in presence of exponentially distributed traps one can infer that they considered *f(l)* to be equal to 1. To clarify the apparent lack of consistency, we discuss the permitted limits of the pre-factor *f(l)* in Eq. (5.9).

In Fig. 5.1 we show a graph of *f(l)* vs *l*, [Eq. (5.9)] for values of *l* from the minimum allowed $l = 1$ (corresponding to $m = 2$) to an arbitrary $l = 50$.

Calculation shows that *f(l)* decreases monotonously, e.g., from 8/9 to 0.51 for values of *l* between 1 and 30. In the limit when *l* tends to infinity, *f(l)* tends to 0.5. We suggest that 0.5 is the value of *f(l)* when the *J(V)* curve in double logarithmic scale becomes vertical. In that case, the description of traps by a continuous exponential distribution ceases to be valid. The traps being filled are then described as being situated on some discrete energy level within the band gap [46], [57]. When *f(l)* is the maximum allowed value of 8/9, all traps are filled, and there is no trap filling taking place. This happens when $m = 2$. We define therefore that the exponential description is valid if $0.5 < f(l) < (8/9)$. Therefore using any of the two extremes in calculation of E_F or N_{total} cannot be justified, worse approximating to a prohibited value 1, even if this will not alter the numerical result significantly. For values of $l < 10$, which are usually obtained practically, one expects shallow traps close to the valence band edge, some of which in fact can be filled by thermal energy.

Figure 5.2 illustrates the effect of space charge on the Fermi level in the SCLC regime, at constant temperature.
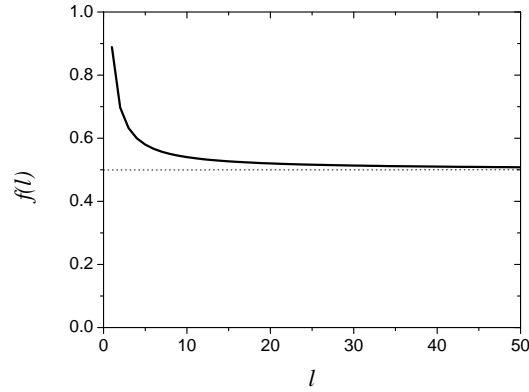
Figure 5.1: *Graph of f(l) vs* l, *Eq. (5.9) for values of* l *from the minimum allowed l = 1 to an arbitrary l = 50. When l tends to infinity f(l) tends to 0.5. f(l) describes the limits of validity of the exponential trap distribution model.*
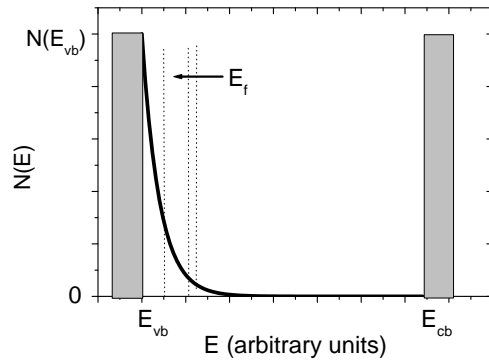
Figure 5.2: *Schematic diagram of the proposed exponentially distributed density of states as a function of energy,* N(E), *at constant temperature.* E_{vb} *and* E_{cb} *mark the edges of the valence and conduction bands respectively. In the band gap, the area under the bold exponential distribution curve indicates the total trap density. Upon application of a high electric field, space charge builds up in the sample, resulting in a shift of the Fermi energy* E_F *towards the valence band, and a corresponding increase in current.*

Upon an increase of the bias voltage, the increased positive space charge will occupy the first available trap states for holes in the bandgap, which corresponds to a shift of E_F towards the valence band edge. [114]

Further, we may rewrite Eq. (5.8) as

$$E_F(V) = k_B T_t ln[f(l)\frac{qd^2N_{total}}{\varepsilon\varepsilon_0} - lnV], \qquad (5.10)$$

where $f(l)$ is the pre-factor with l in Eq. (5.9), and is constant for any given temperature, where the power law $J \sim V^m$, $m > 2$ is satisfied. In the SCLC regime E_F is thus linearly dependent on lnV. The Fermi level $E_F(V)$ will coincide with the valence band edge ($E_F = 0$), only if the right-hand-side of Eq. (5.10) is zero. This takes place when the applied voltage, V, reaches a critical voltage given by

$$V = V_c = f(l)\frac{qd^2N_{total}}{\varepsilon\varepsilon_0}. \qquad (5.11)$$

At the bias voltage V_c all the traps are filled and E_F coincides with the valence band edge energy E_{vb}. V_c obtained for the temperature in question (implicitly expressed in the function $f(l)$) indicates the minimum voltage which is necessary to apply in order to fill up all existing traps at that temperature. Practically, we expect the slope of the J(V) curve to transform itself to 2 as V_c is approached, in conformity with trap free SCLC. If V_c is the same for all temperatures, this indicates that the traps are so deep that at temperatures considered, the energies $k_B T$ are smaller than those required to fill up any significant number of the traps. The variation of V_c, which is directly proportional to the total number of traps in the bulk, with temperature indicates the measure with which temperature is capable of filling up traps. At high temperatures we would expect more traps to be filled thermally than at low temperatures, and the fraction to be filled by voltage should be reduced. The slope of the $J(V)$ curves determined by Eq. (5.5) increases rapidly with decreasing temperature, making $f(l)$ smaller, thus increasing the fraction of the total number of traps that must be filled by injected charges due to applied voltage.

If the obtained trap distribution parameter $E_t = k_B T_t >> k_B T$, then a cross-over point is observed in the log$J$-log$V$ plot, where V_c and the corresponding current density, J_c, are independent of temperature. A plot of E_F vs ln$V$ for different temperatures should yield straight lines that converge at lnV_c. If such a cross-over point is observed in measured J(V) characteristics, one may then estimate the total deep trap density from Eq. (5.5), as

$$N_{total} = \frac{1}{f(l)}\frac{\varepsilon\varepsilon_0 V_c}{qd^2}, \qquad (5.12)$$

with $0.5 < f(l) < (8/9)$. The total trap density in the exponential distribution is therefore greatest for large l, (low T), where $f(l) \rightarrow 0.5$, which corresponds to low temperature, and decreases for small l reaching its minimum when $f(l) = (8/9)$. Thus, from the $J(V)$ characteristics obeying a power law, one may estimate the characteristic energy of the exponential distribution of traps, the trap density at E_t, and at the conduction band edge, and indeed at any energy level within the band gap, the total trap density, the quasi Fermi level, and the activation energy.

5.2 Results and discussion

ITO/PEDOT:PSS/P3HT/Al devices were prepared as described in chapter 4, with the only difference that a PEDOT:PSS layer was spin coated on top of the cleaned, and patterned ITO substrates prior to
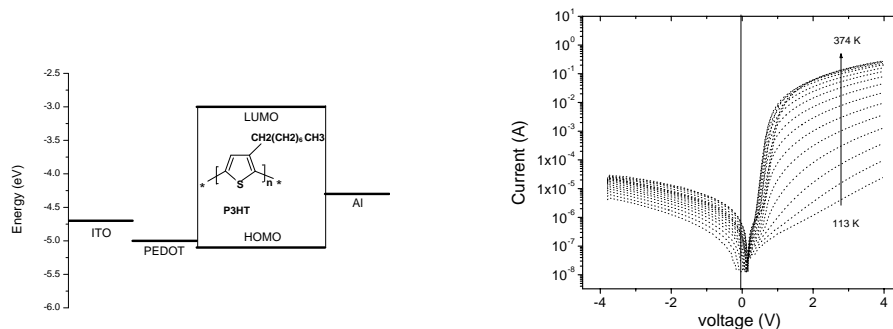
Figure 5.3: *(a)Formula of poly(3-hexylthiophene), and important energy levels of the constituent materials of an ITO/PEDOT:PSS/P3HT/Al hole-only device (under non-equilibrium conditions). Electrode work functions are both in the lower half of the HOMO-LUMO gap of P3HT. (b) Current voltage characteristics of an 85 nm thick ITO/PEDOT:PSS/P3HT/Al device for a temperature range of 113 to 374 K at ~15 K steps, in linear scale. A rectification factor of ~ 5x10^5 was observed at ± 4 V, 304 K.*

spin coating the P3HT. A total of 12 devices made in different batches were studied. All devices were stored in nitrogen atmosphere prior to measurement, which was also done as described in chapter 4. The energy level diagram of the studied ITO/PEDOT:PSS/P3HT/Al devices (under non equilibrium conditions) is shown in Fig. 5.3(a). The inset shows the formula of P3HT. The HOMO of P3HT has been estimated to range between 5.1 and 5.2 eV, from an SCLC analysis of hole only thin film devices [115], cyclic voltametry [116] and photoelectron spectroscopy [117].

The energy gap estimated from absorption spectroscopy is about 2.1 eV, therefore the lowest unoccupied molecular orbital (LUMO) is about -3.0 eV. However, we note that a rigorous estimate of the energy bandgap should also include the exciton binding energy, which is usually a few tenths of an eV. The work functions of ITO, PEDOT and Al are about -4.7, -5.0 and -4.3 eV, respectively. The ITO/PEDOT:PSS/P3HT/Al device is, therefore, a hole only device since in both directions of current flow, the hole injection barrier is smaller than the electron injection barrier.

Figure 5.3(b) shows typical dark current - voltage (*I(V)*) characteristics of as-cast ITO/PEDOT:PSS/P3HT/Al hole only devices of 85 nm thickness in linear scale, in the 113 to 374 K temperature range. High rectification factors of about 5×10^5 were observed in the -4 V to +4 V voltage range at 304 K.

We note that the shape of the curves remained consistent for samples prepared together, and also in separate batches, although the absolute current values varied from sample to sample, the mobilities, charge carrier density, and conductivities are quite comparable for all devices, for the same measurement temperatures.

The curves of Fig. 5.3(b) are re-plotted as current density vs voltage (*J(V)*) in a double logarithmic representation, in Fig. 5.4, corresponding to hole injection through the ITO/PEDOT electrode (forward bias).

At low temperatures, one identifies two different slope regions indicated in Fig. 5.4 by the dotted (slope=1) and dashed (slope>2) lines. As temperature increases, an intermediate region with high slope, which increases with temperature, is observed. The curves then tend to level off to some
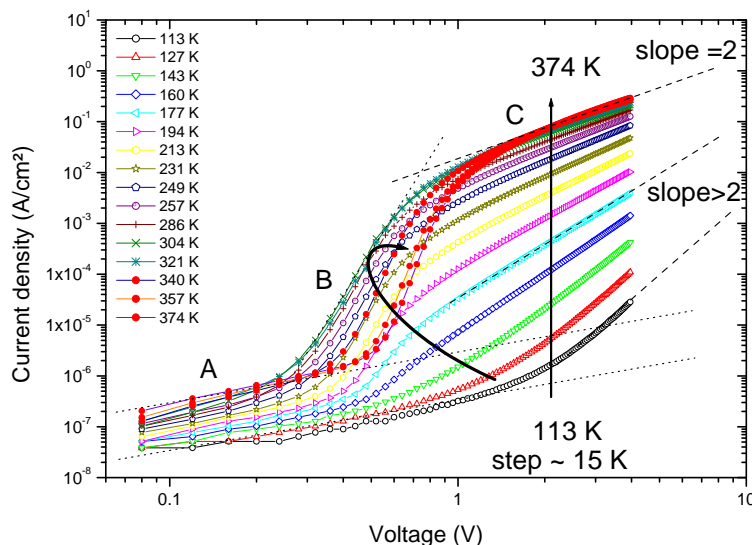
Figure 5.4: *Forward (+ on ITO) dark* J(V) *characteristics of an ITO/PEDOT:PSS/P3HT/Al device (thickness* d=85 nm) *in double logarithmic scale. Regions A has slope = 1, corresponding to ohmic conduction, region B has slope > 2, corresponding to trap filling. The log-log plot at high applied voltage (region C) has a slope = 2 and is described by TFSCLC. This applies only for temperatures above 287 K, otherwise slope > 2, and increases with decrease in temperature.*

constant slope. The dashed lines are a guide for the eye, and they indicate a decrease of slope with increase in temperature. Below 286 K, the slope is greater than 2, and for temperatures above 286 K, the slope is ∼ 2. Note that slope >2 may indicate the filling of traps distributed exponentially in energy. We may approximate that above 286 K, trap free space charge limited conduction is achieved.

Further we remark on the change of tendency to increase current as temperature is increased observed at temperatures above 321 K (filled symbols in Fig. 5.4). This is explained as originating from the evaporation of remnant solvent, water, and oxygen de-doping, which tends to reduce the conductivity of the P3HT [118]. The exponential trap filling region becomes steeper, suggesting a clearer definition of trap energy levels (see section 5.1). Shallow traps which were filled by low voltages seem to have disappeared, as trap filling starts at higher voltages the higher the temperature. The discussion in this paper is valid for the temperatures below 321 K. The electrical properties of P3HT are modified permanently at higher temperatures, due to thermal annealing effects, details of which are a subject of further study.

5.2.1 Trap free space charge limited current

The topmost curve of Fig. 5.4 shows a plot of the forward current density voltage characteristics of an ITO/PEDOT:PSS/P3HT/Al device at 304 ^{o}C in double logarithmic scale.

One can distinguish 3 regions, denoted A, B and C in Fig. 5.4, corresponding to ohmic, charge injection, and space charge limited current respectively.

In region A ($V < 0.3$ V), the applied external electric field is small. The interface barrier blocks charge injection, hence the number of charge carriers participating in the current does not increase. Current depends exclusively on applied field, and on the conductivity of the material. Conduction is due to the intrinsic thermally generated charge carriers, and should obey Ohm's law. For ohmic conduction the slope of logJ vs logV is equal to 1.

We denote region B (0.3 V $< V < 0.7$ V) as charge injection and trap filling region. Applied voltage has passed the threshold of blocking. The number of charges participating in the total current increases with increase in voltage. The bulk material is able to accommodate this increase in charge carriers. We understand this as the overcoming of any built in field across the bulk, which could be the result of the electrode workfunction difference. Rapid increase in current with small increases in voltage is due to the increase in charge carrier density in the bulk. Region B is characterized by slope >2. This region is also described by the Shockley diode equation where current depends exponentially on voltage - in that case the abruptness or spread is expressed in the ideality factor. At some voltage (near 0.7 V), the built-in field is overcome by the applied potential. If the mobility is so low that the extra injected charges cannot be swept to the collecting electrode at the same rate at which they are being injected, space charge then accumulates near the injecting electrode and creates a field that impedes further injection. The rate of increase of current with voltage decreases, until it becomes constant again when all traps are occupied.

We denote Region C ($V > 0.7$ V) as the SCLC region. If the slope>2, this region is usually described by the power law which assumes the filling of traps distributed exponentially within the band gap, the maximum density being at the band edge. If the trap distribution is discrete, then the curve is vertical in region C. The slope therefore can be used as a criterion for comparison of the stretching of the exponential distribution. Low slope implies a gradual (extended) distribution, while higher slope indicates an abrupt distribution. When all traps are filled, trap free space charge limited current (TFSCLC) should then flow. Region C ($V > 0.7$ V) of our $T = 304$ K curve corresponds to (TFSCLC) region since the obtained slope in the double log plot is equal to 2. TFSCLC can be described by Child's law [see Eq. (2.32)]. [57]

We fitted our the experimental data corresponding to temperatures where the *J(V)* exhibited slopes = 2, i.e., between 287 and 374 K, to Eq. (2.32), considering $\varepsilon = 3$, and calculated the mobility under trap free space charge limitation of current. Figure 5.5 shows the calculated mobilities.

We note that when TFSCLC is achieved, both the contact barrier and built in fields are negligible, and the obtained mobility depends only on the properties of the bulk. We obtained a space charge limited hole mobility of 3×10^{-5} cm^2/Vs at 304 K, which tended to a constant value of 4×10^{-5} cm^2/Vs for higher temperatures. This saturation is believed to be an artefact of thermal annealing, which de-dopes P3HT of oxygen and consequently reduces its conductivity (discussed in detail in chapter 8).

5.2.2 Trap limited SCLC

The intermediate region of the *J(V)* curves of Fig. 5.4 (region B) may be described as a trap filling regime. When the slope is greater than 2, as has been observed in this case, one may use the power law $J \sim V^m$, with $m > 2$, to determine the trap energy levels, the trap densities, the total trap density, the activation energy and the quasi-Fermi energies as has been described in Section 5.1.

The slopes, m, of the double logarithmic *J(V)* curves of Fig. 5.4 have been used to calculate the characteristic trap energy levels, E_t, in the band gap of P3HT. We re-plotted Fig. 5.4 and produced the straight lines to high voltages for all temperatures at which the log$J$-log$V$ slope is greater than 2.
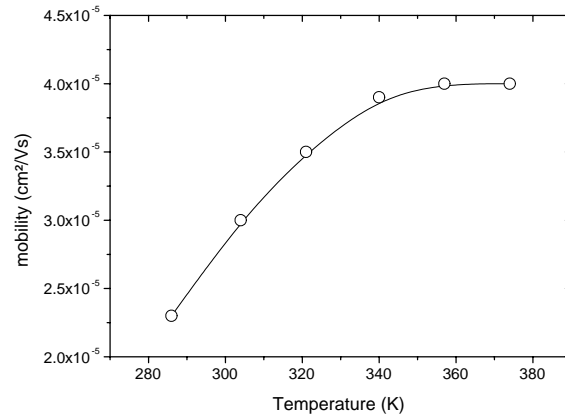
Figure 5.5: *Hole mobilities in an ITO/PEDOT:PSS/P3HT/Al device under forward bias, obtained from TFSCLC fits using Eq. (2.32) are represented as a function of temperature. Slope 2 was obtained only for temperatures between 287 and 374 K.*
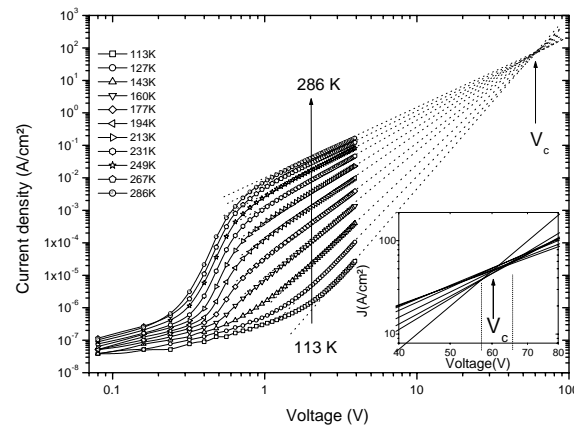
Figure 5.6: *The straight segments of the J(V) characteristics satisfying the power law* $J \sim V^m$, *with* m>2 *produced all meet at a critical voltage* V_c, *where current is independent of temperature. The slope,* m, *decreases with increasing temperature. The inset shows a blown up cross-over point indicating that it is actually a small range of voltages, the mid point of which has been considered as* V_c.
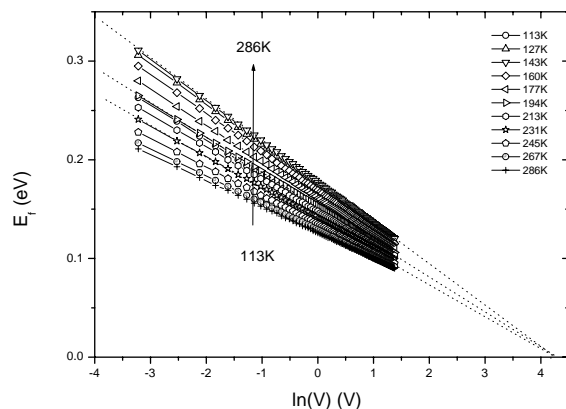
Figure 5.7: *At constant temperature the quasi Fermi energy varies linearly with the natural logarithm of applied voltage. When the quasi Fermi level coincides with the valence band edge, all the curves meet at a critical voltage* V$_c$, *at which all traps are filled, and conduction takes place through the valence band states thereafter. At* V$_c$, *current is independent of temperature*

It can be seen clearly in Fig. 5.6, that the lines meet at some common point, designated as V_c (see section 5.1). This is the critical voltage, at which current becomes independent of temperature.

The inset shows the blown up cross-over point(s) of plots of the straight-line-fit equations to curves of fig 7. We obtained that the cross-over actually takes place within a narrow range of voltages between 58 and 63.2 V, and used the mid point of $V_c = 60.6$ V for the estimation of traps. The spread stems from the fact that V_c is temperature specific (see section 5.1). Substituting it in Eq. (8.1), gives the total trap density to be within the range 2.81×10^{16} to 3.56×10^{16} cm^{-3}, considering the two extremes of *f(l)*. Kumar *et al* [119] estimated the whole term with *l* in Eq. (8.1) to be about 0.5 (within 4%). Nikitenko *et al* [120] found a fitting minimum deep trap density of 1.5×10^{16} cm^{-3} in their P3HT films when they considered a Gaussian distribution of states.

Extrapolation of the straight line fit to the calculated E_t vs T plot (not shown) yields the trap energy at absolute zero temperature. This energy corresponds to the activation energy and is equal to 0.054 eV. At $T > 0$ K, E_t represents activation energy at the temperature in question.

The number of traps at the characteristic energy that marks the width of the trap distribution decreases with increase in trap depth in such a way that the product $N(E_t) \times E_t = \text{constant} = (N_{total}/e)$, from Eq. (5.3). The trap density at the valence band edge at any temperature differs from $N(E_t)$ by a constant multiplier, e, therefore it also decreases with increase in temperature. This can be interpreted as the filling of traps close to the valence band. Raising the temperature fills up shallow energy traps close to the valence band. Therefore, E_t is pushed further into the band gap, but there are fewer traps situated at that energy level.

By substituting the obtained total trap density in Eq. (5.4), we determined the position of the quasi Fermi level as a function of temperature and of applied electric field. Figure 5.7 shows that the quasi Fermi level is linearly dependent on ln$V$, in conformity with theory (see Eq. (5.6)). In Fig. 5.7, the straight lines tend to converge at V_c. We note that this is the critical voltage at which the current

becomes independent of temperature, the Fermi level coincides with the valence band edge, and all traps are filled. Therefore, applying V_c provides sufficient energy equal to the amount of energy that must be supplied to the material in order to fill all the traps, so that any subsequent conduction of current takes place in the valence band. Beyond that critical voltage, current conduction should be trap free, independent of temperature. We note therefore, that both voltage and heat can contribute to the filling up of traps.

5.3 Conclusions

The exponential trap distribution model has been briefly described, and an expression for the calculation of the total trap density was deduced, clarifying the limiting values of a pre-factor that defines the validity of the model. The deduced expression yielded reasonable agreement with our experimental emphJ(V) data. The total deep hole trap density was estimated to be 5×10^{16} cm^{-3}, and the activation, energy at absolute zero temperature, was obtained to be 54 meV. A hole mobility of 3 x10^{-5} cm^2/Vs, at 304 K was also estimated under trap-free space charge conditions.

6 Current limitation in electrode/PCBM/electrode devices

We summarise our findings on the studies of bulk transport properties of PCBM, in which we analyzed temperature dependent current-voltage characteristics of PCBM thin films sandwiched between two electrodes. Two device configurations were studied: ITO/PCBM/Al, and ITO/PEDOT: PSS/PCBM/Al.

6.1 ITO/PCBM/Al devices

ITO/PCBM/Al devices are electron only devices conducting through LUMO of PCBM. The energetic level difference between PCBM HOMO ($\sim$-6.1 eV) and the electrode workfunctions is not expected to favour injection of holes into the PCBM from either electrode. The electrode workfunctions ($\varphi_{ITO}\sim$-4.7 eV, ($\varphi_{Al}\sim$-4.3 eV)) are both in the upper half of the HOMO-LUMO gap of PCBM, i.e., they are closer to the LUMO ($\sim$-3.7 eV). Current - Voltage *(I(V))* curves of an ITO/PCBM/Al device are shown in Fig. 6.1. Rectification behaviour is observed, with rectification factors around 10^2 at ± 1 V. This shows that the injection barriers are different, i.e., it is easier to inject electrons through Al than through PEDOT:PSS. The electrode workfunction difference is also expected to provide an opposing field to current flow when the electron injection is through ITO. It is clear that the conductivity of PCBM increases with temperature, conforming to semiconductor behaviour.

Figures 6.2(a) and (b) show double log J(V) curves the same ITO/PCBM/Al device under reverse and forward bias respectively. In Fig. 6.2(a) the slope = 1 region is observed where Ohm's law is valid. Here there is negligible charge injection from electrodes, and conduction is by thermally generated charge carriers. The curves become non-linear, passing through slope 2, and ultimately the slope is higher than 2 at high applied fields. The region where slope is higher than 2 can be described as a trap filling SCLC region (see chapter 5). The curves at lower temperatures have a higher slope in this region as compared to those at high temperatures. The curves tend to meet at some common point described as the critical voltage V_c, where the current becomes independent of temperature. We estimated the V_c to be equal to 2.214 V and calculated the trap density according to the procedure described in chapter 5. This yielded a total trap density of 1.30×10^{15} cm^{-3}. We note that this is an electron trap density, in contrast to the hole trap density that was calculated for P3HT devices. The electron trap density is maximum at the LUMO and decays exponentially into the HOMO-LUMO gap. Extrapolation of the characterisitc trap parameter to zero kelvin yields an activation energy of 0.015 eV for PCBM.

Under forward bias, although the SCLC region has been observed, the applied fields were not high enough to fill all the traps so that the mobility could be calculated using the TFSCLC model. However, of particular interest is the different V_c to which the extrapolated straight lines would converge in Fig. 6.2(b) as compared to (a). The same procedure yields a $V_c = 41.5$ V and a trap density equal to 2.43×10^{16}, while the activation energy is 0.037 eV. The physical significance of this difference is not clear, but we speculate that this might be due to the differences in the density of surface states created at the respective interfaces during device preparation. This suggests that the conduction of current in the PCBM may not actually take place at the same transport level when electron injection is by different electrodes. To further explore this point, we studied the charge
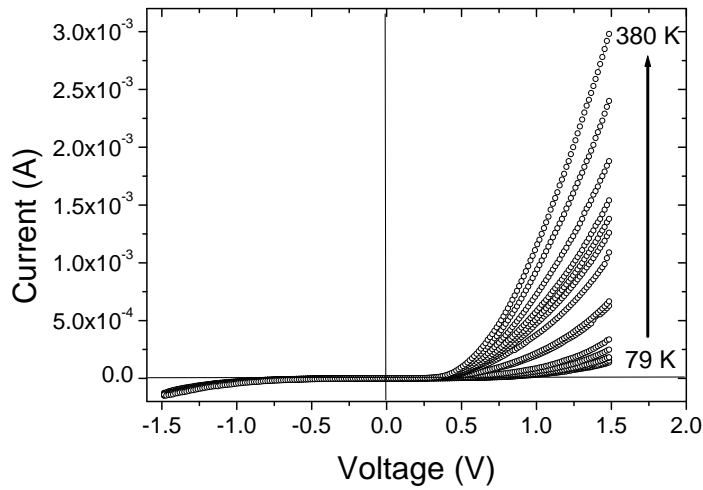
Figure 6.1: *Dark I(V) characteristics of ITO/PCBM/Al device for temperatures ranging from 79 to 380 K at ~20 K intervals, in linear scale.*
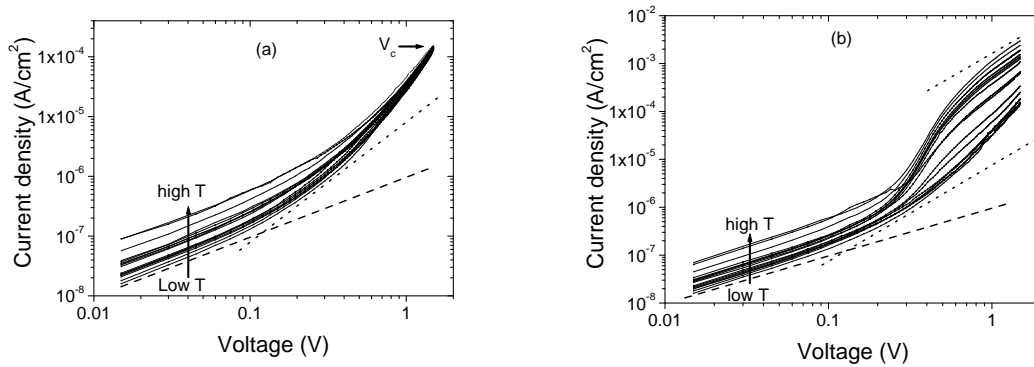
Figure 6.2: *Double-log J(V) plots for an ITO/PCBM/Al device at temperatures between 79 and 380K, under (a) reverse bias (+ on ITO) and (b) forward bias (+ on Al). Dashed lines have slope = 1, and dotted lines have slope=2.*
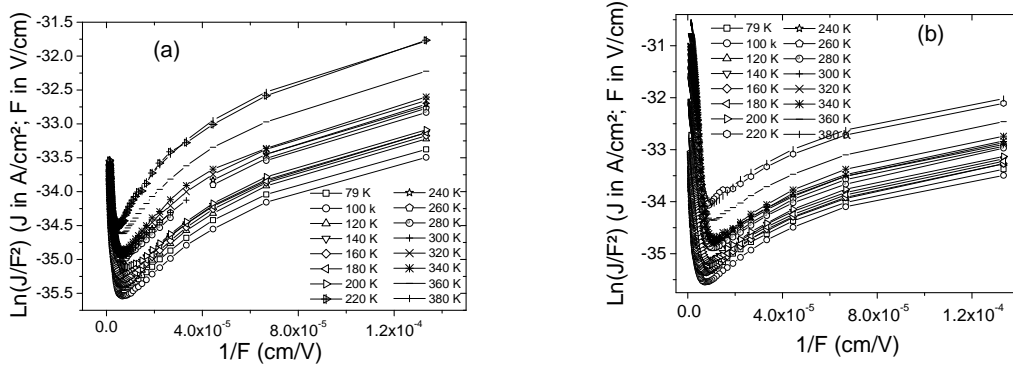
Figure 6.3: *FN curves of an ITO/PCBM/Al device at different temperatures (a) under reverse bias, and (b) under forward bias.*

injection mechanisms.

The Fowler-Nordheim tunneling curves for the same device are shown in Fig. 6.3(a) and (b), corresponding to electron injection using ITO and Al, respectively. The shape of the curves conforms to the theory presented in chapter 4. The straight lines at high fields are attributed to charge injection by tunneling through the barrier at the injecting inteface, while the curved parts of the curves correspond to the thermionic emission contribution to current. It is clear that both mechanisms contribute significantly to the current in both directions of flow. By employing the FN formulation (see section 2.3), we calculated the injection barriers at the respective interfaces for each temperature and obtained an ITO/PCBM electron injection barrier that varied from 1,2 eV at 79 K to 0.6 eV at 300 K, while for the Al/PCBM electron injection barrier we got 0.31 to 0.26 eV, respectively. We also calculated the electron affinity of PCBM from the FN formulation as proposed by Hummelgen et al. [101], in which only the workfunctions of the electrodes, φ, and the slopes of the straight parts, *s*, of the FN curves must be known. The electron affinity is then given by:

$$\chi = \frac{\varphi_2 s_1^{2/3} - \varphi_1 s_2^{2/3}}{s_1^{2/3} - s_2^{2/3}}, \tag{6.1}$$

where the subscripts 1 and 2 refer to ITO and Al, respectively. Such analysis yields a value of -3.9 eV for the LUMO of PCBM in our devices.

We may conclude that space charge limited behaviour in the presence of traps was observed. ITO is blocking for electron conduction into LUMO of PCBM, and Al is blocking the injection of holes into HOMO (reverse bias). Under forward bias (b), an easier injection direction is when Al injects electrons into LUMO of PCBM, which at high enough voltages leads to SCLC behaviour. The Al contact may be considered non-blocking only after a certain applied field has been surpassed, otherwise it is blocking. Injection of holes by ITO into HOMO of PCBM is considered negligible when we consider the rigid Schottky barrier between the two materials.

6.2 ITO/PEDOT:PSS/PCBM/Al devices

The additional layer of PEDOT:PSS enhances the asymmetry of the electrodes sandwiching the PCBM. Figure 6.4(a) shows the respective energy levels of the materials making up the studied
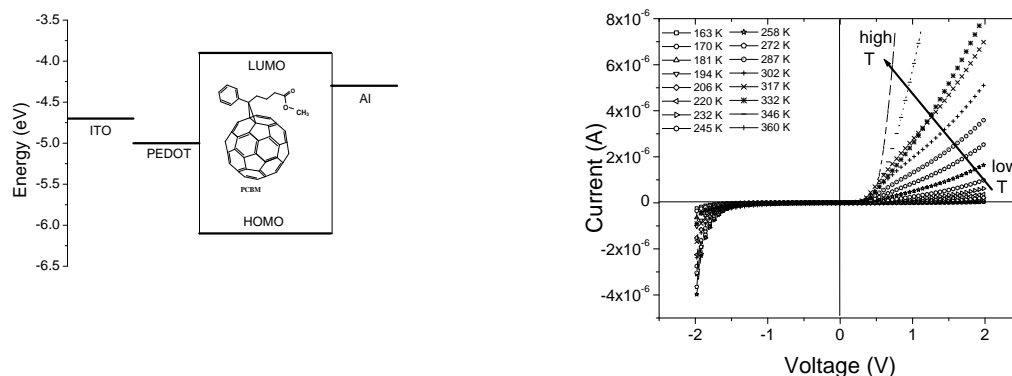
Figure 6.4: *Dark I(V) curves for an as-cast ITO/PEDOT:PSS/PCBM/Al device, at different temperatures.*

ITO/PEDOT:PSS/ PCBM/Al devices, and (b) shows the obtained *I(V)* characteristics in linear scale. Rectification factor is enhanced by 3 orders of magnitude to $\sim 10^5$ in comparison to $\sim 10^2$ obtained for ITO/PCBM/Al devices. The 'turn-on' voltage is clearly smaller for forward bias in comparison with reverse bias. This suggests the overcoming of a smaller charge injection barrier under forward bias. It is reasonable to imagine that the predominant charge injection is that of electrons into LUMO of PCBM through Al, rather than hole injection through PEDOT:PSS since the later is more than 1 eV energetic level difference from HOMO of PCBM. This assumption means that the device is electron dominated. Under reverse bias, the PEDOT:PSS is still more than 1 eV away from the LUMO of PCBM, but Al is even further away with almost 2 eV away from HOMO. We assume that hole injection will be negligible when compared to electron injection. If this is the case, the studied device becomes an electron-only device, in both directions of current flow.

Figure 6.5(a) shows the semi-log plot of J(V) characteristics of an ITO/PEDOT:PSS/PCBM/Al device under forward bias. Symbols show the experimental ponts, while continuous lines are the resulting J(V) curves from simulation using Child's law for TFSCLC (Eq. 2.32). The simulation matches the experimental curves at high applied voltages, showing that at those voltages both contact barriers and built in fields are no longer significant, and the current is trap-free-space-charge-limited. The fitting mobilities are presented in Figure 6.5(b). The mobilities are low, of the order 10^{-5} cm^2/Vs at room temperature, and the injection of electrons through the Al electrode overwhelms the transport properties. We may conclude that the current in this case is bulk transport limited, and that the contact between Al and PCBM may be ohmic. [57]

FN curves for hole injection through Al are shown in Fig. 6.6(a) and (b) for reverse and forward bias, respectively. It seems that there is some field which tends to reduce the current from the expected constant thermal contribution at constant temperature. The thermal contribution, in (a), disappears at a higher field the lower the temperature. The field at which it disappears could be correlated to the built-in field of these devices, and therefore to the open circuit voltage. The open circuit voltage in polymer solar cells increases with decrease in temperature (see chapter 7).

Figure 6.6(b) shows FN curves for hole injection through ITO/PEDOT. Straight line portions show compliance with the tunneling of charge carriers through a triangular barrier. We can conclude that tunneling is the dominant charge injection mechanism in this case. The reduction of the rate of increment at high fields is attributed to the discussed trap free space charge limited conduction. There is no more trap filling taking place above certain applied fields.
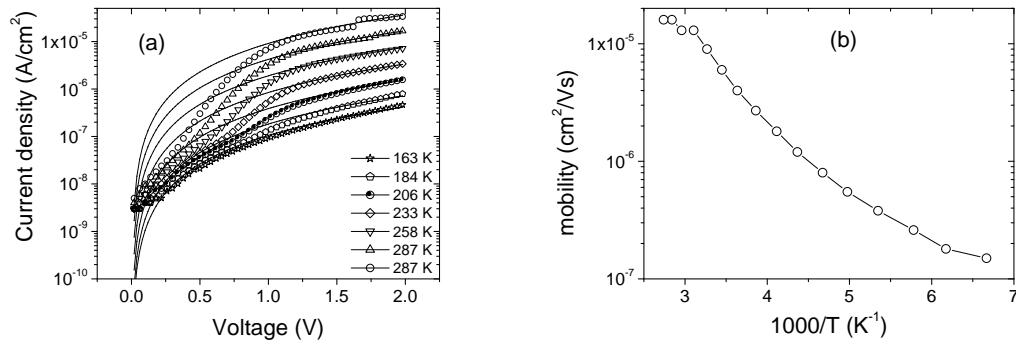
Figure 6.5: *(a) Experimental (symbols) dark J(V) curves and TFSCLC fits (lines) for a forward biased ITO/PEDOT:PSS/PCBM/Al device, at different temperatures. (b) Semi-log plot of the fitting electron mobility as a function of 1000/T.*
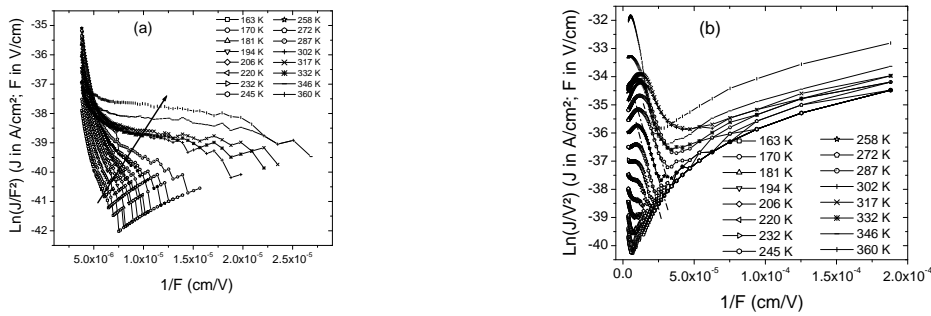
Figure 6.6: *FN curves for hole injection into an ITO/PEDOT/ PCBM/Al device (a) through Al, (b) through ITO/PEDOT at different temperatures.*

6.3 Conclusions

In this chapter we have shown that the Al/PCBM contact is ohmic for electron injection, but only after surpassing certain applied fields, otherwise it is blocking. We have shown that the J(V) curves can be described using the exponential trap distribution model. We have discussed that the introduction of the PEDOT:PSS layer leads to an enhancement of the rectification factor by 3 orders of magnitude. In the case of the ITO/PEDOT:PSS/PCBM/Al devices, TFSCLC model has been used to estimate the electron mobility, which is dependent on temperature. At room temperature this mobility is of the order 10^{-5} cm^2/Vs, comparable with the observed hole mobilities estimated in chapter 5.

7 Influence of thermal annealing on the electrical properties of P3HT based devices

The effects of thermal annealing on the bulk transport properties of poly(3-hexylthiophene) (P3HT) were studied by analyzing room temperature current-voltage characteristics of the polymer thin films sandwiched between ITO/PEDOT:PSS and aluminium electrodes, before and after an annealing step. It was observed that annealing takes place in two steps: (1) De-doping of the polymer of impurities such as oxygen, remnant solvent, water, etc, leading to a decrease in the conductivity of the film, and (2) thermally induced motion of the polymer chains leading to closer packing, and thus stronger inter-chain interaction, and consequently increase in conductivity. Annealing reduces the density of trapping states within the sample. We also observed that the ITO/PEDOT:PSS/P3HT hole injection barrier increases on annealing the ITO/PEDOT:PSS/ P3HT/Al thin film devices. Further we discuss the implications of these observations on the improvement of the ITO/PEDOT:PSS/ P3HT:PCBM/Al solar cells.

7.1 Introduction

It has been observed that the external quantum efficiency of solar cells employing P3HT as electron donor, and a fullerene derivative [6,6]-phenyl-C61 butyric acid methyl ester (PCBM) as acceptor, improves on annealing the solar cells. The temperature and annealing duration are important, as are the actual conditions and procedure of annealing. Padinger *et al.* [6] obtained the best increase in power conversion efficiency after annealing their P3HT:PCBM solar cells at 75 ^{o}C for 5 to 6 minutes. The energy conversion efficiency increased from 0.4 to 2.5%, i.e. over six times the value for as cast devices. They attributed the improvement of short circuit current density, J_{sc}, from 2.5 to 7.5 mA/cm^2, to increased charge carrier mobility in the blend presumed to be due to enhanced crystallization of the polymer during the annealing process. The increases in open circuit voltage and fill factor were attributed to the burning of shunts. Parker [55] reported that heat treatment improves the quantum efficiency of the polymer film because of a change of morphology at the polymer electrode interface. Change of bulk morphology has also been considered responsible for observed improvement in performance of polymer-fullerene devices.

Both PCBM [121] and regioregular P3HT [122] are known to crystallize in thin films under respective appropriate conditions. The significant improvement of performance, stability and lifetime of P3HT based devices after an annealing step at temperatures between 60 ^{o}C and 120 ^{o}C has been attributed to crystallization of PCBM, of P3HT, or both; contact quality improvement; interdiffusion improving donor-acceptor orbital overlap; film drying by evaporation of moisture and remnant solvent; oxygen de-doping of the polymer; phase separation of donor and acceptor materials; densification/ reordering of the polymer film, etc. [123] , [124] , [118] , [6].

However, it is still unclear whether the assumed re-ordering of the P3HT would really lead to crystallization, and hence an improvement in hole mobility, considering the different annealing conditions reported by various authors. In this respect it is not clear why the output characteristics improve on annealing the device, whether crystallization of P3HT is good for the solar cell or not, what role is played by PCBM, and by the electrodes. It is therefore necessary to understand the influences that
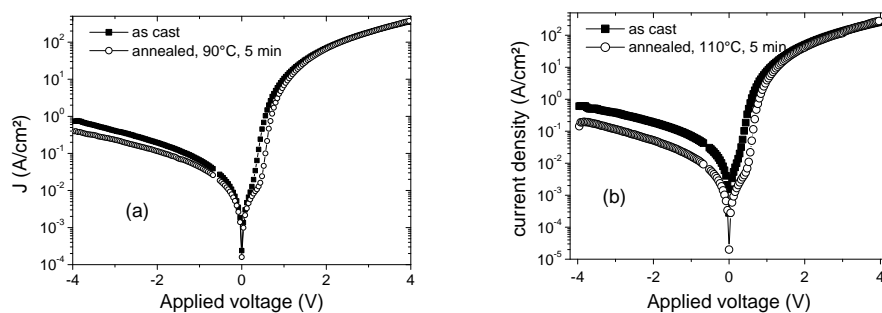
Figure 7.1: J(V) *curves of ITO/PEDOT:PSS/ P3HT/Al devices in semi-logarithmic scale before and after annealing at (a) 90°C for 5 min, and (b) 110 °C for 5 minutes.. Current is lower for the annealed device, indicating lower conductivity. The onset of the exponential region is shifted to the right, i.e. to higher voltage.*

lead to the observed improvements in order to prescribe an optimization procedure based on thermal annealing. In order to shed light on the role played by P3HT in the blend device, and hence by elimination, possible role of PCBM, we undertook the study of ITO/PEDOT:PSS/ P3HT/Al devices, where preparation was the same as that for ITO/PEDOT:PSS/ P3HT:PCBM/Al heterojunction solar cells, except that the active layer comprised of P3HT alone, without PCBM.

7.2 Results and Discussion

The electrical conductivity of P3HT is expected to increase accompanied with increased crystallinity and coplanarity of main chains after heat treatment. The increase of coplanarity of thiophene rings on a main chain brings the enhancement of effective conjugation length and of intra-chain carrier mobility. Thus, the mobility of charge carrier and the conductivity are expected to increase after the heat treatment. However, reduced conductivities have been observed after heat treatment [125].

7.2.1 Low temperature annealing

Figure 7.1 shows typical dark current density - voltage [*J(V)*] characteristics of as-cast ITO/PEDOT:PSS/ P3HT/Al hole only devices in semi-logarithmic scale, at 290K.

High rectification factors of $\sim 5 \times 10^5$ were observed at 4V. The current density for devices annealed at 90°C and 110°C are lower than those for their respective as-cast counterparts. We explain the reduction in current after the annealing step as resulting from de-doping the polymer of impurities such as oxygen, water and remnant solvent. This de-doping is more severe in the 110°C annealed device as compared to the 90°C case, hence the latter exhibits much lower currents.

During production and solution preparation of P3HT oxygen is absorbed from the environment. Therefore, despite inert ambient-based device fabrication and electrical characterization, significant concentrations of oxygen are expected to be embedded in the films. This oxygen dopant serves to improve the conductivity of the P3HT through the production of localised states within the π-π^* gap. [118] Annealing at temperatures below 110 °C for 5 minutes frees the polymer of trapped impurities (e.g. remnant solvent, water, and oxygen), but the annealing temperature and duration are below some threshold value of supplied energy, so the polymer chains may remain in their as-
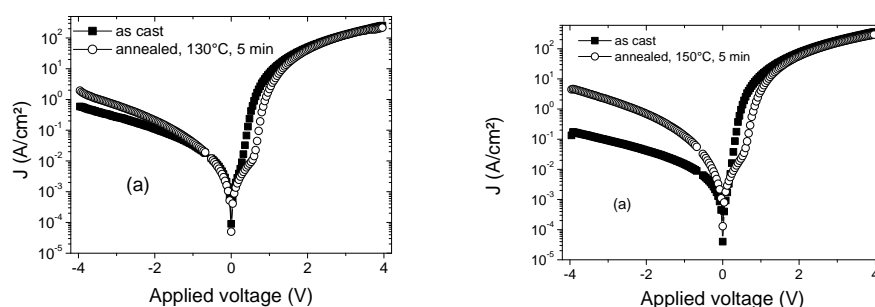
Figure 7.2: J(V) *curves of ITO/PEDOT:PSS/ P3HT/Al devices in semi-logarithmic scale before and after annealing at (a) 130 °C for 5 minutes, and (b) 150 °C for 5 min. Current is 2 orders of magnitude higher for the 150 °C annealed device, indicating higher conductivity. The onset of the exponential region is shifted to the right.*

cast positions. Oxygen de-doping leads to a decrease in conductivity. We conclude that reduction of free volume and consequent increase inter-chain interaction are therefore negligible under these annealing conditions.

Mattis *et al.* [118] showed, through Rutherford backscattering spectrometry, that indeed oxygen is one of the substances given off when P3HT thin film devices are heated, and that the amount of oxygen given off increases with annealing temperature. For devices annealed at temperatures higher than 100 ^{o}C, they could not detect any remaining traces of oxygen in their samples. Nakazono *et al.* [125] also suggested that the density of charge carriers induced by the structural defects and by the oxygen or moisture may decrease upon heat treatment, leading to reduction in conductivity. Traps are a particular problem in fabricating n-channel semiconductor devices, for example, because oxygen itself is reduced easily enough to act as an electron trap when devices are operated in air [126]. Oxygen captures the electrons and retains them thereby making available a higher number of holes in the HOMO of P3HT to contribute to the current. The observed reduction in conductivity may therefore be interpreted as the reduction in electron trapping centers, and hence reduction of trap induced hole density.

7.2.2 High temperature annealing

Devices annealed for 5 minutes at 130 ^{o}C and those annealed at 150 ^{o}C (see Fig. 7.2) showed higher, reverse, and low voltage forward, current densities as compared to their as-cast counterparts.

Higher increases were for devices annealed at 150 ^{o}C. We attribute this to film reordering, possibly leading to crystallization of the P3HT. Charge transport through conjugated polymer films requires intimate electrical contact between the polymer segments. The high spin coating and solvent evaporation speeds tend to dry the polymer chains under tension of the centrifugal and friction forces. Film ordering in as-cast films is poor since spin coating tends to leave the polymer chains lying in the plane of the film [127], so that there is rarely a single polymer chain bridging the electrodes in an electrode/polymer film/electrode sandwich device. Thermally annealing a polymer film above its glass transition temperature, T_g, allows the freely flowing chains in the polymer melt to untangle into lower energy conformations, and an enhanced crystallization of the polymer may take place [122].

The glass transition temperature of P3HT is around 12 ^{o}C [122] and its melting temperature is

69

220 ^oC [128]. The crystal of P3HT is formed by aligned chains which are stacked on top of each other, with the thiophene ring forming a planar alternating 'up-down' conformation and the alkyl side chains pointing perpendicularly to the stacking direction [122]. The presumed straightening of the polymer strands upon annealing would lead to better chain packing and thus an increase in the degree of inter-chain interactions in annealed films relative to as-cast films, so charge may be conducted along as well as across chains. Thus, along with the enhanced crystallization, the hole conductivity of the P3HT increases dramatically [129]. The high mobility in regioregular PH3T is attributed to the formation of extended polaron states as a result of self-organization in the films [130].

When the P3HT is saturated with injected charge the space charge conductivity decreases slightly (see Figs 7.1 and 7.2). This is because the amount of charge that this material is now able to accommodate when traps are all filled, is now smaller, therefore the amount of charge available for "unlimited" conduction is also smaller. Annealing at 150 ^oC increases the conductivity at low fields. After impurity dedoping, the polymer chains also have enough energy to move and "wiggle" into low energy conformations, thereby reordering and possibly increasing crystallinity. The chains then pack closer together, and "dangling bonds" may rejoin, increasing chain length, thereby further reducing the trap density. We attribute shallow traps to the impurity states while deep traps should be due to unperturbed polymer chain length. Impurities possibly disappear on annealing.

Very high temperatures induce conformational changes within the P3HT and may degrade device performance. The protruding alkyl chains cause torsioning along the backbone of the molecule. The torsioning of the P3HT chain decreases the conjugation length, therefore increasing the bandgap, and drastically reducing the conductivity of the film. The physical change is irreversible, permanently harming the electrical characteristics of the device. Further, the differences in the expansion coefficients of the polymer and the inorganic materials constituting the device may lead to buckling which takes place in order to relieve tensile stress, resulting in a wavy metal surface. Annealing at such high temperatures may lengthen the lifetime but reduce the efficiency. [131]

7.2.3 Annealing the same device several times

Annealing the same device several times (Fig. 7.3) shows clearly that annealing is a two stage process leading first to a decrease in conductivity, which subsequently increases. Fig 7.4(a) shows current density vs anneal count for the reverse-bias data of Fig. 7.3.

The current decreases and reaches a minimum, then it increases, surpassing the as-cast measured current. Both impurity dedoping and film ordering effects may take place simultaneously all the time, but one effect is more effective than the other. The minimum indicates the situation when the effect of impurity dedoping is overtaken by that of thermally induced polymer chain reorganization. In the following subsections we discuss the forward bias curves of devices before and after annealing them.

Figure 7.4(b) shows forward bias *J(V)* curves of the devices, annealed several times, in a double logarithmic representation, corresponding to hole injection through the ITO/PEDOT:PSS electrode.

At low voltages, the slopes of the *J(V)* curves in log-log plot, of Fig. 7.4(b), are about 1 for both the as-cast and annealed device (region A), and increase gradually to higher than 2 (region B), leveling off to 2 at high voltages (region C). For the as-cast device the transition from low slope is gradual, suggesting the filling of traps of continuous distribution in energy. The filling of traps starts at lower voltages for the as cast device, in comparison to the annealed device, suggesting that the as cast device has shallow traps. It would appear that most of such shallow traps have disappeared in the
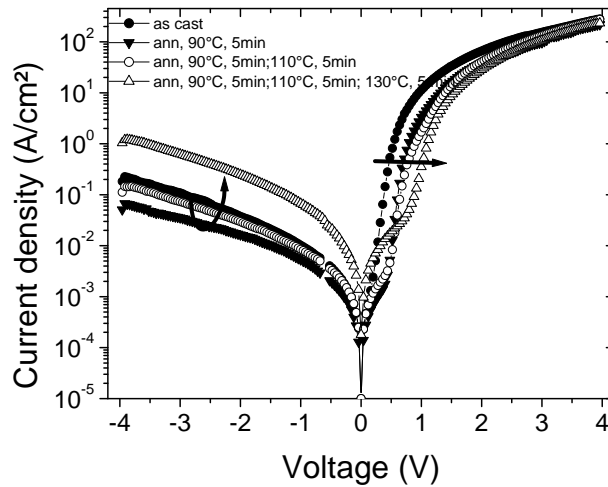
Figure 7.3: J(V) *curves of ITO/PEDOT:PSS/ P3HT/Al device in semi-logarithmic scale before and after annealing the same device several times as indicated in the legend. Under reverse, and low voltage forward, bias, J first decreases then increases with each further annealing step, as indicated by the curved arrow. The straight arrow indicates a shift of the onset of the exponential region of the curves to high voltages, with each further annealing step. The current is lower at high forward bias voltages.*
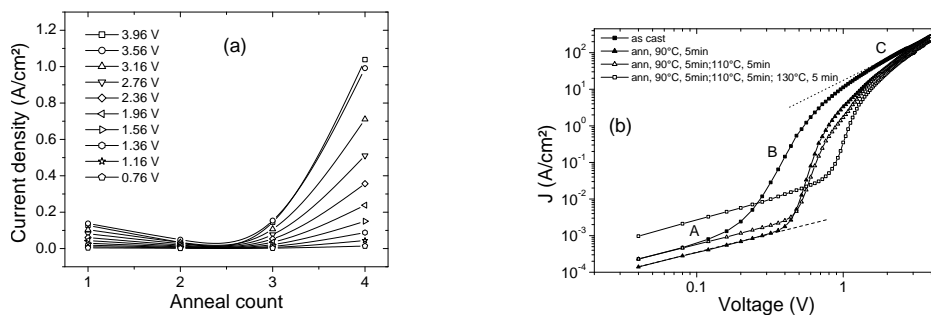
Figure 7.4: *(a) Current density of an ITO/PEDOT:PSS/ P3HT/Al device before, and after each annealing step (extracted from the data of Fig.3) at different reverse voltages. The current density first decreases, then increases indicating that the final result is due to a 2-stage process. (b) Dark double-log* J(V) *characteristics of an ITO/PEDOT:PSS/ P3HT/Al device under forward bias, before and after each annealing step. Regions A have slope = 1 (dashed line), corresponding to ohmic conduction, regions B have slopes greater than 2, corresponding to charge injection, and region C to SCLC.*

case of the annealed device, since trap filling now starts at a much higher voltage with each further annealing step. This confirms that the density of shallow traps decreases on annealing, and that the observed increase in current after annealing several times is due to another effect, not related to those traps. The transition from ohmic to SCLC is nearly abrupt, giving rise to an almost vertical section in the double *J(V)* characteristics, indicating that the traps are more defined in energy. Vertical *J(V)* curves means that traps are situated in a discrete energy level within the π-π* gap.

7.2.4 Barrier modification

Annealing modifies the ITO/PEDOT:PSS/P3HT hole injection barrier. Such modification may be understood through the employment of Fowler-Nordheim (FN) theory (see chapters 2 and 4), which predicts that if charge injection from the electrodes is governed by quantum mechanical tunneling through a triangular interface barrier, then a plot of $\ln(J/F^2)$ vs $1/F$ yields a straight line whose slope is directly proportional to $\phi^{3/2}$, where ϕ the potential barrier at that interface. [50] Here $F=V/d$ is the applied electric field, *V* is applied voltage and d is the thickness of the device. Additionally, it was shown that the total current in a device may be modeled by the sum of the current due to charges that are injected through tunneling (FN mechanism) and that due to charges injected thermionically over the barrier (Richardson-Schottky mechanism), where for a constant temperature, the thermionic contribution may be considered constant. Such consideration yields a minimum in the FN plots delimiting the transition from thermionic to tunneling dominated injection as the field is increased. [132] The thermionic effect is dominant at high temperatures and low fields, while the tunneling effect is dominant at low temperatures and high fields.

Figure 7.5 shows the FN curves for the data of Fig. 7.2 of ∼70 nm thick devices. The curves consist of straight line portions at high fields (tunneling), and curved portions at low fields (thermionic emission). At very high fields, the curves deviate from straight lines because there is so much injected charge, which overwhelms the transport capabilities of the polymer, and hence builds up space charge which resists further charge injection. The slopes of the straight parts are clearly larger for the annealed device, than for the as-cast device. The slopes of the FN curves increase each time on further annealing, therefore ITO/PEDOT:PSS/P3HT hole injection barrier increases. The barrier increases for all studied annealing temperatures from 90 to 150 ^{o}C. On the other hand it is clear that the magnitude of the thermionic contribution is higher for the as-cast device, than when the device is annealed at 90 ^{o}C, supporting the suggestion that the number of thermally generated charge carriers available for conduction is higher in that device, because the impurities in the bulk of the as cast P3HT film immobilize electrons. This also supports the idea that such traps are shallow and can be filled thermally even at 290 K. The number of free holes is therefore high for as cast devices.

At high forward voltages above 2 V, as-cast and annealed *J(V)* curves coincide. One would expect therefore to get the same space charge limited characteristics. Although the intrinsically generated hole density increases on annealing the devices at high temperatures, it is equally negligible at high voltages, and space charge limits the current in much the same way as in as-cast devices. However, for the most interesting region for opto-electronic devices like LEDs and solar cells, most of the shallow traps have disappeared on annealing.

It is important to note that the impurity dedoping process and thermally induced chain re-ordering may take place at the same time in P3HT based devices at the studied temperatures. This is because the glass transition temperature of P3HT is about 12 ^{o}C, and limited film ordering should start to take place around this temperature. However it is not the dominant effect at low temperatures and for the employed duration of annealing. At high temperatures evaporation of remnant solvent, water vapour,
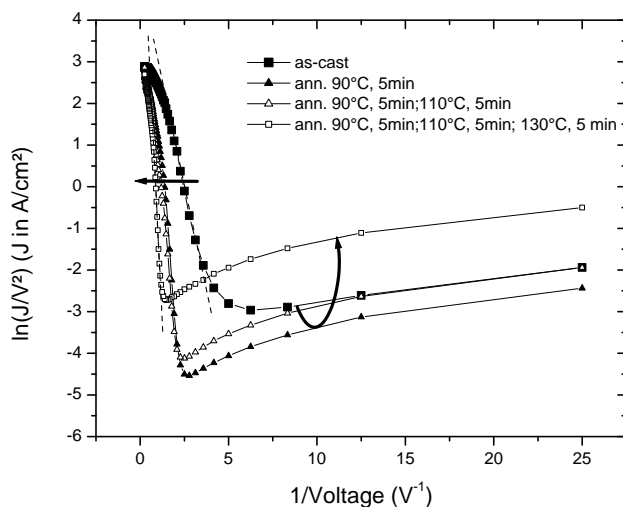
Figure 7.5: *Fowler-Nordheim plots for hole injection into an ITO/PEDOT:PSS/ P3HT/Al device through the ITO/PEDOT:PSS electrode, before and after each annealing step. The slope of the straight line region (dashed lines) increases after annealing, indicating a corresponding increase in the hole injection barrier. The curved parts of the FN plots indicate the current contribution of thermionically injected holes. This current, related to thermally generated charge carriers, decreases after the first annealing step, then increases subsequently on further annealing.*

and oxygen dedoping should quickly take place and the polymer chains receive more thermal energy, allowing them some significant reordering.

Increase of potential barrier, implies some difficulty in hole injection into HOMO of P3HT at low voltages. But because of impurity dedoping, some traps have been emptied, and polaronic states which participated in conduction are not there anymore. There is need to supply higher energy to fill up the traps, i.e., to increase the charge density in the bulk. Therefore the detrapped impurities were shallow. Being shallow, they could be filled thermally even at a temperature of 290 K. As they disappear, the density of thermally generated charge carriers is reduced. Therefore the reverse, and low voltage forward, bias currents are smaller for the annealed device. The observed abrupt increase in forward current for annealed devices indicates the filling of deep traps distributed in a narrow energy band, suggestive of deep traps related to chain length. But the material can hold only a fixed maximum amount of charge, with or without traps so although trap filling is slow for the as-cast device, when all traps are filled, we expect the same TFSCLC for both cases. We can therefore conclude that the charge carrier density, or the capacity for injection at low voltages has been affected, and not the mobility.

7.3 Conclusions

In conclusion, thermal annealing of P3HT films occurs in two stages, the first of which is impurity de-doping leading to a reduction of conductivity, and the second which involves thermal motion

of polymer chains resulting in reordering, and possibly crystallization, leading to an increase in conductivity.

8 P3HT:PCBM bulk heterojunction devices in the dark and under illumination

We report the development of a bulk heterojunction polymer/fullerene solar cell based on regioregular P3HT, as an electron donor, and a soluble fullerene derivative PCBM, as an electron acceptor. ITO/PEDOT:PSS/P3HT:PCBM/Al devices were studied in the dark and under illumination. We discuss some experimentally observed factors influencing the performance of illuminated devices, and suggest some optimum values for improved performance. We also discuss the role of the PEDOT:PSS layer in the generation of open circuit voltage in these devices.

8.1 Dark *I(V)* curves

The ITO/PEDOT:PSS/P3HT:PCBM/Al device is a double carrier device injecting holes through the ITO/PEDOT:PSS electrode into HOMO P3HT, and electrons through Al into LUMO PCBM. An active layer consisting of a mixture of P3HT/PCBM at a 1:1 mass ratio dissolved in chloroform at 5mg/ml was spin coated (speed 1000 rpm) on top of a dry PEDOT:PSS film to give a thin film of about 100 nm. Al contacts were deposited on the active layer by thermal evaporation in a high vacuum (thickness $\sim$ 100 nm). Typical dark current-voltage *I(V)* curves of an ITO/PEDOT:PSS/P3HT:PCBM/Al device are presented in Fig. 8.1. This device exhibits diode like behaviour, and rectification factors as high as 7×10^{-5} were observed at +/- 2.94 V.

8.1.1 Charge injection in the dark

To determine the charge injection mechanisms in these devices we analysed the *J(V)* data using the Fowler-Nordheim tunneling theory and the Richardson-Schottky thermionic emission theory as described in chapters 2 and 4. Figure 8.2 shows FN curves of the device under reverse bias (a), corresponding to electron injection through the ITO/PEDOT:PSS electrode, and to hole injection through the Al electrode.

According the FN theory, the $\ln(J/V^2)$ vs 1/V curves should give straight lines if charge injection is by tunneling through the interfacial barrier. The part of the curves in Fig.8.2 with negative slope is attributed to tunneling, while the positive slope indicates the field independent thermionic emission contribution to the current. For temperatures above, and including, 303 K, the curves conform to the proposed sum of the two contributions to current (see chapter 4). Below 303 K, the curves have negative slope, with the curves tending to curve upwards, and at some inflexion points the curves curve downwards, until they reach some minimum. The curves have been truncated at the points when the current changes from negative to positive, even when negative bias is still applied. The observation of positive currents when negative bias is applied indicates that there must be some additional field in the device which tends to suppress the thermionic emission contribution. When the applied field is high, this internal field is insignificant, and the tunneling contribution may be easily observed, however, at low applied fields, this field becomes important, and at some stage even becomes greater than the applied field, thereby changing the direction of flow of the current. The internal field stops all thermionically generated charges until a certain field overcomes it. The
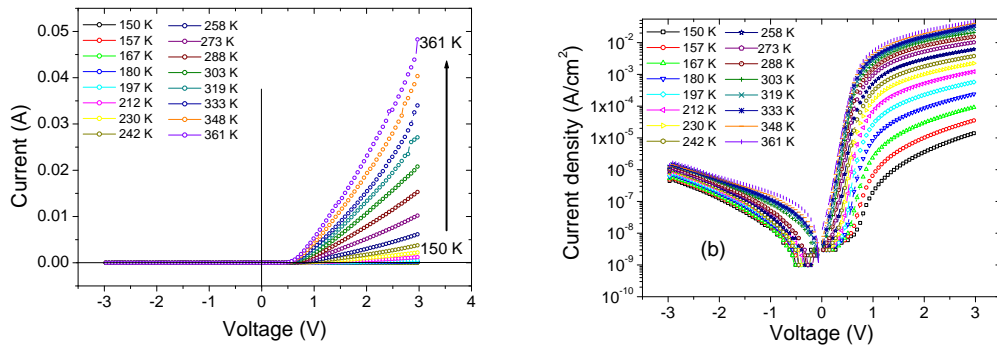
Figure 8.1: *(a) Dark I(V) and (b) dark J(V) characteristics of an ITO/PEDOT:PSS/P3HT: PCBM/Al solar cell at temperatures ranging from 150 to 361 K at ∼ 15 K steps in linear and semi-log scale, respectively. Rectification factors as high 7×10^{-5} were observed at +/- 2.94 V, at 300 K.*
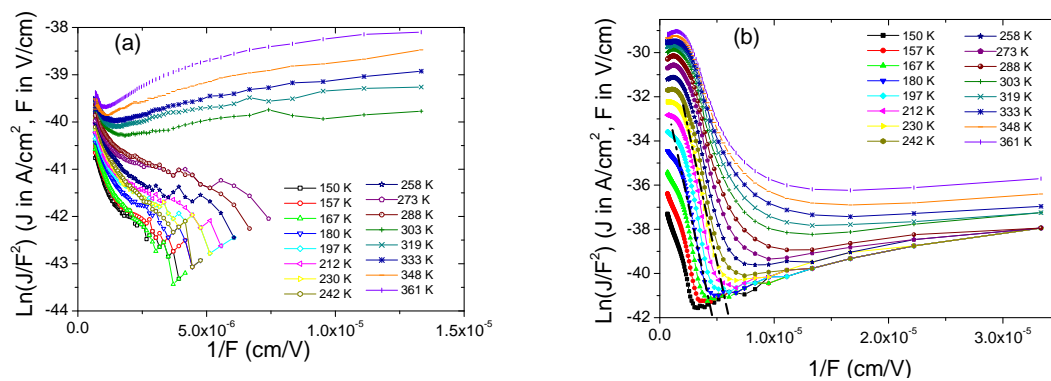
Figure 8.2: *FN curves of an ITO/PEDOT: PSS/P3HT: PCBM/Al solar cell (a) under reverse bias, and (b) under forward bias at different temperatures.*

magnitude of such a field may be visualised at the turning point in the FN curves. According to Fig. 8.2, the minimum in the curves occurs at high fields (to the left) at low temperatures, and at lower fields(to the right) as temperature increases. The locus of the minima indicates the lowest measurable current, of 1 nA, in our experimental setup. We suggest that the observed minima occur at the built in voltage of the device and is related to the open circuit voltage of the device. In this case the open circuit voltage will be expected to be high at low temperatures, and to decrease as the temperature is increased. This has been observed for illuminated devices (see section 7.1.4.). As temperature increases, the density of thermally generated charge carriers increases, and may generate a potential difference in the same way that light does.

Figure 8.2(b) shows forward bias FN curves for the same device described above, corresponding to hole injection through ITO/PEDOT and electron injection through Al. The shape of the FN curves conforms to the proposed sum of thermionic and tunneling contributions. The thermionic emission contribution increases with temperature. Straight segments of the curves observed at high fields are attributed to the tunneling of charge carriers into the device. In this case, it is difficult to say if the tunneling charges are electrons, or holes, but by comparing the tunneling fields needed to for electrons to tunnel into LUMO of PCBM, and those fields needed for holes to tunnel into PEDOT and HOMO of P3HT, we suggest that the charge injection should predominantly be holes. There is a very small variation of the thermionic emission current contribution with increase in temperature. Since the thermionic emission contribution is quasi constant in the low temperature range, the field at which tunneling takes over decreases with increase in temperature. This is because in accordance with inequality (4.7), the number of thermally generated carriers is negligible as compared to the injected charges. This means that to overwhelm the 'same' number of thermally generated carriers, a smaller applied electric field is needed the higher the temperature, in conformity with the proposed theory. This is different from the ITO/P3HT/Al devices of chapter 4, where changes in temperature led to significant changes in the number of thermally generated free charge carriers. In that case larger fields are needed to overwhelm the increased thermally generated charge carrier density. We suggest that although the same temperature ranges are considered in both cases, in the composite device discussed here, the additional thermally generated charge carriers are trapped by PCBM, becoming unavailable for conduction.

At still higher applied electrical fields, the FN curves tend to level off from the straight lines, indicating a reduced conductivity, as compared to the straight line region. We suggest that this is the region when all possible traps have been filled through tunneling, and space charge accumulates at the close to the injecting electrodes.

Figures 8.3 show the Richardson-Schottky (RS) thermionic emission curves of the ITO/PEDOT:PSS/ P3HT:PCBM/Al device whose I(V) curves have been presesnted in Fig. 8.1. Figure 8.3(a) corresponds to electron injection into HOMO of P3HT and hole injection into PCBM. We suggest that the characteristics are determined by holes. In the RS plots, straight lines indicate charge injection by thermionic emission. Such a description fits only at high temperatures (indicated by broken lines), suggesting high interface barrier inder reverse bias. Deviations from straight lines are due to the contribution of tunnelling. Figure 8.3(b) corresponds to electron injection into LUMO of PCBM through Al, and hole injection into HOMO of P3HT through ITO/PEDOT:PSS. The RS plots are straight lines in the whole range of the temperatures considered, indicating that the barriers to charge injection are small.
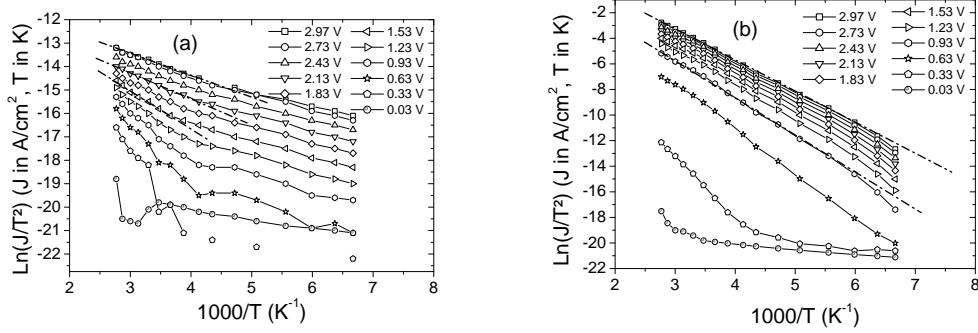
Figure 8.3: *RS thermionic emission curves for (a) reverse biased, and (b) forward biased ITO/PEDOT: PSS/ P3HT:PCBM/Al solar cell under darkness and different bias voltages. The broken lines are guides for the eye showing regions where the curves can be approximated to straight lines.*
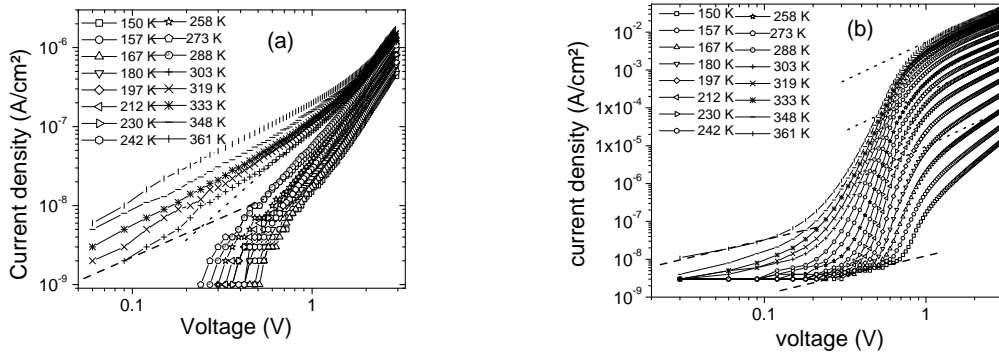
Figure 8.4: *Double logarithmic plots for dark* J(V) *characteristics of an ITO/PEDOT: PSS/ P3HT: PCBM/Al device at different temperatures. (a) under reverse bias, and (b) under forward bias.*

8.1.2 Charge transport in the dark

We replotted the *I(V)* curves of Fig. 8.1 in double logarithmic representation in Figs. 8.4(a) and (b). Slope =1 in this representation indicates compliance with Ohm's law, while slope 2 indicates trap free space charge conduction. Slopes greater than 2 indicate the filling of traps, which can be of different levels and distributions.

Under forward bias (Fig. 8.4b), continuous lines indicate slope = 1, and dotted lines indicate slope = 2. The rest of the curves have slopes greater than 2 indicating the trap filling regime, which also corresponds to charge injection into the bulk. Charge injection into the device is by tunneling, and the bulk is able to use up all injected charge in the conduction of current, until such a point when the bulk becomes saturated, and injected charge starts to accumulate near the injecting electrode. When all possible traps are filled, the slope becomes 2 in conformity with Child's law (Eq. (2.32)).

In the P3HT:PCBM blend, the total current is composed of both electrons and holes. One can then talk of an effective mobility of charge carriers [46]. We have simulated the J(V) data of Fig.

8.4 (b) using Child's law considering that the dielectric permittivity is 3.9 and device thickness = 90 nm. The simulated curves (lines) together with measured data (symbols), are presented in Fig. 8.5 (a). The only variable in this case was considered to be the effective mobility. The fitting mobilities are plotted in a $\log(\mu)$ vs 1000/T plot in Fig. 8.5 (b). The obtained straight line can be attributted to thermal activation of the effective mobility under TFSCLC.
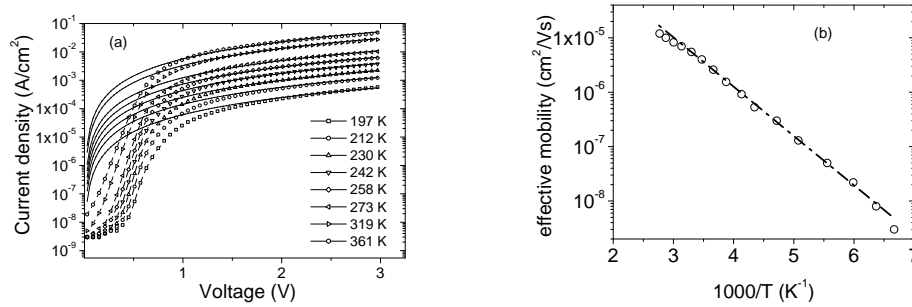
Figure 8.5: *(a) Semi logarithmic plots for dark* J(V) *characteristics of an ITO/PEDOT: PSS/ P3HT: PCBM/Al device at different temperatures (symbols). Solid lines represent the TFSCLC fit using Child's law. (b) The fitting effective mobility vs 1000/T.*

8.2 J(V) under illumination

8.2.1 Illuminated *J(V)* at room temperature

Typical current density-voltage characteristic curves of an ITO/PEDOT:PSS/P3HT:PCBM/Al solar cell have been plotted in a semi-logarithmic representation in Fig. 8.6 at different light intensities from 0.1mW/cm^2 to 100mW/cm^2 at T=300 K.

The dark *J(V)* characteristic curve (not shown) demonstrates typical diode-like behaviour. Under illumination, the rectification ratio decreases from 400 at 0.1 mW/cm^2 to 7 at 100 mW/cm^2 at $\pm$ 1.2 V. This is a common feature of polymer based solar cells, but the underlying reasons remain unclear.
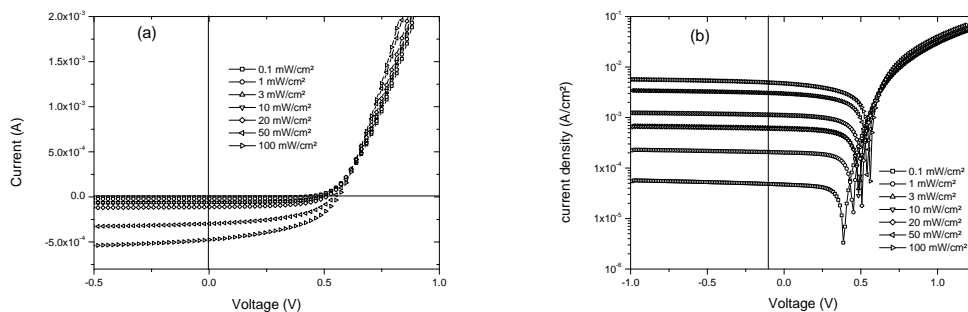
Figure 8.6: *(a) I(V) characteristic curves of an ITO/PEDOT: PSS/ P3HT:PCBM/ Al solar cell plotted in linear scale, and (b) J(V) curves in semi-log scale.*
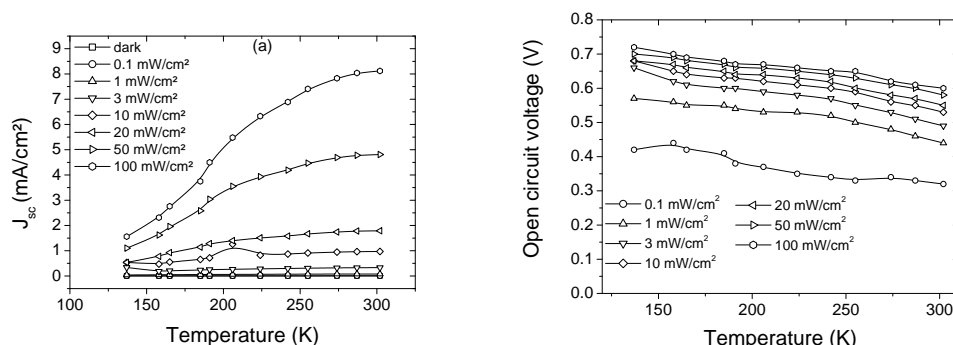
Figure 8.7: *Output characteristics of an ITO/PEDOT:PSS/ P3HT:PCBM/Al solar cell: (a) Short circuit current density, J_{sc}, vs temperature at different incident light intensities, (b) Open circuit voltage vs temperature, for various white light illumination intensities.*

We suggest that this is due to photoconductivity, where light increases the number of charge carriers participating in the conduction of current.

8.2.2 Temperature dependent *J(V)* curves

Typical output characteristics like power conversion efficiency, η, open-circuit voltage, V_{oc}, short-circuit current density, J_{sc}, and fill factor, FF, of an ITO/PEDOT:PSS/P3HT:PCBM/Al solar cell in the temperature range 137 to 302 K, at 100 mW/cm^2 white light illumination are shown in Table 8.1, and in Fig. 8.7.

Temp (K)	J_{sc} (mA/cm^2)	V_{oc} (V)	FF (%)	eff (%)
137	1.56	0.72	18.27	0.21
158	2.31	0.70	19.39	0.31
165	2.76	0.69	20.07	0.38
185	3.75	0.68	21.54	0.55
191	4.50	0.67	22.98	0.69
206	5.48	0.67	28.38	0.92
224	6.33	0.66	32.24	1.19
242	7.41	0.65	35.95	1.73
255	7.83	0.62	41.76	2.03
274	8.04	0.61	45.38	2.23
302	8.12	0.60	49.81	2.43

Table 8.1: Typical output parameters of an ITO/PEDOT:PSS/ P3HT:PCBM/Al solar cell in the temperature range 137 to 302 K, at 100 mW/cm^2 white light illumination.

We observed an increase of the short circuit current density with temperature as shown in Fig. 8.7(a). This can be understood by considering that the current output of a solar cell is proportional to the number of generated charge carriers and to their mobility. At low temperatures few charge carriers are thermally generated and are not easily transported, therefore the current, without illumination, is low. As the temperature increases, charge carrier mobility and therefore conductivity,
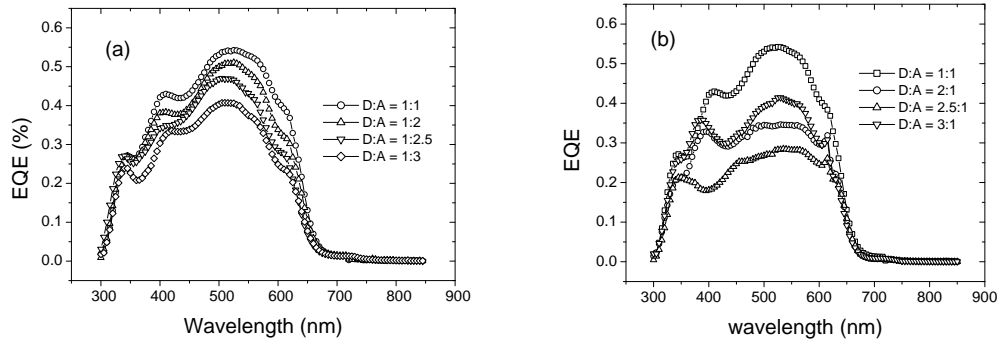
Figure 8.8: *EQE spectrum for illuminated ITO/PEDOT: PSS/ P3HT:PCBM/ Al solar cells of different donor-acceptor (D:A) weight ratio compositions. (a) The EQE decreases with increase in PCBM content for D/A mass ratio <1, and (b) EQE decreases with increase in P3HT content for D/A mass ratio >1.*

should also increase.

The open circuit voltage, on the other hand, decreases almost linearly with increase in temperature. Extrapolation of a straight line fit for the voltage vs temperature curve at 100 mW/cm^2 white light illumination yielded a possible maximum of 0.75 V for this device. The origin of the open circuit voltage is discussed in a later section.

8.3 Improvement of efficiency of P3HT-PCBM solar cells

The power conversion efficiency, η, of solar cells is calculated using the formula:

$$\eta = \frac{J_{sc}Voc}{P_{light}}FF, \tag{8.1}$$

where J_{sc} is the short circuit current density, V_{oc} is the open circuit voltage, and *FF* is the fill factor (see chapter 2). Areas in which there is room for improvement are perhaps best identified by returning to the steps involved in the generation of the photovoltaic effect: exciton creation, exciton diffusion, Donor-acceptor electron transfer, carrier transport to electrodes, and electron transfer at electrodes.To improve the performance of solar cells it is therefore necessary to explore ways in which to increase these 3 factors, and we discuss our experimental observations on how these may be optimised.

8.3.1 Influence of active layer composition on the output characeristics of P3HT:PCBM solar cells

Solar cells of different donor-acceptor mass ratio were prepared within the same batch. External Quantum Efficiency (EQE) and light intensity dependent *J(V)* measurements were done at room temperature before, and after annealing the cells on the same hot plate, for 2 minutes at 120 °C. Typical EQE measurements obtained after the annealing are presented in fig. 8.8, where the ratios are by weight.

A 1:1 D:A weight ratio gives the cell with the highest external quantum efficiency, in agreement with Chirvase *et al.* [133]. A deviation from this ratio reduces the efficiency of the solar cells. Figure
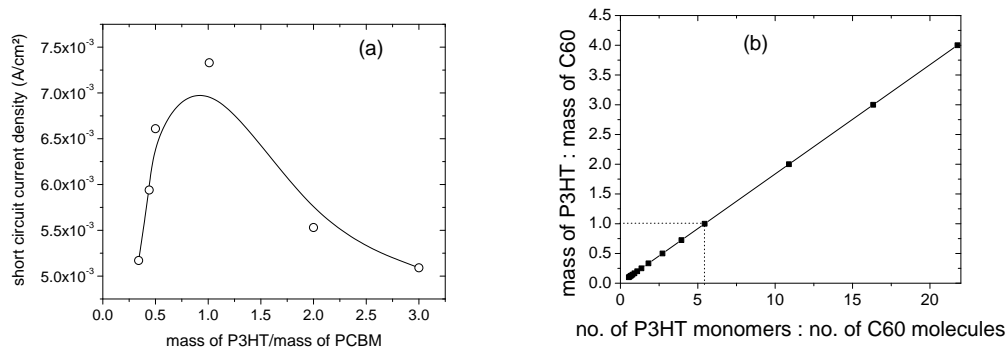
Figure 8.9: *(a) Graph showing the dependence of the short circuit current(estimated from EQE spectra) on the D/A mass ratio. (b) The relationship between weight ratio and molecular number ratio in a P3HT:PCBM composite film. The dotted lines indicate the optimum solar cell composition corresponding to 1:1 by mass, which is equivalent to about 6 P3HT monomer units for each PCBM molecule.*

8.9(a) shows the dependence of the short circuit current density calculated from EQE (see chapter 2) on the donor:acceptor weight ratio for cells prepared in the same batch.

In order to analyse the significance of the above finding, we performed a simple calculation to determine the number of P3HT monomer units corresponding to each PCBM molecule within the composite layers.

Molecular weight of single monomer units of P3HT and of PCBM molecules have been calculated using the formula:

$$m = \frac{M_w}{N_A},\qquad(8.2)$$

where M_w is molar mass, N_A is Avogadro's number = 6.02257×10^{23}. By considering the molecular weight of each single C, H, and S that constitute one monomer unit of P3HT, we obtain that the molecular weight of P3HT monomer = 167.2951 g / mol, therefore, using Eq. (8.2), mass of one monomer unit of P3HT $= 2.778 \times 10^{-22}$ g. Similarly, molecular weight of PCBM = 910.9019 g / mol, hence, mass of one molecule of PCBM $= 1.512 \times 10^{-21}$ g. The molecular mass ratio is therefore m(P3HT) / m(PCBM) = 0.184, or m(PCBM) / m(P3HT) = 5.445. The ratio m(P3HT)/m(PCBM) is also equal to the number ratio of molecules, n(P3HT)/n(PCBM).

The mass composition of the active layer may be calculated using Eq. (8.3):

$$M(PCBM) = \frac{m(PCBM)}{m(P3HT)} M(P3HT).\qquad(8.3)$$

where m = mass of a single molecule, or monomer unit, and M = mass of a specimen. By fixing the mass of P3HT for example, one can calculate the corresponding mass for PCBM, as required. An example of such a calculation yielded the results that have been plotted in Fig. 8.9(b).

It appears that the obtained optimum D:A weight ratio of about 1:1 corresponds to a molecular ratio of one PCBM molecule to about six monomers of polythiophene. Such an outcome is logical when we consider the fact that the electron affinity of C_{60} is equivalent to 6 electrons and assume that one photon breaks only one double-bond, and at any one given time a P3HT monomer can have

only one bond broken. The characterization of C_{60} as an electron acceptor capable of accepting as many as six electrons [91] candidates it as the acceptor in blends with conjugated polymers as good photoexcited electron donors. When the number of P3HT monomers for each PCBM molecule, increases to more than 6, the P3HT monomers will shield each other from the PCBM, and thus the number of ultrafast electron transfers is reduced. On the other hand, too much PCBM becomes redundant in the solar cell, and the efficiency will be reduced. If clusters of PCBM are larger than the exciton diffusion lengths, for example, recombination of the generated electron-hole pairs may occur before the exciton reaches the exciton splitting interface.

8.3.2 Effects of film composition on morphology, and *J(V)* characteristics

The morphology of the active layer plays a critical role in determining the performance of polymer fullerene solar cells. We observed that thermally annealing the fabricated solar cells increased their efficiency and improved their stability in the atmosphere. EQE and light dependent *J(V)* measurements were done before and after thermally annealing P3HT:PCBM solar cells of different donor acceptor ratios. The same solar cells described above were investigated. Figures 8.10 (a) to (d) show the EQE curves before and after annealing for the 1:1, 1:2, 1:2.5 and 1:3 D:A ratios respectively. The inset to each figure is the ratio of the current output after annealing to that before. An interesting peculiarity is that the improvement in EQE by annealing seems to follow the D:A ratio, e.g., a 1:1 cell impoved its efficiency by just slightly above 1, a 1:2 cell by about 2, and 1:3 D:A cell improved its efficiency by about 3 times. The 1:1 cell has the least percentage change in J_{sc}, suggesting minimal changes in the morphology. The 1:3 cell has the largest percentage change, suggesting large variations in film morphology.

This result tends to confirm the notion that the 1:6 D:A ratio by molecular numbers is the optimum, so if the weight ratio is 1:1, the improvement observed on thermal annealing may be due to a homogeneous re-distribution of the mixture. In higher weight ratio cells, it was observed that thermal annealing leads to the formation of clusters identified as PCBM, in a sea of 1:6 P3HT:PCBM blend, by number. AFM surface profiles for 1:1, 1:2, and 1:3 blends are shown in Fig. 8.11. We confirm that these clusters are indeed PCBM crystals because the AFM pictures of the same solar cells being discussed here, had large clusters for the 1:3 weight ratio cells, decreasing commensurate with decrease in weight ratio, as observed also by [133]. For the 1:1 weight ratio cells, only very small crystals of PCBM were observed. The aggregated PCBM islands in a sea of 1:1 composition are dead parts of the cell since the innermost molecules will not be available for charge transfer. They are therefore shielded and this reduces the efficiency of charge separation, as observed in the decreased power conversion efficiences of the polymer-fullerene solar cells with high PCBM content. Further, every pure PCBM cluster takes up space and therefore reduces the active area available for intercepting the incident radiation. The crystals protrude out of the plave of the film, and this may have adverse effects on the properties of the interface of the film with the Al top contact.

We also studied the effects of film composition *J(V)* characteristics. Figure 8.12 shows the the illuminated *I(V)* characterisitics of cells made from blends of different donor-acceptor weight ratios. The slope of the *J(V)* curve when it crosses the voltage axis indicates the magnitude of the series resistance, while the slope as the *J(V)* curve crosses the current density axis indicates the magnitude of the parallel resistance. The series resistance is smallest, and the parallel resistance biggest, for a 1:1 mass ratio. The fill factor is therefore largest for that same ratio. V_{oc} is independent of P3HT:PCBM mass ratio, but J_{sc} increases with decrease in the D:A weight ratio. The series resistances become larger with increase of the PCBM content, and the parallel resistances become smaller, thereby re-
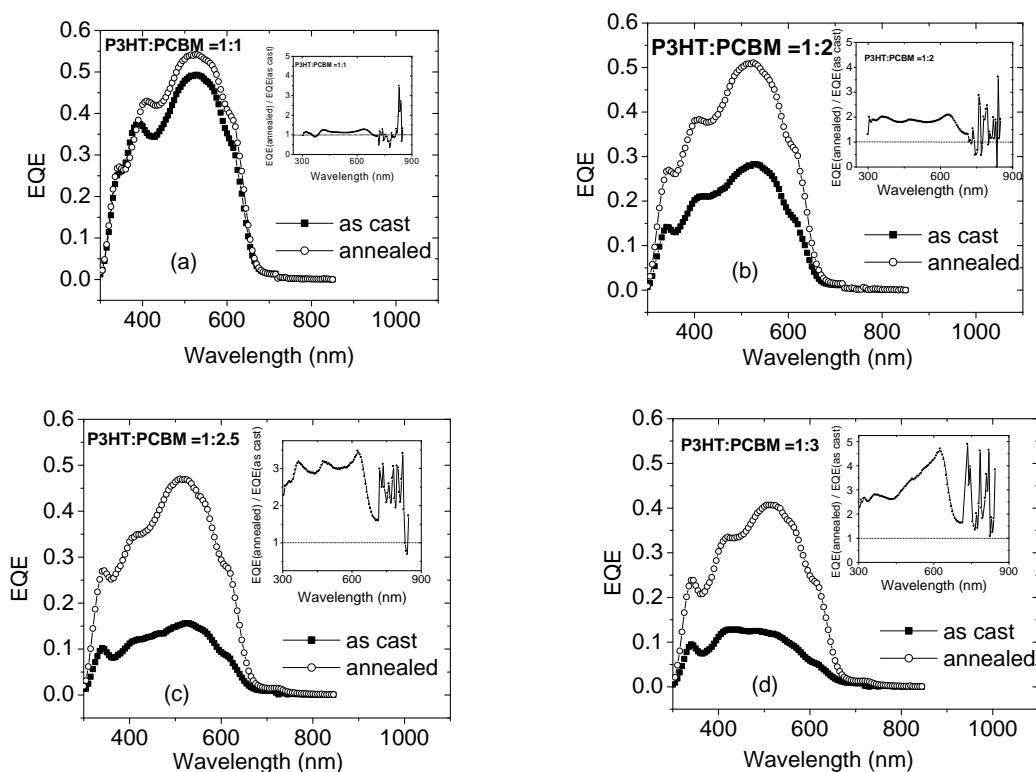
Figure 8.10: *EQE before and after annealing:-comparison of percentage increases in J$_{sc}$ for different donor:acceptor weight ratios. The inset shows the fraction of the change observed in the spectrum after annealing, in each case. This scales up with the increase of acceptor.*

ducing the fill factors.

Figure 8.13 shows the dark curves of solar cells of different active layer compositions. The dark *J(V)* curves of annealed cells indicate that the conductivity of films containing a smaller amount of PCBM is higher as compared to those with large concentrations of PCBM, at high voltages above 0.65V. This range has been described as the trap filled SCLC range.

Forward bias dark *J(V)* curves in double logarithmic scale showing the ohmic, exponential trap filling, and the trap-free space charge limited current regimes. When all possible states are conducting (TF-SCLC), the conductivity decreases monotonously with increase in PCBM concentration. The 1:1 cell has small changes in efficiency, while largest changes in efficiency have been recorded for the 1:3 cell, though the efficiency still remains the lowest for this cell.

8.3.3 Implications of barrier modification due to annealing

We observed ib chapter 6 that the barrier is modified by thermal annealing, and we discuss the implication on the output characteristics of ITO/PEDOT:PSS/ P3HT/PCBM/Al solar cells. The active layer consisted of a 1:3 P3HT:PCBM mass ratio in a 10 mg/ml chloroform solution. We measured external quantum efficiencies (EQE) of the cells at 290K before determining their *J(V)* characteristics. The cells were then annealed at 120 ^{o}C for 2 minutes in a glove box with nitrogen atmosphere, and EQE, and *J(V)* determined at 290 K again. In Fig. 8.14 we present the EQE curves of an as-cast
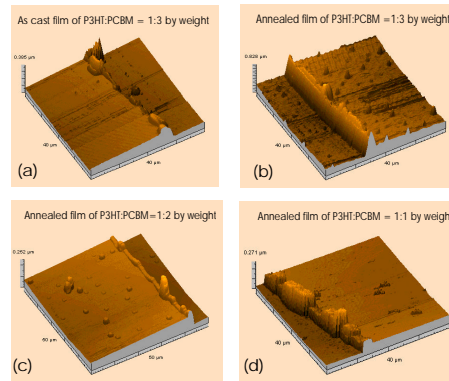
Figure 8.11: *Surface pictures of films of P3HT:PCBM blends of different weight ratios: (a) as cast (1:3); (b) annealed (1:3); (c) annealed (1:2); and (d) annealed (1:1), taken by a Burleigh Vista atomic force microscope (AFM). The structures observed in annealed films are attributed to crystallisation of PCBM. The annealing temperature was 120 °C for 2 minutes under inert atmosphere.*

and subsequently annealed ITO/PEDOT:PSS/ P3HT:PCBM/Al solar cell.

The area under the EQE curves gives the short circuit current density. The EQE increased dramatically on annealing these devices, at 120 °C for 2 minutes, resulting in a short circuit current density increase from 1.84 to 5.17 mA/cm^2 at 100 mW/cm^2 white light illumination. Figure 8.15(a) shows the dark *J(V)* characteristics before and after annealing the solar cells.

The current decreased by more than 1 order of magnitude under reverse bias, and under forward bias before the onset of the exponential region. Such a decrease is in conformity with the observed effects for the P3HT devices annealed at 90 °C, and those annealed at 110 °C (see Fig. 7.1). However, at high forward voltages, the annealed device exhibits a much higher current, also by close to 1 order. The reduction in reverse bias current and the increase in forward bias current result in increased rectification factors from 1.1 to 401.1 (400 times!), at 1 V. The biggest increase in the forward current is just after the exponential region, suggesting that at some high voltage, the two curves may actually merge as in the P3HT devices (see Figs. 7.1, 7.2 and 7.3). Polymer ordering temperatures may not have been reached by annealing the devices at 120 °C for 2 min.

FN plots of the dark *J(V)* characteristics indicate straight lines at high voltages suggesting the tunneling of holes into the HOMO of P3HT under forward bias. These plots indicate a larger slope for the annealed device, than for the as-cast device, similar to the observed for P3HT devices. The hole injection barrier (ITO/PEDOT: PSS/P3HT) therefore increases after annealing the solar cell. The observed annealing effects may therefore be triggered by barrier modification and impurity de-doping. Current decreases! Therefore the observed increase in external quantum efficiency, and hence short circuit current density cannot be explained by mobility increase in the blend. If it increases at all, then that increase is not the dominant effect.
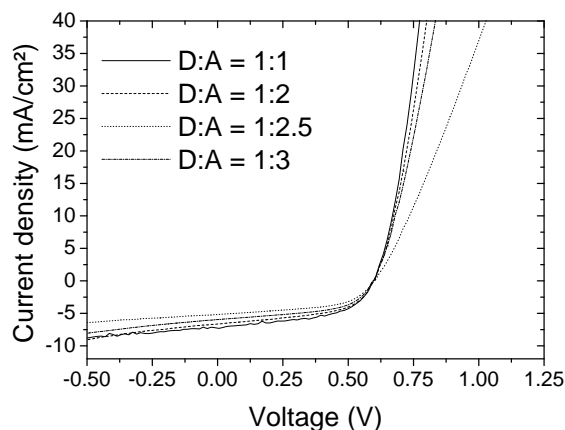
Figure 8.12: *Comparison of the illuminated* J(V) *characteristics of ITO/PEDOT: PSS/ P3HT:PCBM/Al cells made from blends of different Donor-Acceptor weight ratios.*
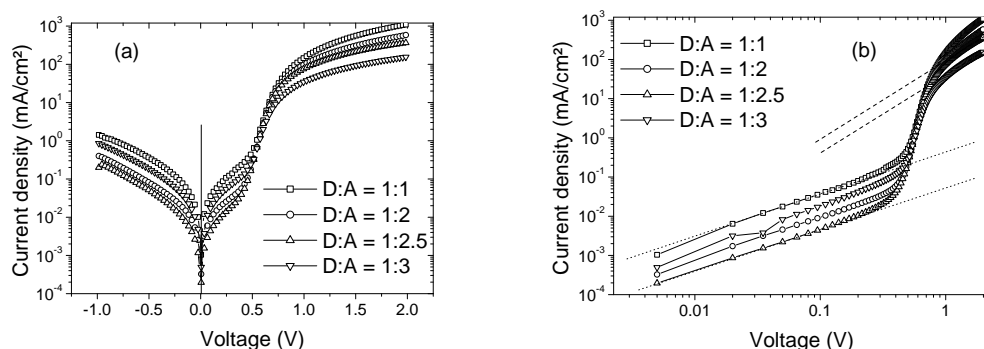
Figure 8.13: *Dark* J(V) *characteristics of ITO/PEDOT: PSS/ P3HT:PCBM/Al solar cells with active layer compositions of different D:A mass ratios in (a) semi-log and (b) double log plots (Dotted lines have slope = 1 and dashed lines have slope = 2).*

Figure 8.15(b) shows the corresponding 100 mW/cm^2 illuminated cell *J(V)* characteristics in semi-logarithmic representation. The open circuit voltage, V$_{oc}$, and the short circuit current J$_{sc}$ of the annealed device are higher in for the annealed solar cell. Table 8.2 shows a comparative summary of the output characteristics of the ITO/PEDOT:PSS/ P3HT:PCBM/Al solar cell before and after annealing.

We note that the increase of the ITO/PEDOT:PSS/P3HT hole injection barrier implies an increase in an internal electric field which favours the motion of holes from P3HT HOMO to PEDOT:PSS, and ultimately to ITO. The increase in such a field implies more effective blocking of electrons and an efficient collection of holes by ITO through PEDOT:PSS at zero bias. The *V$_{oc}$* increases after thermal annealing (Figs. 8.15(b) and 8.16). Charge injection becomes more difficult, but collection improves.
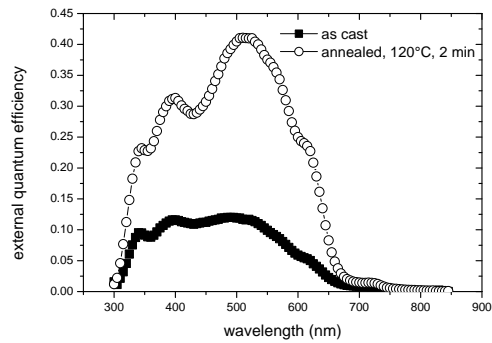
Figure 8.14: *Dramatic increase in EQE of a 1:3 weight ratio ITO/ PEDOT:PSS/ P3HT:PCBM/Al solar cell after annealing for 2 min at 120°C. The area under the curve gives the short circuit current density, and it increased by 3.2 times, from 1.6 mA/cm^2 to 5.17 mA/cm^2 for an AM1.5 solar spectrum.*

Device	J_{sc} (mA/cm^2)	V_{oc} (V)	FF (%)	eff (%)
As cast	1.835	0.485	28.864	0.255
Annealed	5.170	0.605	53.338	1.669
% increase	181.9	24.7	86	554.5

Table 8.2: Comparative summary of the output characteristics of the ITO/PEDOT:PSS/P3HT: PCBM/Al solar cell before, and after annealing.
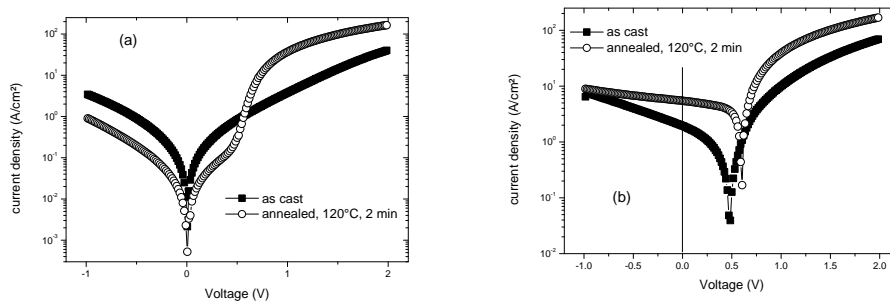
Figure 8.15: *Semi-logarithmic representation of* J(V) *curves of ITO/PEDOT: PSS/ P3HT/ PCBM/Al solar cell before and after annealing at 120°C for 2 minutes: (a) under darkness, and (b) under 100 mW/cm^2 white-light-illumination. J$_{sc}$ and V$_{oc}$ both increase after annealing.*

8.3.4 Implications of impurity dedoping

It is not expected that electrons trapped by the O_2 can participate in the current, instead they are immobilized, giving the polymer a chance to remain with a high number of holes for conduction. These holes can not recombine with the trapped electrons. Once trapping centers are reduced, the number of recombinations in the polymer increases, thereby reducing the hole density. PCBM may not trap such low energy electrons, hence it is not expected that they could be transferred to PCBM, it captures only excited electrons that have reached the LUMO of P3HT. Therefore dedoping the polymer of oxygen, water and remnant solvent do not increase the mobility of charge carriers, it merely reduces the density of holes participating in the current, which therefore decreases.

Impurity dedoping has good implications for conductivity when the ITO/PEDOT:PSS/P3HT:PCBM/Al solar cell is illuminated. Ultra-fast photo-induced electron transfer from P3HT to PCBM occurs with an efficiency close to 100%. [7] Both the holes and the electrons participate in the current. The overall effect is that the number of electron transfers to the PCBM increases, since fewer of the electrons are captured and immobilized as in the case of abundant oxygen presence. It is therefore to be expected that the current should be higher in the illuminated annealed device. The failure to reach 100% electron transfer efficiency may be related to the remaining impurity materials that may compete with PCBM, but immobilize the captured electrons. The number of electrons conducted through the PCBM LUMO has increased, and may balance the number being conducted through P3HT LUMO. The number of scattering centers is also reduced, and overall conductivity increases. We suggest that the major contributor to this increase is the increase in charge carrier density participating in the current, rather than mobility since for the dark $J(V)$, the current decreased anyway, even if the number of scattering centers had also decreased. Figure 8.16 shows $J(V)$ curves of illuminated ITO/PEDOT: PSS/P3HT/Al device of Fig. 7.1(b) before and after annealing at 110 ^{o}C for 5 minutes.

Note that the illuminated current is lower for annealed device. This is because there is no additional charge transfer taking place, and that although the number of holes increased due to photo-excitation, it has not reached the same level as when impurities simply immobilized the electrons.

Further, thermally induced inter-diffusion may increase the overlap of wave functions between P3HT and PCBM making charge transfer easier. During the annealing, a rush of colour is observed after about 20 s which we attribute to the motion of PCBM molecules as they rush to occupy the sites left by impurities like oxygen and H_2O. Possible crystallization of PCBM may also create easier percolation paths for electrons towards the Al electrode.

High temperature annealing induces stronger inter-chain interactions, which promotes bi-polaronic recombination of charge carriers. Although strong inter-chain interactions increase the mobility of holes in the polymer, it has a negative effect on quantum efficiency. Padinger et al [6] observed that annealing P3HT:PCBM solar cells at 75 ^{o}C increased the quantum efficiency to some maximum within 5 to 6 minutes, but longer annealing durations at the same temperature reduced the overall efficiency 'dramatically' again. This suggests that strong inter-chain interactions may not be as important as the dedoping the polymer of oxygen and evaporation of remnant solvent and water. Strong inter-chain interactions also reduce the rectification ratio.

We have shown that the annealing temperatures and duration, at which high improvement in external quantum efficiency in P3HT:PCBM bulk heterojunction solar cells is achieved, are within the range when the polymer is dedoped of oxygen, we therefore suggest that increase in mobility due to reordering of P3HT is not the dominant effect in this case. When O_2 leaves the film, the number of immobilized electrons is reduced, therefore there is an increased number of electrons participating in the generation of current. Additionally the conglomeration of PCBM conduces to the appropri-
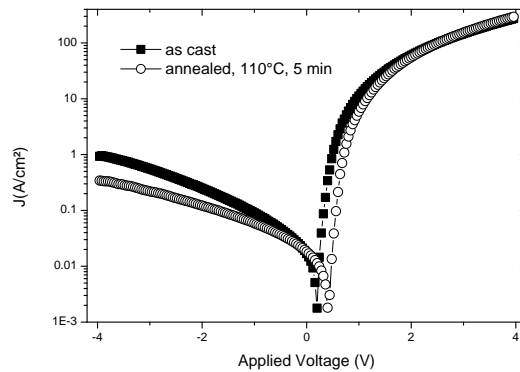
Figure 8.16: *J(V) semi-logarithmic representation of 100 mW/cm^2 white-light-illuminated ITO/ PE-DOT: PSS/ P3HT/Al device before and after annealing at 110° C for 5 minutes. The current under both reverse and forward bias, is lower after annealing. V$_{oc}$ increases after annealing.*

ate ratio optimum for electron transfer. The increase in quantum efficiency of the ITO/PEDOT: PSS/P3HT:PCBM/Al after an annealing step is therefore explained.

8.4 Origin and limit of open circuit voltage

The built-in potential of solar cells, which can be estimated from the open circuit voltage V_{oc}, is an essential parameter of thin film photovoltaic devices, influencing charge dissociation and charge collection and thus mirroring the diode principle as well as the photophysical properties of the materials. Therefore, the question of the built-in potential is directly related to an extensively discussed phenomenon, the origin of the open circuit voltage V_{oc}. For the design of future solar cells it is important to understand whether the V_{oc} of bulk heterojunction devices can be determined by the choice of the electrodes and whether the V_{oc} is a bulk property, or an electrode property, or a combination of both.

It has been demonstrated that for a photodiode, based on a single layer of a conjugated polymer, the V_{oc} scales with the work function difference between electrodes, and thus follows the metal-insulator-metal (MIM) model. [134] In bilayer devices made by electron- and hole-accepting polymers, the V_{oc} also scales linearly with the work function difference, however, with an additional contribution depending on the light intensity. [135] This contribution is due to the accumulation of charge carriers at the organic/organic interface, giving rise to a diffusion current which must be compensated by a drift current at open circuit.

We have investigated the current limiting mechanisms in single, double and blend layer devices sandwiched between various electrodes in order to get an insight into the role of each material in photovoltaic generation in the polymer-fullerene solar cell. Illuminated *J(V)* characteristics of selected devices are presented in Appendix 2. The objective was to respond to the controversial question of the origin of open circuit voltage in illuminated polymer-fullerene devices.

8.4.1 The Role of the PEDOT:PSS layer in the generation of V_{oc}

Bulk-heterojunction devices show unusually high open circuit voltage values. These values cannot be explained by the metal-insulator-metal (MIM)model that has been often used for organic light emitting diodes. The origin of open circuit voltage in polymer-fullerene bulk heterojunctions has become a controversial subject since Brabec *et al.* [136] discussed that their observed V_{oc} was more than what the electrode work function difference could give, and therefore suggested that the maximum open cicuit voltage was given by the energetic difference between the LUMO of acceptor and HOMO of donor. Since then there has been a lot of studies to try and substantiate this notion. To date it seems to be the most accepted among the scientists working on polymer-fullerene heterojunction solar cells. In this section, we explore the development of this understanding and suggest that the role of PEDOT:PSS, as the charge separating interface, in the cell must also be taken into account.

1. • Brabec *et al.* [136] varied the metal negative contact and observed that the V_{oc} was rather insensitive to variations in the metal electrode workfunction. They also varied the fulllerene acceptor strength and obtained a direct correlation of V_{oc} with acceptor strength. Their conclusions were that the quasi-Fermi levels of the fullerene pin the Fermi level of the negative metal electrode. The positive electrode used was ITO coated with PEDOT:PSS, and the negative electrode in all cases was Al. The active layer consisted of a 1:1 toluene solution of MDMO-PPV:fullerene spin coated film, where the fullerene was either Azafulleroid (-0.67 V), Ketolactam (-0.53 V), PCBM (-0.69 V) or C_{60} (-0.6 V). These values were based on redox behaviour determined by cyclic voltametry. According to the values of the first reduction potential published by these authors, the strongest electron acceptor is Ketolactam, while the weakest is PCBM. In their plots of average V_{oc} vs first reduction potential, they obtained a slope equal to 0.8 (a strong correlation indeed), and for the maximum V_{oc}, the slope gave 100 % correlation. The main conclusions were that the MIM picture cannot adequately describe the V_{oc} of polymer fullerene devices because the workfunction difference of the ITO and Al electrodes would imply only a 0.4 V potential difference as opposed to the obtained 0.55 to 0.72 V.

2. *Comment:* While these conclusions sound valid and reasonable, the analysis suffers from only one flaw. The role of PEDOT:PSS in these devices has been ignored completely. If this were taken to be the positive electrode, all the obtained voltages would fall in a range that could be described by the metal-insulator-metal (MIM) model. We suggest that the MIM picture is true if the sandwiched material were a pure insulator, and that the role of PEDOT:PSS electrode in the device should also have been considered. We note that in P3HT:PCBM devices with symmetrical contacts, Al/P3HT:PCBM/Al we did not observe an open circuit voltage under illumination (see table 8.3).

It is therefore important that the electrodes must have different workfunctions, so that a built in electric field will favour flow of electrons in one direction and holes in the other. On the other hand, our Al/PEDOT:PSS/P3HT:PCBM/Al devices gave open circuit voltages up to 0.28 V at 300K, clearly demonstrating that it is not only the outer electrodes playing a role in generating the V_{oc}. PEDOT:PSS is indeed the electrode to consider, as well as the interfacial barrier it forms with the outer electrode.

3. • Inspired by the results obtained by Brabec *et al.* [137], Kymakis *et al.* [138] studied bilayer devices consisting of an ITO positive electrode, Poly-octylthiophene (P3OT) layer, single wall carbon nanotubes (SWNT) layer, and Al negative electrode. It is interesting to note that this device did not contain a PEDOT:PSS layer, however the SWNTs are separated from the positive electrode by the P3OT layer. We note that these devices have a different configuration when compared to the bulk heterojunction devices described in [137]. In these devices, the observed V_{oc} was 0.7 V, which

Device	$q(\chi_{out}-\chi_{in})$	J_{sc} (mA/cm^2)	V_{oc} (V)	FF (%)	eff (%)	Remarks
ITO/P3HT/Au	0.1	0	0	-	-	MIM
Al/P3HT/Au	0.1	0	0	-	-	MIM
ITO/P3HT/Al	0.4	$\sim 1 \times 10^{-5}$	0.26	-	-	MIM
ITO/PEDOT:PSS/P3HT/Al	0.4	0.391	0.46	37.46	0.068	MIM(X)
ITO/PCBM/Al	0.4	0.11	0.35	31	0,31	MIM
Al/PCBM/Al	0	0	0	-	-	MIM
ITO/PEDOT:PSS/PCBM/Al	0.4	0.329	0.66	26.11	0.057	MIM(X)
Al//P3HT:PCBM/Al	0	0	0	-	-	MIM
Al/PEDOT:PSS/blend/Al	0	0.929	0.276	24.54	0.0006	MIM(X)

Table 8.3: Output characteristics of illuminated devices of different configurations. All devices in which the PEDOT:PSS layer is present can not be described by the simple MIM picture, unless the PEDOT:PSS is considered as the inner electrode, with χ=5.1 to 5.2 eV. (blend=P3HT:PCBM).

is higher than 0.4 V that would be expected from the Al-ITO electrode workfunction difference. They also observe that the MIM picture does not adequately describe the V_{oc} of such devices, and suggest that the V_{oc} is generated due to the exciton dissociation at the P3OT/SWNT interface. The V_{oc} is therefore attributed to the LUMO$_{acceptor}$ - HOMO$_{donor}$ difference as concluded by Brabec *et al.* in their devices. They also studied the effect of the difference in the work function between the two electrodes (ϕ_{ITO} -ϕ_{metal}) on the V_{oc} by studying P3OT-SWNT based devices and varying the metal of the negative electrode. For the four different metals utilized, V_{oc} varied by a total variation of 0.1 V for a 0.8 eV variation of the ϕ_{metal}. This result indicates that the work function of the metal has no significant effect on the V_{oc} , opposite to what would be expected if V_{oc} was determined only by the difference in the contact metal work functions according to the MIM model. They therefore concluded as well that the SWNTs pinned the metal workfunction to their quasi-Fermi levels, suggesting that the metal electrodes form ohmic contacts with the percolation paths of the SWNTs. Their illuminated ITO/P3OT/Al devices gave a V_{oc} of 0.35 V in conformity with the MIM model, and concluded therefore that such a model works only in high purity polymers, like the polythiophenes.

4. *Comment:* Based on the conclusions given in 3., it should be reasonable to imagine that the positive electrode (ITO) should also be pinned to the quasi Fermi level of the P3OT. The conclusions in 3. should be expected due to the configuration of their device, which is completely different from the ones described by Brabec (see 1.).

5. ● As a counter-study of the origin of open circuit voltage reported by Brabec *et al* (see 1.), Kim *et al.* [139] studied polymer fullerene solar cells with the same configuration but instead, varied the ionisation potential of the polymer. In this case they used MEH-PPV (Ionisation potential (I$_p$) = 4.9 eV), P-DMOP-PPV (I$_p$ = 4.52 eV), or P-DMOP-CO-MEH-PPV (5.44 eV) blended with PCBM, and sandwiched between ITO/PEDOT:PSS and Al electrodes. The obtained open circuit voltages were 0.66 V, 0.73 V, and 0.77 V respectively confirming that the V_{oc} indeed scales with the ionisation potential of the donor, since in this case the acceptor strength is constant.

6. *Comment:* As in 1., the role of PEDOT:PSS is completely ignored. If it had been considered as the positive electrode, the V_{oc} obtained would have easily fallen within range of the MIM picture. However their conclusions seem to indicate as well the pinning of the PEDOT:PSS electrode to the

polymer transport levels (quasi Fermi levels). Studies have already shown that P3OT, PPV, and P3HT form ohmic contacts with the ITO/PEDOT:PSS electrode. [110]

7. • Mihailetchi *et al.* [140] argued that the obtained correlation of 100 % between acceptor strength and maximum V_{oc} in bulk heterojunction polymer-fullerene solar cells is to be expected in case of ohmic contacts, meaning that the negative and positive electrodes match the lowest unoccupied molecular orbital (LUMO) of the acceptor and the highest occupied (HOMO) level of the donor, respectively. The maximum V_{oc} for this case is thus governed by the bulk material properties. In case of non-ohmic contacts, a reduced V_{oc} with magnitude [(LUMO$_{acceptor}$ - HOMO$_{donor}$) - ($\phi_{electrode1}$ - ($\phi_{electrode2}$)] is expected, according to the MIM model. Furthermore, the band bending at the ohmic contacts reduce the open circuit voltage by typically 0.2 V for each contact. These voltage losses strongly reduce the maximally attainable V_{oc} in an OC1C10-PPV:PCBM bulk heterojunction solar cell at room temperature. However, a weak variation of the V_{oc} of only 160 meV has been observed when varying the work function of the negative electrode from 5.1 eV (Au) to 2.9 eV (Ca) (see 1.). This deviation from the MIM model has been explained by pinning of the electrode Fermi level to the reduction potential of the fullerene.

8. *Comment:* These authors take the PEDOT:PSS electrode as the positive electrode and are able to account for the maximally obtainable V_{oc} in the MIM picture, by considering the ohmicity of the contacts, and effects of band bending. However their model could not accommodate the Au and Pd electrodes, and had to invoke the dipole formed by the Au/polymer interface.

9. •By dedoping PEDOT:PSS to different levels Frohne et al. [141] varied the 'equilibrium potential' (workfunction) of the PEDOT:PSS 'electrode' from the commercially available ($\sim$-5.1±0.1 eV) to even past the PCBM acceptor levels ($\sim$-3.9 eV), and studied the V_{oc} of ITO/PEDOT:PSS/MDMO-PPV:PCBM/Al solar cells. Interestingly, the V_{oc} decreased as the equilibrium potential of PEDOT:PSS approached the PCBM acceptor levels, where it became zero. Beyond the PCBM acceptor levels, obtained J_{sc} and V_{oc}s were 'inverted', i.e., photogenerated electric fields had opposite direction indicating that the internal built-in field had also changed direction. Doping PEDOT:PSS until its equilibrium potential reaches or surpasses the HOMO of MDMO-PPV led to a reduction in Voc and this was attributed to a 'fobidden potential range', in which PEDOT:PSS is able to oxidise MDMO-PPV.

10. *Comment:* The studies described in 9. indicate that the presence of PEDOT:PSS in the device is not trivial. Its workfunction, which can be controlled by varying the 'doping concentration' influences the obtained open circuit voltage directly. With these results we are inclined to think that the PEDOT:PSS also pin the ITO workfunction to its transport levels, in the same way that has been suggested for PCBM and the metallic outer electrode. In order to generate a voltage, asymmetrical contacts are a necessity if the conduction in the bulk is spatially homogeneous. It has been shown that PEDOT:PSS is important as the positive electrode. We propose that the bulk heterojunction P3HT:PCBM active layer behaves as an n-doped material - P3HT doped with PCBM, and the PEDOT:PSS as a p-doped material - PEDOT doped with PSS. The analysis of the bulk heterojunction ITO/PEDOT:PSS/P3HT:PCBM/Al heterojunction solar cell may therefore be considered as ITO/p-doped/n-doped/Al solar cell. The bulk heterojunctions between P3HT and PCBM enhance the probability of photogenerated excitons dissociating at those interfaces.

We suggest that the open circuit voltage is dependent on the energetic levels of p and n dopants and on their concentrations within the donor and acceptor materials (see Eq. 2.6). PCBM introduces a transport level in the band gap of P3HT in the same fashion as an n dopant does. PSS on the other hand, introduces a transport level in PEDOT making it a p-type material. The junction formed should therefore be expected to behave like a p-n junction, and the open circuit voltage is determined by the

transport level of the n type material (P3HT:PCBM) and the transport level of the p type material (PEDOT:PSS) which both tend to pin the electrode workfunctions to their respective transport levels. Dedoping PEDOT:PSS beyond the acceptor levels of PCBM makes PEDOT:PSS more n than the P3HT:PCBM blend, and a reversed V_{oc} is obtained.

8.5 Conclusions

We conclude that the ideal solar cell is one with a homogeneous P3HT:PCBM distribution in a 1:1 weight ratio, which corresponds to 6 P3HT monomer units for each PCBM molecule, so as to maximise on the number of exciton dissociating heterojunctions in the bulk. This ensures high fill factors, implying high parallel resistance, and low series resistance, as well as maximising the absorption of radiation and creation of electron-hole pairs, and therefore high internal quantum efficiency. Symmetrical electrodes on such a film produce no voltage, therefore there is need to select asymmetrical electrodes in such a way as to provide minimal resistance to the collection of the generated charge carriers. The negative electrode must form an ohmic contact with the transport level of the PCBM, while the positive electrode must first filter the charge carriers, i.e., block the passage of electrons and allow only holes to travel through it. The (PEDOT:PSS)/(P3HT:PCBM) interface is therefore the charge carrier separating interface while the P3HT/PCBM heterojunctions provide exciton dissociating interfaces, which on their own cannot generate a voltage. The ITO is needed since it is easier to contact with external wires as compared to the PEDOT:PSS from our experimental point of view. However, although the ITO/PEDOT:PSS interface is ohmic, a small loss of V_{oc} may be observed due to band bending which may unavoidably occur at that interface. The P3HT:PCBM/Al interface cannot be considered as a charge separating interface because in as much as Al is able to receive electrons from the PCBM, it is equally capable of providing electrons to fill up the holes in P3HT since both materials are in contact with the Al. On the other hand, PEDOT:PSS is a well known hole conductor.

9 Conclusions and Recommendations

9.1 Conclusions

The following are the main conclusions resulting from this work:

- We have shown that hole transport in P3HT is bulk limited when injection is through the ITO/ PEDOT:PSS interface. The J(V) characteristics can be described by space charge limited currents taking into account an exponential distribution of traps within the bandgap of P3HT. We also addressed an inconsistency in the analysis of exponentially distributed traps and calculation of activation energy. We obtained that the TFSCLC hole mobility in P3HT at room temperature is of the order 10^{-5} cm^2/Vs.

- We have shown that electron injection from Al into PCBM is bulk transport limited, which leads to trap free space charge limited currents at sufficiently high applied voltages. We determined the mobility of electrons in the PCBM devices to be 10^{-5} cm^2/Vs at room temperature, i.e., same order as hole mobility in P3HT devices.

- A study of P3HT:PCBM blend devices yielded an effective TFSCLC charge carrier mobility of the order 10^{-5} cm^2/Vs at room temperature.

- We have determined that the optimum exciton splitting donor-acceptor network consists of a homogeneously distributed ratio of 1:1 weight ratio, corresponding to 6 monomer units of P3HT to 1 PCBM molecule. Any deviation from this optimum introduces shielding effects, which tend to reduce efficiency of the solar cells.

- We have shown that the role of PEDOT:PSS in the bulk heterojunction solar cell is that of providing the charge separation interface in the solar cell. Bulk heterojunctions provide an increased exciton splitting network, but cannot alone separate the electrons from the holes. The open circuit voltage should therefore be related to the transport level of PEDOT:PSS and the transport level introduced by PCBM within the band gap of P3HT. The maximum voltage is determined by these transport levels.

- We have shown that the observed improvement of the performance of P3HT:PCBM solar cells, with the optimum ratio, is related to impurity dedoping of P3HT, as well as interdiffusion that improves the overlap of the donor and acceptor wavefunctions. We rule out crystallisation of P3HT as the reason for improvement, and confirm that the crystalline PCBM islands within the material, formed during annealing, become 'dead' parts of the cell. If their size is bigger than the exciton diffusion length, the photogenerated excitons may recobine before reaching an exciton splitting interface.

- We have developed the theoretical understanding and shown that the total current in an electrode/ polymer/ electrode device may be successfully modelled as being due to the sum of contributions of tunneling currents and thermionic emission currents.

- Conclusions reached on studying separate components can be used in explaining some of the features of the composite device.

9.2 Recommendations

There is still room for improvement of efficiency of solar cells based on P3HT:PCBM blends. When this work was started, efficiencies around 1% were the norm, but on finalising, 2.5 to 3 % efficient solar cells can easily be produced. As we believe there is still some scope for the improvement of polymer-fullerene solar cells before commercialisation can be considered, we recommend the following:

- Further studies of electrode/polymer electrode devices should be done in order to determine the electrode materials which can best be pinned to the Fermi levels of the polymer and fullerene respectively. The model developed here could be used in the drawing of both quantitative, and qualitative results in this respect.

- The optimum conditions for thermal annealing must be refined.

- Effects of solvent on the morphology based on real experiments is yet to be studied so that the best solvent is utilised in the preparation of solar cells.

- Conductivity and transmissivity of PEDOT:PSS should be optimised for hole transport in the solar cell.

- Suitable materials for the encapsulation of polymer-fullerene solar cells must be studied in order to protect the cells against the environmental water vapour and oxygen, which tend to reduce their lifetime drastically.

- Scientists working on the development of polymer solar cells should not be discouraged, the science is still young. It took 88 years from discovery to commercialisation of silicon solar cells. It could take less for polymer solar cells if the impetus is not lost.

10 Appendices

Appendix 1: Derivation of J(T) for metal/polymer/metal structures, from the FN formulation.

(extracted from M. Koehler and I. A. Hümmelgen, Appl. Phys. Lett. 70, 3254 (1997)

Under the scope of the rigid band model, the injection of charge carriers into the polymer proceeds via tunneling through a triangular barrier at the electrode polymer interface. The current density *J* depends on the flux *P(W)dW* of carriers that emerge from the metal with energy between *W* and *W+dW*,

$$J = \int_{-\infty}^{+\infty} p(W)dW, \tag{10.1}$$

where q is the magnitude of the electronic charge. Assuming that the carriers inside the metal remain in thermal equilibrium in spite of those that are tunneling from the metal, *P(W)* is given by the product of the equilibrium flux of electrons incident on the interface *N(W)* and the quantum mechanical probability that the carrier penetrates the barrier *D(W)*, thus:

$$P(W) = D(W) \cdot N(W). \tag{10.2}$$

The equilibrium flux of charge carriers with the *x* component of the linear momentum between p_x and p_x+dp_x and energy between *W* and *W+dW* is found by integrating the product of the density of states, the *x* component of the velocity and the Fermi Dirac distribution function over all p_y and p_z. The number *N(W)* is then

$$N(W) = \frac{4\pi m k_B T}{h^3} \ln\left[1 + exp\left(-\frac{W-\mu}{k_B T}\right)\right], \tag{10.3}$$

where *m* is the effective mass of the considered charge carrier, k_B is Boltzmann's constant, *h* is the Planck constant and *μ* is the Fermi energy (chemical potential) of the metal.

In the Wenzel-Kramers-Brillouin (WKB) approximation the tunneling probability for a triangular barrier is:

$$D(W) = exp\left[-\frac{8\pi\sqrt{2m}W^{3/2}}{3Fqh}\right] \tag{10.4}$$

where *F* is the electric field strength applied to the polymer. Equation (10.4) is obtained by setting the reference potential as null at the interface. Substituting Eq. (10.3) and (10.4) in (10.2),

$$P(W)dW = \frac{4\pi m k_B T}{h^3} exp\left[-\frac{8\pi\sqrt{2m}W^{3/2}}{3Fqh}\right] \ln\left[1 + exp\left(-\frac{W-\mu}{k_B T}\right)\right] dW \tag{10.5}$$

Since the major contributions to the tunneling current come from the carriers with energies in the neighbourhood of μ, the exponent in $D(W)$ can be approximated by the first two terms of a Taylor expansion around $W = \mu$. Equation (5) then becomes:

$$P(W)dW = \frac{4\pi m k_B T}{h^3} exp\left[-\frac{8\pi\sqrt{2m}\phi^{3/2}}{3Fqh}\right] exp[\beta(W-\mu)]\ln\left[1+exp\left(-\frac{W-\mu}{k_B T}\right)\right] dW, \quad (10.6)$$

where ϕ is the energy barrier height at the interface and

$$\beta = \frac{2\sqrt{2m}\phi^{1/2}}{3Fqh} \quad (10.7)$$

The FN theory is obtained aproximating the logarithmic function in Eq. (10.6) by a step function at $W = \mu$. This approximation is valid for $q/k_B T \gg 1$. However, for metal/polymer interfaces in which the barrier height has typically only thenths of an electron volt, this is no longer a good approximation at room temperature. For a more precise description of the current density as a function of F, it is ncessary to integrate over the logarithmic function in Eq. (10.6). The tunnel current presents then a temperature dependence from Eqs. (10.1) and (10.6), given by:

$$J(T) = q\left(\frac{4\pi m k_B T}{h^3}\right) exp\left(-\frac{4\sqrt{2m}\phi^{3/2}}{3Fqh}\right)\int_0^\infty \xi^{\beta k_B T-1}\ln\left(1+\frac{1}{\xi}\right)d\xi \quad (10.8)$$

where $\xi = exp[(W-\mu)/k_B T]$. The equation resulting from part integration of Eq. (10.8) is of a standard form and the current density becomes:

$$J(T) = \frac{q^2 \pi k_B T}{h^2}\left(\frac{m^*}{2\phi_B}\right)^{1/2}\cdot F \cdot exp\left(-\frac{8\pi\sqrt{2m^*}\phi_B^{3/2}}{3hqF}\right)\cdot\frac{1}{sin(\beta\pi k_B T)}. \quad (10.9)$$

(c.f. Eq. 2.32)

$$* * *$$

Appendix 2: Output characteristics of illuminated P3HT and PCBM devices

Output characteristics of single layer P3HT devices
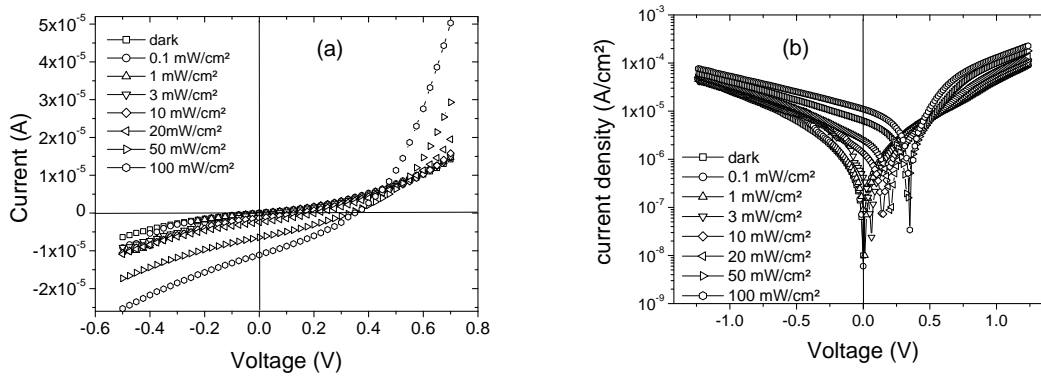
Figure 10.1: *(a) Linear I(V) and (b) semi-logarithmic representation of J(V) curves of an ITO/ PCBM/ Al device at 300 K, under illumination of different intensities.*

Under illumination a potential difference is generated. Output characteristics under white light illumination at 100 mW/cm^2 300 K gave: V_{oc} = 0.35 V; FF = 31 %; J_{sc} = 0.11 mA/cm^2; and Eff. = 0,31 %. Figures 10.1 show the obtained *J(V)* characteristics for ITO/PCBM/Al devices. Photogenerated voltages of up to 0.375 V were recorded for these devices. The obtained V_{oc} can be described by the MIM picture.

Al/P3HT/Al devices

Device preparation involved the deposition of Al electrodes on cleaned glass substrates, by thermal deposition in high vacuum. P3HT was subsequently spin coated, followed by thermal deposition again of Al electrodes. Al/P3HT/Al devices are hole only devices conducting through HOMO of P3HT. These electrodes limit charge injection until a electric field (>5x10^6 V/cm) has been applied. The *J(V)* characteristics show symmetrical behaviour for both directions of hole injection (see Fig. 10.2). This suggests that the method of preparation is adquate, and avoids the formation of a significant oxide layer on the Al contact deposited on glass.

We observed no open circuit voltage under illumination. This suggests the need of an electrode work function difference to generate open circuit voltage. The electrode workfunction difference provides a built-in field across P3HT so that photo-generated electron-hole pairs are separated. What this means is that electrons will find a favourable field to move towards the Al electrode, and holes diffuse to the ITO electrode. This is a typical metal-insulator-metal picture, where the maximum achievable photovoltage would be given by the electrode workfunction difference divided by the electronic charge.
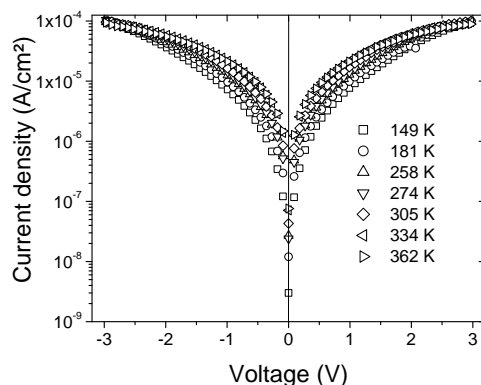
Figure 10.2: Dark J(V) *plot of an Al/P3HT/Al device for different temperatures. Symmetrical behaviour is observed in both directions of current flow.*

* * *

Output characteristics of double layer PV devices

ITO/PEDOT:PSS/P3HT/Al devices
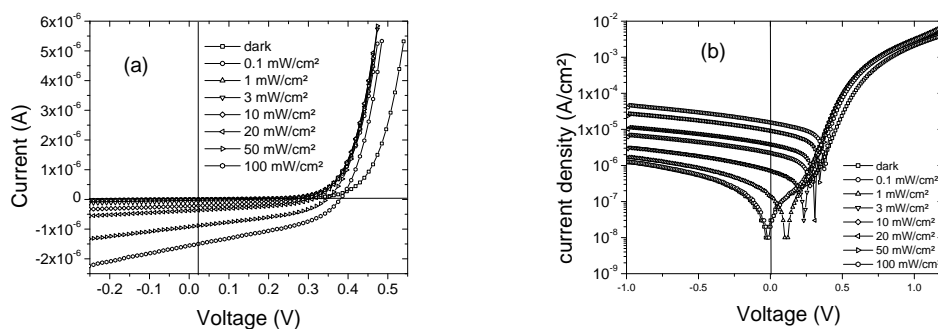
Figure 10.3: *(a) I(V) and characteristics of an illuminated ITO/PEDOT: PSS/P3HT/Al device in linear scale at different light intensities. (b) semi-logarithmic plot of the J(V) characteristics.*

The *I(V)* and *J(V)* curves are presented in Figs. 10.3(a) and (b) respectively. Typical output characteristics are presented in Table 10.1. Note the high open circuit voltage obtained (about 0.46 V at 100 mW/cm^2 white light illumination, at 300K). We also note that measurable currents (up to more than 0.3 mA/cm^2) were obtained. The question yet to be answered is what role the PEDOT:PSS layer plays in this device. The open circuit voltage is slightly more than what the MIM picture predicts. Considering ITO ($\varphi \sim$ 4.7 eV) and Al ($\varphi \sim$0.43 eV) outer electrodes work function difference would suggest maximum open circuit voltage for the device to be around 0.4 V. For now, PEDOT:PSS improves the rectification properties of the device, and influences the open circuit voltage. If PEDOT:PSS ($\phi \sim$ 5.0 eV)is considered to be the positive electrode, the obtained V_{oc} could be described

Light intensity	J_{sc} (mA/cm^2)	V_{oc} (V)	FF (%)	eff (%)
0,1 mW/cm^2	1.20×10^{-4}	0.01	157.14	0.004
1 mW/cm^2	3.94×10^{-3}	0.08	24.67	0.008
3 mW/cm^2	1.70×10^{-2}	0.24	27.53	0.038
10 mW/cm^2	5.14×10^{-2}	0.39	33.94	0.067
20 mW/cm^2	9.03×10^{-2}	0.42	37.91	0.072
50 mW/cm^2	2.33×10^{-1}	0.44	39.58	0.081
100 mW/cm^2	3.91×10^{-1}	0.46	37.46	0.068

Table 10.1: Output characteristics of an illuminated ITO/PEDOT:PSS/ P3HT/Al device.

by the MIM picture.

For the analysis of the opto-electrical behaviour of ITO/PEDOT:PSS/P3HT/Al devices, two questions arise: Is this a single layer device, where PEDOT:PSS is one of the electrodes, or is it a double layer device, with PEDOT:PSS acting as a p-type semiconductor? In this case would the P3HT be considered an n-type material?
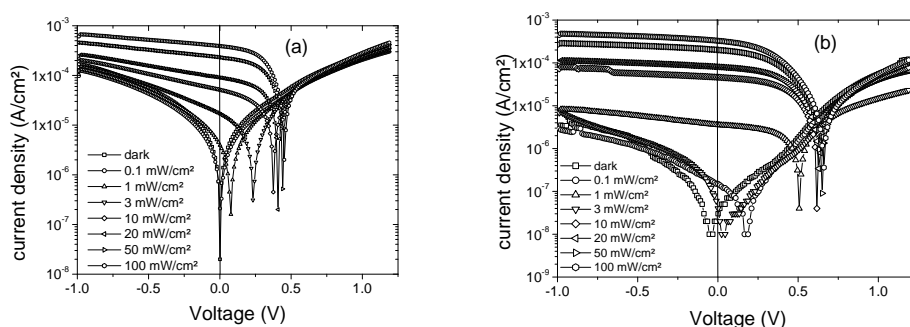
Figure 10.4: *Illuminated* J(V) *curves of an as-cast ITO/PEDOT/PCBM/Al device (a) and after a thermal annealing step (b) at different illumination intensities. High open circuit voltages of above 0.65 V were observed.*

ITO/PEDOT:PSS/PCBM/Al devices

Typical output parameters of an illuminated ITO/PEDOT:PSS/ PCBM/Al device are presented in Table 10.2. Both the V_{oc} and the short circuit current density are much higher for these devices, as compared to ITO/PCBM Al devices. With PEDOT:PSS, higher open circuit voltages (>650 mV) are obtained, and also higher currents (>0.35mA/cm^2). On annealing the devices, up to $\sim$ 740mV V_{oc} was obtained. The obtained V_{oc} is comparable to that obtained for the solar cell (see chapter 7). This raises the question of the origin of V_{oc}. HOMO of P3HT is not present in this device. We assume that the ITO does not limit hole collection once these have passed into PEDOT:PSS. In this case the obtained V_{oc} is attributed to LUMO$_{(PCBM)}$- HOMO$_{(PEDOT:PSS)}$ difference. It is assumed that the quasi Fermi level of PCBM pins the Al electrode workfunction while the HOMO of PEDOT:PSS should pin the ITO electrode workfunction. The maximally realizable V_{oc} in these devices should therefore be when all states are filled and transport levels concide with the HOMO and LUMO of PEDOT:PSS and PCBM respectively - about 1.1 V. The role of traps, charge carrier mobility, density

Light intensity	J_{sc} (mA/cm^2)	V_{oc} (V)	FF (%)	eff (%)
0,1 mW/cm^2	4.00E-05	0.03	17.65	0.000
1 mW/cm^2	1.50×10^{-4}	0.18	30.13	0.001
3 mW/cm^2	3.56×10^{-3}	0.52	45.07	0.028
10 mW/cm^2	4.62×10^{-2}	0.63	37.44	0.109
20 mW/cm^2	8.05×10^{-2}	0.64	34.44	0.089
50 mW/cm^2	2.02×10^{-1}	0.65	28.96	0.076
100 mW/cm^2	3.29×10^{-1}	0.66	26.11	0.057

Table 10.2: Output characteristics of an illuminated ITO/PEDOT:PSS/PCBM/Al device.

and the role of the different electrodes in creating the V_{oc} still have to be determined.

$$* * *$$

Output characteristics of single layer bulk heterojunction PV devices

Al/P3HT:PCBM/Al device

Al/P3HT:PCBM/Al devices are electron only devices conducting through LUMO of PCBM. Dark $J(V)$ curves of these devices are represented by the semi-log plots of Fig. 10.5(a). TFSCLC was observed for both directions of current flow. Al seems to make an ohmic contact with the PCBM:P3HT composite. We assume that the transport level in this case is LUMO PCBM, implying that this device is an electron only device, and the acceptor levels are used for the conduction rather than the P3HT. It has already been shown that Al limits injection into HOMO of P3HT. Note that Al's workfunction falls in the lower half of the P3HT HOMO-LUMO gap (see chapters 4 and 5). Slope 1 and 2 are observed in the log log plots both for as-cast and for annealed devices. Higher currents though, are observed for the annealed device.
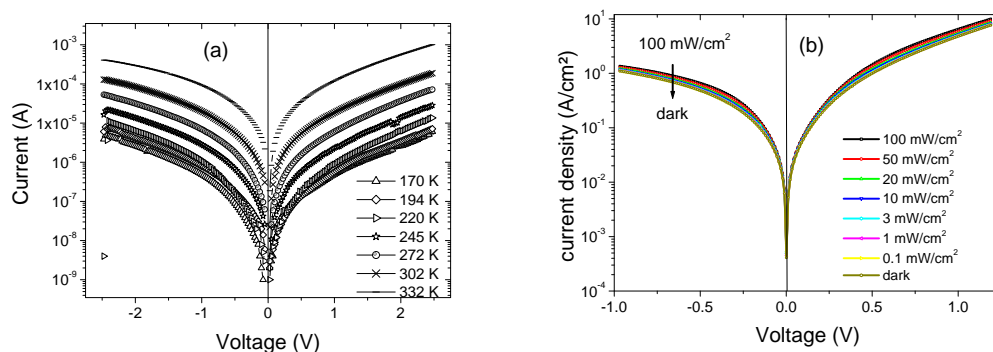
Figure 10.5: *Semi logarithmic plots of (a) dark I(V) characteristics of an Al/P3HT:PCBM/Al device at different temperatures, (b) illuminated characteristics at 300K for different illumination intensities.*

Figure 10.5(b) shows the illuminated characteristics of an Al/P3HT:PCBM/Al device. No open circuit voltage was recorded for these devices. This clearly demonstrates the need to have asymetrical
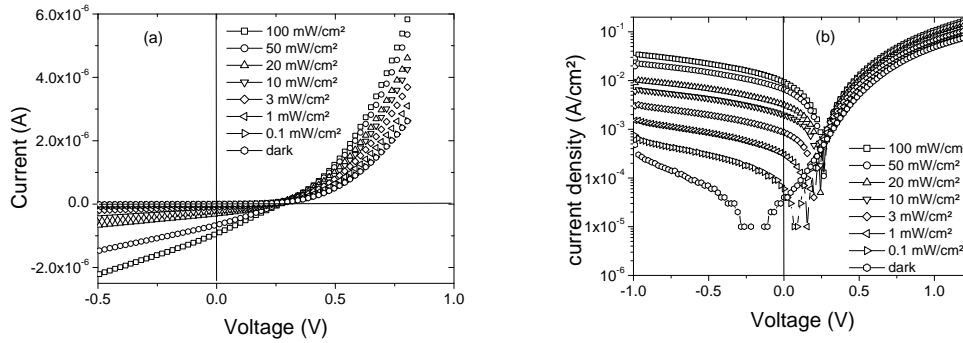
Figure 10.6: *(a) I(V) curves of an Al/PEDOT:PSS/P3HT:PCBM/Al device under illumination of different intensities in linear scale (b) J(V) curves of the same device in semi-logarithmic scale.*

electrodes in order to be able to collect one type of charge at either electrode, and to generate a voltage.

Output characteristics of double layer bulk heterojunction PV devices

Al/PEDOT:PSS/P3HT:PCBM/Al device

For Al/PEDOT:PSS/P3HT/PCBM/Al devices, the open circuit voltage was developed independent of the fact that both outer electrodes are of Aluminum. This situation reminds of the silicon crystal solar cell where both outer electrodes are Al, the pd is thought to occur due to the difference in the conduction properties of the PEDOT:PSS and the P3HT:PCBM blend. PEDOT:PSS is known to be a p-type material (see chapter 3). We may speculate that P3HT:PCBM behaves like an n type material. In any case it is sufficient that one must be more n (or more p) than the other in order for a voltage to be generated. P-n junction theory should therefore apply. The short circuit current density is however small since the Al/PEDOT:SS interface blocks hole conduction.

Light intensity	J_{sc} (μA/cm^2)	V_{oc} (V)	FF (%)	eff (%)
0,1 mW/cm^2	0.006	0.078	28.85	0.0014
1 mW/cm^2	0.030	0.166	28.85	0.0058
3 mW/cm^2	0.086	0.210	31.96	0.0019
10 mW/cm^2	0.197	0.232	33.76	0.0015
20 mW/cm^2	0.314	0.254	31.18	0.0012
50 mW/cm^2	0.655	0.265	27.51	0.0010
100 mW/cm^2	0.929	0.276	24.54	0.0006

Table 10.3: Output characteristics of an illuminated Al/PEDOT:PSS /P3HT:PCBM/Al device.

Even with similar outer electrodes, a potential difference is generated. Introducing PEDOT:PSS (an electron blocking layer) makes the electrodes asymmetrical. A clear reverse and forward direction is observed in the *I(V)* curves (Fig. 10.6), the device shows rectifying behaviour. The fact that PV effect is observed for this device indicates that the field created by the electrodes is important in the solar cell. Without the PEDOT:PSS layer, the PV effect is not observed. We may conclude that

with symmetrical electrodes, there are equal chances of generated electrons and holes travelling to both electrodes with the same rate, therefore a potential difference can not be established.

Introduction of the PEDOT:PSS layer slows down electrons and makes an easy path for holes, hence a potential difference is observed, with more holes at the PEDOT:PSS/Al electrode. This demonstrates that PEDOT:PSS must also be considered in the analysis of voltage generation in bulk heterojunction solar cells. It might therefore constitute a mistake to consider the generated open circuit voltage in polymer fullerene solar cells to be limited by the workfunction difference of outer electrode materials. (We discuss this point in detail in section 7.3.4.) The observed V_{oc} is therefore in conformity with work-function difference of PEDOT:PSS and Al, namely within the range 0 V to 0.8 V. Up to 0.28 V were recorded at 300 K, 100 mW/cm^2 for our illuminated Al/PEDOT:PSS /P3HT:PCBM/Al devices. The limiting value could be higher, as the incident light is by no means considered to saturate the device. Further, the Al positive electrode is highly reflecting.

$$* * *$$

Bibliography

[1] D. Y. Goswami, F. Kreith, and Jan F. Kreider. *Principles of Solar Engineering*. Taylor and Francis, Philadelphia, 2000.

[2] J. Shinar. *Organic Light Emitting Devices: A Survey*. Springer Verlag, New York, 2002.

[3] C. J. Brabec, V. Dyakonov, J. Parisi, and N. S. Sariciftci. *Organic Photovoltaics: Concepts and Realization*. Springer Verlag, Berlin, 2003.

[4] T. Markvart and L. Castaner. *Practical Handbook of Photovoltaics, Fundamentals and Applications*. Elsevier, Oxford, 2003.

[5] C. D. Dimitrakopoulos and D. J. Mascaro. Organic thin-film transistors: A review of recent advances. *Organic Electronics*, 45:11, 2001.

[6] F. Padinger, R. S. Rittberger, and N. S. Sariciftci. Effects of postproduction treatment on plastic solar cells. *Adv. Funct. Mater.*, 13:1, 2003.

[7] P. Schilinsky, C. Waldauf, and C. J. Brabec. Recombination and loss analysis in polythiophene based bulk heterojunction photodetectors. *Appl. Phys. Lett.*, 81:3885, 2002.

[8] H. Sirringhaus, N. Tessler, and R. Friend. Integrated optoelectronic devices based on conjugated polymers. *Science*, 280:1741, 1998.

[9] J. A. Duffie and W. A. Beckman. *Solar Engineering of Thermal Processes*. J. Wiley, new York, 1991.

[10] S. L. Sargent. A compact table of blackbody radiation functions. *Bull. Of the Meteorological Soc.*, 53:360, 1972.

[11] E. Lorenzo. *Solar Electricity, Engineering of Photovoltaic Systems*. James and James, London, 1994.

[12] C. K. Chiang, C. R. Fincher, Y. W. Park, A. J. Heeger, H. Shirakawa, E. J. Louis, S. C. Gau, and A. G. MacDiarmid. Electrical conductivity in doped polyacetylene. *Phys. Rev. Lett.*, 39:1098, 1977.

[13] F. Garnier R. Hajlaoui, A. Yassar, and P. Srivastava. Flexible light-emitting diodes made from soluble conducting polymers. *Science*, 265:1684, 1994.

[14] L. Torsi, A. Dodabalapur, L. J. Rothberg, A. W. P. Fung, and H. E. Katz. Intrinsic transport properties and performance limits of organic field-effect transistors. *Science*, 272:1462, 1996.

[15] Y. Yang and A. J. Heeger. A new architecture for polymer transistors. *Nature*, 372:344, 1994.

[16] A. R. Brown, A. Pomp, C. M. Hart, and D. M. de Leeuw. Logic gates made from polymer transistors and their use in ring oscillators. *Science*, 270:972, 1995.

[17] G. Yu, J. Gao, J. C. Hummelen, F. Wudl, and A. J. Heeger. Polymer photovoltaic cells: Enhanced efficiencies via a network of internal donor-acceptor heterojunctions. *Science*, 270:1789, 1995.

[18] N. C. Greenham, S. C. Moratti, D. D. C. Bradley, R. H. Friend, and A. B. Holmes. Efficient light-emitting diodes based on polymers with high electron affinities. *Nature*, 365:628, 1993.

[19] D. Braun and A. J. Heeger. Visible light emission from semiconducting polymer diodes. *Appl. Phys. Lett.*, 58:1982, 1991.

[20] R. H. Friend, R. W. Gymer, A. B. Holmes, J. H. Burroughes, R. N. Marks, C. Taliani, D. D. C. Bradley, D. A. Dos Santos, J. L. Bredas, M. Lögdlund, and W. R. Salaneck. Electroluminescence in conjugated polymers. *Nature*, 397:121, 1999.

[21] G. G. Wallace, P. C. Dastoor, D. L. Officer, and C. O. Too. Conjugated polymers: New materials for photovoltaics. *Chem. Innov.*, 30:14, 2000.

[22] N. S. Sariciftci. Role of buckminsterfullerene in organic photoelectric devices. *Progr. Quant. Electron.*, 19:131, 1995.

[23] M. Grandstrom, K. Petritsch, , A. C. Arias, A. Lux, M. R. Anderson, and R. H. Friend. Laminated fabrication of polymeric photovoltaic diodes. *Nature*, 395:257, 1998.

[24] H. Antoniadis, L. J. Rothberg, F. Papadimitrakopoulos, M. Yan, M. E. Galvin, and M. A. Abkowitz. Enhanced carrier photogeneration by defects in conjugated polymers and its mechanism. *Phys. Rev. B*, 50:14911, 1994.

[25] H. Rost S. Barth, H. Bässler and H. H. Hörhold. Extrinsic and intrinsic dc photoconductivity in a conjugated polymer. *Phys. Rev. B*, 56:3884, 1997.

[26] S. Barth and H. Baessler. Intrinsic photoconduction in ppv-type conjugated polymers. *Phys. Rev. Lett.*, 79:4445, 1997.

[27] C. J. Brabec, G. Zerza, N. S. Sariciftci, G. Cerullo, S. DeSilvesteri, S. Luzatti, and J. C. Hummelen. Tracing photoinduced electron transfer process in conjugated polymer/fullerene bulk heterojunctions in real time. *Chem. Phys. Lett.*, 340:232, 2001.

[28] P. W. M. Blom, M. J. M. de Jong, and J. J. M. Vleggaar. Electron and hole transport in poly(p-phenylene vinylene) devices. *Appl. Phys. Lett.*, 68:3308, 1996.

[29] P. W. M. Blom, M. J. M. de Jong, and M. G. van Munster. Electric-field and temperature dependence of the hole mobility in poly(p-phenylene vinylene). *Phys. Rev. B*, 55:R656, 1997.

[30] W. Brutting, S. Berleb, and A. Mückl. Device physics of organic light-emitting diodes based on molecular materials. *Organic Electronics*, 2:1, 2001.

[31] H. Ishii and K. Seki. Energy level alignment at organic/metal interfaces studied by uv photoemission: breakdown of traditional assumption of a common vacuum level at the interface. *IEEE Trans. Electron Devices*, 44:1295, 1997.

[32] I. G. Hill, A. Rajagopal, A. Kahn, and Y. Hu. Molecular level alignment at organic semiconductor-metal interfaces. *Appl. Phys. Lett.*, 73:662, 1998.

[33] I. G. Hill, A. J. Makinen, and Z. H. Kafafi. Distinguishing between interface dipoles and band bending at metal/tris-(8-hydroxyquinoline) aluminum interfaces. *Appl. Phys. Lett.*, 77:1825, 2000.

[34] W. R. Salaneck, K. Seki, A. Kahn, and J. J. Pireaux. *Conjugated Polymer and Molecular Interfaces: Science and Technology for Photonic and Optoelectronic Applications*. Dekker, New York, 2001.

[35] C. Shen, A. Kahn, and J. Schwartz. Chemical and electrical properties of interfaces between magnesium and aluminum and tris-(8-hydroxy quinoline) aluminum. *J. Appl. Phys.*, 89:449, 2001.

[36] N. Koch, A. Elschner, J. Schwartz, and A. Kahn. Organic molecular films on gold versus conducting polymer: Influence of injection barrier height and morphology on current-voltage characteristics. *Appl. Phys. Lett.*, 82:2281, 2003.

[37] A. Rose. Space-charge-limited currents in solids. *Phys. Rev.*, 97:1538, 1955.

[38] A. J. Campbell, D. D. C. Bradley, and D. G. Lidzey. Space-charge limited conduction with traps in poly(phenylene vinylene) light emitting diodes. *J. Appl. Phys.*, 82:6326, 1997.

[39] P. S. Davids, Sh. M. Kogan, I. D. Parker, and D. L. Smith. Charge injection in organic light-emitting diodes: Tunneling into low mobility materials. *Appl. Phys. Lett.*, 69:2270, 1997.

[40] F. Feller, C. Rothe, M. Tammer, D. Geshke, and A. P. Monkman. Temperature dependence of the space charge distribution in injection limited conjugated polymer structures. *J. Appl. Phys.*, 91:9225, 2002.

[41] F. Feller, D. Geshke, and A. P. Monkman. Spatial distribution of space charge in conjugated polymers. *Appl. Phys. Lett.*, 79:779, 2001.

[42] P. W. Blom and M. C. J. M. Vissenberg. Charge transport in poly(p-phenylene vinylene) light-emitting diodes. *Mater. Sci. Eng.*, 27:53, 2000.

[43] M. Kiy, I. Biaggio, M. Koehler, and P. Guenter. Conditions for ohmic electron injection at the mg/alq3 interface. *Appl. Phys. Lett.*, 80:4366, 2002.

[44] S. M. Sze. *Semiconductor devices*. Wiley, New York, 1998.

[45] M. Koehler and I. A. Hümmelgen. Temperature dependent tunneling current at metal/polymer interfaces - potential barrier height determination. *Appl. Phys. Lett.*, 70:3254, 1997.

[46] K. C. Kao and W. Hwang. *Electrical Transport in Solids, with particular reference to organic semiconductors*, volume 14 of *International Series in the Science of the solid State*. Pergamon Press, Oxford, 1981.

[47] R. R. Das, P. Battacharya, W. Perez, Ram S. Katiyar, and A. S. Bhalla. Leakage current characteristics of laser-ablated *srbi2nb2o9* thin films. *Appl. Phys. Lett.*, 81:880, 2002.

[48] D. Braun. Electronic injection and conduction processes for polymer devices. *J. Polymer Science B*, 41:2622, 2003.

[49] H. K. Henisch. *Semiconductor Contacts, An approach to ideas and models, International Series of Monographs on Physics No. 70*. Clarendon Press, Oxford, 1984.

[50] R. H. Fowler and L. Nordheim. Electron emission in intense electric fields. *Proc. R. Soc. London, Ser. A*, 119:173, 1928.

[51] C. Lee, J. Y. Park, Y. W. Park, Y. H. Ahn, D. H. Hwang D. S. Kim, and T. H. Zyung. Temperature dependence of the electroluminescence and the photoluminescence of a silyl-disubstituted poly(p-phenylenevinylene) derivative. *J. Korean Phys. Soc.*, 35:S291, 1999.

[52] D. V. Khramtchenkov, H. Baessler, and V. I. Arkhipov. A model of electroluminescence in organic double-layer light-emitting diodes. *J. Appl. Phys.*, 79:9283, 1996.

[53] R. N. Marks, D. D. C. Bradley, R. W. Jackson, P. L. Burn, and A. Holmes. a. *Synth. Met.*, 55-57:4128, 1993.

[54] X. Wei, M. Raikh, Z. V. Vardeny, Y. Yang, and D. Moses. Photoresponse of poly(para-phenylenevinylene) light-emitting diodes. *Phys. Rev. B*, 49:17480, 1994.

[55] I. D. Parker. Carrier tunneling and device characteristics in polymer light-emitting diodes. *J. Appl. Phys.*, 75:1656, 1994.

[56] P. S. Davids, I. H. Campbell, and D. L. Smith. Device model for single carrier organic diodes. *J. Appl. Phys.*, 82:6319, 1997.

[57] M. A. Lampert and P. Mark. *Current Injection in Solids*. Academic Press, New York, 1970.

[58] M. Abkowitz, J. S. Facci, and J. Rehm. Direct evaluation of contact injection efficiency into small molecule based transport layers: Influence of extrinsic factors. *J. Appl. Phys.*, 83:2670, 1998.

[59] M. Abkowitz, J. S. Facci, and M. Stolka. Behavior of an ideal injecting contact on a trap-free polymer. *J. Appl. Phys.*, 63:1892, 1993.

[60] Ray Swati, R. Banerjee, N. Basu, A. K. Batabyal, and A. K. Barua. Properties of tin doped indium oxide thin films prepared by magnetron sputtering. *J. Appl. Phys.*, 54:3497, 1983.

[61] A. J. R. Sheats, H. Antoniadis, M. Hueschen, W. Leonard, J. Miller, R. Moon, D. Roitman, and A. Stocking. Organic electroluminescent devices. *Science*, 273:884, 1996.

[62] P. E. Burrows, V. Bulovic, S. R. Forrest, L. S. Sapochak, D. M. McCarty, and M. E. Thompson. Reliability and degradation of organic light emitting devices. *Appl. Phys. Lett.*, 65:2922, 1994.

[63] J. C. Scott, J. H. Kaufman, P. J. Brock, R. DiPietro, J. Salem, and J. A. Goitia. Degradation and failure of meh-ppv light-emitting diodes. *J. Appl. Phys.*, 79:2745, 1996.

[64] C. C. Wu, C. I. Wu, J. C. Sturm, and A. Kahn. Surface modification of indium tin oxide by plasma treatment: An effective method to improve the efficiency, brightness, and reliability of organic light emitting devices. *Appl. Phys. Lett.*, 70:1348, 1997.

[65] J. C. C. Fan and J. B. Goodenough. X-ray photoemission spectroscopy studies of sn-doped indium-oxide films. *J. Appl. Phys.*, 48:3524, 1977.

[66] L. Groenendaal, F. Jonas, D. Freitag, H. Pielartzik, and J. R. Reynolds. Poly(3,4-ehylenedioxythiophene) and its derivatives: Past, present, and future. *Adv. Mater.*, 12:481, 2000.

[67] K. Book, H. Baessler, A. Elschner, and S. Kirchmeyer. Hole injection from an ito—pedt anode into the hole transporting layer of an oled probed by bias induced absorption. *Organic Electronics*, 4:227, 2003.

[68] T. Johansson, L. A. A. Pettersson, and O. Inganas. Conductivity of de-doped poly(3,4-ethylenedioxythiophene). *Synth. Met.*, 129:269, 2002.

[69] P. D. Andersson, D. Nilsson, P. O. Svensson, M. Chen, A. Malmström, T. Remonen, T. Kugler, and M. Berggren. Active matrix displays based on all-organic electrochemical smart pixels printed on paper. *Adv. Mater.*, 14:1460, 2002.

[70] O. Diels and K. Alder. Diene synthesis ...proposal by h. c. starck- manufacturers of pedot:pss. *Ann*, 460:98, 1928.

[71] J. H. Burroughes, D. D. C. Bradley, A. R. Brown, R. N. Marks, K. Mackay, R. H. Friend, P. L. Burn, and A. B. Holmes. Light-emitting diodes based on conjugated polymers. *Nature*, 347:539, 1990.

[72] P. K. H. Ho, M. Granström, R. H. Friend, and N. C. Greenham. Ultrathin self-assembled layers at the ito interface to control charge injection and electroluminescence efficiency in polymer light-emitting diodes. *Adv. Mater.*, 10:769, 1998.

[73] G. Gustafsson, Y. Cao, G. M. Treacy, F. Klavetter, N. Colaneri, and A. J. Heeger. Flexible light-emitting diodes made from soluble conducting polymers. *Nature*, 357:477, 1992.

[74] T. Kugler, A. Andersson, A. B. Holmes, X. Li, and W. R. Salaneck. Buried interfaces: poly(p-phenylene-vinylene)-on-ito. *Synth Met.*, 100:163, 1999.

[75] F. Nüesch, L. J. Rothberg, E. W. Forsythe, Q. T. Le, and Y. Gao. A photoelectron spectroscopy study on the indium tin oxide treatment by acids and bases. *Appl. Phys. Lett.*, 74:880, 1999.

[76] K. W. Wong, H. L. Yip, Y. Luo, K. Y. Yong, W. M. Lau, K. H. Low, H. F. Chow, Z. Q. Gao, W. L. Yeung, and C. C. Chang. Blocking reactions between indium-tin oxide and poly (3,4-ethylene dioxythiophene):poly(styrene sulphonate) with a self-assembly monolayer. *Appl. Phys. Lett*, 80:2788, 2002.

[77] X. Crispin, A. Crispin, M. P. de Jong, S. Marciniak, W. Osikowicz, S. Jönsson, M. Fahlman, T. Kugler, L. J. van IJzendoorn, M. J. A. de Voigt, and W. R. Salaneck. Stability of indium tin oxide/polymer interfaces. *Mat. Res. Soc. Symp. Proc.*, 747:V5.5.1, 2002.

[78] S. Karg, J. C. Scott, J. R. Salem, and M. Angelopoulos. Increased brightness and lifetime of polymer light-emitting diodes with polyaniline anodes. *Synth. Met.*, 80:111, 1996.

[79] A. Elschner, F. Bruder, W. W. Heuer, F. Jonas, A. Karbach, S. Kirchmeyer, S. Thurn, and R. Wehrmann. Pedt / pss for efficient hole-injection in hybrid organic light-emitting diodes. *Synth. Met.*, 111-112:139, 2000.

[80] J. C. Carter, I. Grizzi, S. K. Heeks, D. J. Lacey, S. G. Latham, P. G. May, O. Ruiz de-los Panos, K. Pichler, C. R. Towns, and H. F. Wittmann. Operating stability of light-emitting polymer diodes based on poly(p-phenylene vinylene). *Appl. Phys. Lett.*, 71:34, 1997.

[81] S. A. Carter, M. Angelopoulos, S. Karg, P. J. Brock, and J. C. Scott. Polymeric anodes for improved polymer light-emitting diode performance. *Appl. Phys. Lett.*, 70:2067, 1997.

[82] A. J. M. Berntsen, P. V. D. Weijer, Y. Croonen, C. T. H. F. Liedenbaum, and J. J. M. Vleggaar. Stability of polymer light-emitting diodes. *Philips J. Res.*, 51:511, 1998.

[83] J. S. Kim, P. K. H. Ho, P. D. S. Thomas, R. H. Friend, F. Cacialli, G. W. Bao, and S. F. Y. Li. X-ray photoelectron spectroscopy of surface-treated indium-tin oxide thin films. *Chem. Phys. Lett.*, 315:307, 1999.

[84] T. M. Brown, J. S. Kim, R. H. Friend, F. Cacialli, R. Daik, and W. J. Feast. Built-in field electroabsorption spectroscopy of polymer light-emitting diodes incorporating a doped poly(3,4-ethylene dioxythiophene) hole injection layer. *Appl. Phys. Lett.*, 75:1679, 1999.

[85] G. Folcher, H. Cachet, M. Froment, and J. Bruneaux. Anodic corrosion of indium tin oxide films induced by the electrochemical oxidation of chlorides. *Thin Solid Films*, 301:242, 1997.

[86] M. P. D. Jong, D. P. L. Simons, M. A. Reijme, L. Z. V. Ijzendoorn, A. W. D. V. D. Gon, M. J. A. D. Voigt, H. H. Brongersma, and R. W. Gymer. Indium diffusion in model polymer light-emitting diodes. *Synth. Met.*, 110:1, 2000.

[87] H. Y. Mao, B. Xu, and S. Holdcroft. Synthesis and structure-property relationships of regioirregular poly(3-hexylthiophenes). *Macromolecules*, 26:1163, 1993.

[88] R. D. McCullough, R. D. Lowe, M. Jayaraman, and D. L. Anderson. Design, synthesis, and control of conducting polymer architectures: structurally homogeneous poly(3-alkylthiophenes). *J. Org. Chem.*, 58:904, 1993.

[89] T. A. Chen, X. W. Reuben, and D. Riecke. Regiocontrolled synthesis of poly(3-alkylthiophenes) mediated by rieke zinc: Their characterization and solid-state properties. *J. Am. Chem. Soc.*, 117:233, 1995.

[90] M. M. Erwin, J. McBride, A. V. Kadavanich, and S. J. Rosenthal. Effects of impurities on the optical properties of poly-3-hexylthiophene thin films. *Thin Solid Films*, 409:198, 2002.

[91] P. M. Allemand, A. Koch, F. Wudl, Y. Rubin, F. Diederich, M. M. Alvarez, S. J. Anz, and R. L. Whetten. Two different fullerenes have the same cyclic voltammetry. *J. Am. Chem. Soc.*, 113:1050, 1991.

[92] H. Kroto, J. Heath, S. O'Brien, R. Curl, and R. Smalley. a. *Nature*, 318:162, 1985.

[93] W. Krätschmer, L. Lamb, and K. Fostiropoulos D. Huffman. a. *Nature*, 347:354, 1985.

[94] J. P. Lu, X. P. Li, and R. M. Martin. Ground state and phase transitions in solid c60. *Phys. Rev. Lett.*, 68:1551, 1992.

[95] R. Tycko, G. Dabbagh, R. M. Flemming, R. C. Haddon, A. V. Makhia, and S. M. Zahurak. Molecular dynamics and the phase transition in solid c60. *Phys. Rev. Lett.*, 67:1886, 1991.

[96] P. A. Heiney, J. E. Fisher, A. R. McGhie, J. W. Romanow, A. M. Denestejn, J. P. McCauley, A. B. Smith, and D. E. Cox. Orientational ordering transition in solid c_{60}. *Phys. Rev. Lett.*, 66:2911, 1991.

[97] E. A. Katz, D. Faiman, K. Iakoubovskii, A. Isakina, K. A. Yagotintsev, M. A. Strzhemechny, and I. Balberg. Effect of the disorder/order phase transition on the electrical and photoelectrical properties of c_{60} thin films. *J. Appl. Phys.*, 93:3401, 2003.

[98] R. C. Haddon, A. S. Perel, R. C. Morris, T. T. Palstra, A. F. Hebard, and R. M. Flemming. C_{60} thin film transistors. *Appl. Phys. Lett.*, 67:121, 1995.

[99] E. Frankevich, Y. Maruyama, and H. Ogata. Mobility of charge carriers in vapor-phase grown c_{60} single crystal. *Chem. Phys. Lett.*, 214:39, 1993.

[100] V. D. Mihailetchi, J. K. van Duren, P. W. M. Blom, J. C. Hummelen, R. A. J. Janssen, J. M. Kroon, M. T. Rispens, W. J. H. Verhees, and M. M. Wienk. Electron transport in a methanofullerene. *Adv. Funct. Mater.*, 13:43, 2003.

[101] I. A. Hümmelgen, S. Roman, F. C. Nart, L. O. Peres, and E. L. de Sa. Polymer and polymer/metal interface characterization via fowlernordheim tunneling measurements. *Appl. Phys. Lett.*, 68:3194, 1996.

[102] I. D. Parker, Y. Cao, and C. Y. Yang. Lifetime and degradation effects in polymer light-emitting diodes. *J. Appl. Phys.*, 85:2441, 1999.

[103] H. Vestweber, J. Pommerrehne, R. Sander, R. F. Mahrt, A. Greiner, W. Heity, and H. Bässler. Majority carrier injection from ito anodes into organic light-emitting diodes based upon polymer blends. *Synth. Met.*, 68:263, 1995.

[104] P. E. Burrows and S. R. Forrest. Electroluminescence from trap-limited current transport in vacuum deposited organic light emitting devices. *Appl. Phys. Lett.*, 64:2285, 1994.

[105] E. Ettedgui, H. Razafitrimo, Y. Gao, and B. R. Hsieh. Band bending modified tunneling at metal/conjugated polymer interfaces. *Appl. Phys. Lett.*, 67:2705, 1995.

[106] J. R. de Lima, C. Schreiner, I. A. Huemmelgen, C. C. M. Fornari, Jr., C. A Ferreira, and F. C. Nart. Charge injection from polyaniline-poly (methylmethacrylate) blends into poly (p-phenylene vinylene). *J. Appl. Phys.*, 84:1445, 1998.

[107] V. I. Arkhipov, P. Heremans, E. V. Emilianova, G. J. Adiaenssens, and H. Baessler. Charge carrier mobility in doped semiconducting polymers. *Appl. Phys. Lett.*, 82:3245, 2002.

[108] V. Kumar, S. C. Jain, A. K. Kapoor, W. Geens, T. Aernauts, J. Poortmans, and R. Mertens. Carrier transport in conducting polymers with field dependent trap occupancy. *J. Appl. Phys.*, 92:7325, 2002.

[109] A. J. Campbell, M. S. Weaver, D. G. Lidzey, and D. D. C. Bradley. Bulk limited conduction in electroluminescent polymer devices. *J. Appl. Phys.*, 84:53, 1998.

[110] W. P. Blom and M. C. J. M. Vissenberg. Charge transport in poly(p-phenylene vinylene) light-emitting diodes. *Material Science and Engineering Reports*, 27:53, 2000.

[111] S. C. Jain, W. Geens, A. Mehra, V. Kumar, T. Aernouts, J. Poortmans, R. Mertens, and W. Willander. Injection- and space charge limited-currents in doped conducting organic materials. *J. Appl. Phys.*, 89:3804, 2001.

[112] R. D. Gould and B. A. Carter. Electrical conduction and trapping distributions in zno and zno-sn composite varistors. *J. Phys. D: Appl. Phys.*, 16:L201, 1983.

[113] V. Kumar, S. C. Jain, A. K. Kapoor, J. Poortmans, and R. Mertens. Trap density in conducting organic semiconductors determined from temperature dependence of jv characteristics. *J. Appl. Phys.*, 94:1283, 2003.

[114] S. J. Tans, R. G. Miedema, L. J. Geerligs, C. Dekker, J. Wu, D. Neher, and D. Wegner. Electronic transport in monolayers of phthalocyanine polymers. *Nanotechnology*, 14:1043, 2003.

[115] D. Chirvase, Z. Chiguvare, M. Knipper, J. Parisi, V. Dyakonov, and J. C. Hummelen. Temperature dependent characteristics of poly(3 hexylthiophene)-fullerene based heterojunction organic solar cells. *J. Appl. Phys.*, 93:3376, 2003.

[116] R. Valaski, L. M. Moreira, L. Micaroni, and I. A. Hummelgen. Charge injection and transport in electrochemical films of poly(3-hexylthiophene). *J. Appl. Phys.*, 92:2035, 2002.

[117] M. Onoda, K. Tada, A. A. Zakhidov, and K. Yoshino. Photoinduced charge separation in photovoltaic cell with heterojunction of p- and n-type conjugated polymers. *Thin Solid Films*, 331:76, 1998.

[118] B. A. Mattis, P. C. Chang, and V. Subramanian. Effect of thermal cycling on performance of poly(3-hexylthiophene) transistors. *Mat. Res. Soc. Symp. Proc.*, 771:L10.35.1, 2003.

[119] V. Kumar, S. C. Jain, A. K. Kapoor, J. Poortmans, and R. Mertens. Trap density in conducting organic semiconductors determined from temperature dependence of jv characteristics. *J. Appl. Phys.*, 94:1283, 2003.

[120] V. R. Nikitenko, H. Heil, and H. von Seggern. Space-charge limited current in regioregular poly-3-hexyl-thiophene. *J. Appl. Phys.*, 94:2480, 2003.

[121] M. T. Rispens, A. Meetsma, R. Rittberger, C. J. Brabec, N. S. Sariciftci, and Jan C. Hummelen. Influence of the solvent on the crystal structure of pcbm and the efficiency of mdmo-ppv:pcbm plastic solar cells. *Chem. Commun.*, 17:2116, 2003.

[122] Y. Zhao, G. X. Yuan, P. Roche, and M. Leclerc. A calorimetric study of the phase transitions in poly (3 hexylthiophene). *Polymer*, 36:2211, 1995.

[123] T. Ahn, H. L. Lee, and S. H. Han. Effect of annealing of polythiophene derivative for polymer light-emitting diodes. *Appl. Phys. Lett.*, 80:392, 2002.

[124] J. Liu, Y. Shi, and Y. Yang. Solvation-induced morphology effects on the performance of polymer-based photovoltaic devices. *Adv. Funct. Mater.*, 11:420, 2001.

[125] M. Nakazono, T. Kawai, , and K. Yoshino. Effects of heat treatment on properties of poly(3-alkylthiophene). *Chem. Mater.*, 6:864, 1994.

[126] G. Horowitz. Organic field-effect transistors. *Adv. Mater.*, 10:365, 1998.

[127] D. McBranch, I. H. Campbell, D. L. Smith, and J. P. Ferraris. Optical determination of chain orientation in electroluminescent polymer films. *Appl. Phys. Lett.*, 66:1175, 1995.

[128] C. Yang, F. P. Orfino, and S. Holdcroft. A phenomenological model for predicting thermochromism of regioregular and non-regioregular poly(3-alkylthiophenes). *Macromol.*, 29:6510, 1996.

[129] J. J. Dittmer, E. A. Marseglia, and R. H. Friend. Electron trapping in dye/polymer blend photovoltaic cells. *Adv. Mater.*, 12:1270, 2000.

[130] D. Fichou. Structural order in conjugated oligothiophenes and its implications on opto-electronic devices. *J. Mater. Chem.*, 10:571, 2000.

[131] J. Kim, J. Lee, C. W. Han, N. Y. Lee, and I. J. Chung. Effect of thermal annealing on the lifetime of polymer light-emitting diodes. *Appl. Phys. Lett.*, 82:4238, 2003.

[132] Z. Chiguvare, J. Parisi, and V. Dyakonov. Current limiting mechanisms in indium-tin-oxide/poly3-hexylthiophene/aluminum thin film devices. *J. Appl. Phys.*, 94:2440, 2003.

[133] D. Chirvase, J. Parisi, J. C. Hummelen, and V. Dyakonov. Influence of nanomorphology on the photovoltaic action of polymer-fullerene composites. *Nanotechnology*, 15:1317, 2004.

[134] J. Liu, T. F. Guo, and Y. Yang. Effects of thermal annealing on the performance of polymer light emitting diodes. *J. Appl. Phys.*, 91:1595, 2002.

[135] C. M. Ramsdale, J. A. Barker, A. C. Arias, J. D. MacKenzie, R. H. Friend, and N. C. Greenham. The origin of the open-circuit voltage in polyfluorene-based photovoltaic devices. *J. Appl. Phys.*, 92:4266, 2002.

[136] C. J. Brabec, A. Cravino, D. Meissner, N. S. Sariciftci, M. T. Rispens, L. Sanchez, J. C. Hummelen, and T. Fromherz. The influence of materials work function on the open circuit voltage of plastic solar cells. *Thin Solid Films*, 403-404:368, 2002.

[137] C. J. Brabec, A. Cravino, N. S. Sariciftci, Minze T. Rispens, J. C. Hummelen, D. Meissner, T. Fromherz, and Luis Sanchez. Origin of the open circuit voltage of plastic solar cells. *Adv. Funct. Mater.*, 11:374, 2001.

[138] E. Kymakis, E. Alexandrou, and G. A. J. Amaratunga. High open-circuit voltage photovoltaic devices from carbon-nanotube-polymer composites. *J. Appl. Phys.*, 93:1764, 2003.

[139] H. Kim, S. H. Jin, H. Suh, and K. Lee. Origin of the open circuit voltage in conjugated polymer-fullerene photovoltaic cells. *SPIE, USA*, 4:5215, 2003.

[140] V. D. Mihailetchi, P. W. M. Blom, J. C. Hummelen, and M. T. Rispens. Cathode dependence of the open-circuit voltage of polymer:fullerene bulk heterojunction solar cells. *J. Appl. Phys.*, 94:6849, 2003.

[141] H. Frohne, S. E. Shaneen, C. J. Brabec, D. C. Müller, N. S. Sariciftci, and K. Meerholz. Influence of the anodic work function on the performance of organic solar cells. *Chemphyschem*, 9:795, 2002.

Curriculum Vitae

Published papers

- 1. Trap limited hole mobility in semiconducting poly(3-hexylthiophene), Z. Chiguvare, and V. Dyakonov, Physical Review B (Accepted for publication in Physical Review B, October 2004.)

- 2. Current limiting mechanisms in indium tin oxide/poly 3-hexylthiophene/aluminium thin films, Z. Chiguvare, J. Parisi, and V. Dyakonov, Journal of Applied Physics 94, 2440 (2003).

- 3. Electrical and optical design and characterisation of a regioregular polythiophene-fullerene heterojunction polymer solar cell, D. Chirvase, Z. Chiguvare, J. Parisi, M. Knipper, V. Dyakonov, and J. C. Hummelen, Synthetic Metals 138, 299 (2003).

- 4. Temperature dependent characteristics of poly (3hexylthiophene) - fullerene heterojunction organic solar cells, D. Chirvase, Z. Chiguvare, M. Knipper, J. Parisi, V. Dyakonov, and J. C. Hummelen, Journal of Applied Physics 93, 3376 (2003).

- 5. Electronic properties of polymer-fullerene solar cells studied with light-induced electron spin resonance and admittance spectroscopy V. Dyakonov, I. Riedel, Z. Chiguvare, C. Deibel, J. Parisi, C. J. Brabec, N. S. Sariciftci and J. C. Hummelen, Organic and Polymeric Materials and Devices - Optical, Electrical and Optoelectronic Properties, MRS Proceedings 725, P.7.10 (2002)

Conferences and workshop papers

1. Investigation of current limiting mechanisms within polymer-fullerene solar cells, E. von Hauff, V. Dyakonov, J. Parisi, Z. Chiguvare , and I. Riedel, Paper presentation at the International Conference on the Physics, Chemistry and Engineering of Solar Cells (SSCELL-2004) - Badajoz, Spain - 13-15 May 2004

2. Realisation of polymer-fullerene solar cells without charge transport limitations, V. Dyakonov, J. Parisi, I. Riedel, and Z. Chiguvare, Paper Presentation at the Quantsol Conference, 14-20 March 2004 - Badgastein, Austria.

3. Effect of thermal annealing on characteristic traps in poly(3-hexylthiophene) Thin Films, Z. Chiguvare, J. Parisi, and V. Dyakonov, Poster presented at the Germany Physical Society Conference - Regensburg, Germany 08-12 Mar 2004

4. Electrical and optical design and characterisation of a regioregular polythiophene- fullerene heterojunction polymer solar cell, D. Chirvase, Z. Chiguvare, J. Parisi, V. Dyakonov, and J. C. Hummelen, Poster Presentation for the E-MRS Spring Meeting 2002 - June 18 to 21- Strasburg, France.

5. Influence of temperature and illumination intensity on the current - voltage characteristics of polymer-fullerene solar cells, V. Dyakonov, I. Riedel, Z. Chiguvare, D. Chirvase, J. Parisi, L. Lusten, D. Van der Zande, and J. C. Hummelen, - Paper presented at the Germany Physical Society Seminar - Regensburg, Germany 11-15 March 2002

6. Photoinduced absorption spectroscopy on MDMO-PPV/PCBM composites, M. Knipper, M. Pientka, S. Boeger, Z. Chiguvare, I. Riedel, J. C. Hummelen, J. Parisi, and V. Dyakonov, Poster presented at the Germany Physical Society Conference - Regensburg, Germany 11-15 Mar 2002

7. Current limiting mechanisms in poly(3 hexylthiophene) thin film devices, Z. Chiguvare, E. von Hauff, J. Parisi, and V. Dyakonov, Poster presentation for the E-MRS Spring Meeting 2003 - June 10 to 13 - Strasburg, France

8. Principles of operation of organic solar cells, Z. Chiguvare, - Paper presented at: The 2nd Seminar of Material Science Workgroups on Electronically Active Substances - Hanse Science College - Delmenhorst, Germany - 7 to 8 February 2002.

Curriculum Vitae
PERSONAL DETAILS

NAME	Zivayi, CHIGUVARE
SEX	Male
DATE OF BIRTH	26 October 1969
PLACE OF BIRTH	Marondera, Zimbabwe
NATIONALITY	Zimbabwean
DRIVING LICENCE	Class 4 (Zimbabwean)
MARRITAL STATUS	Married (2 children)
LANGUAGES	English, Spanish, German and Shona
CONTACT ADDRESS	Zivayi_Chiguvare@Yahoo.com

ACADEMIC PROFILE

	Degree level	Institution	Degree Class	Year
1	PhD Physics	University of Oldenburg- Germany	Magna cum laude (1)	2001-05
2	MSc in Applied Physics	University of Zimbabwe	Merit	1996-97
3	BSc (Hons.) in Physics	University of Zimbabwe	2.1	1995
4	Lic. in Physics Education	E. J. Varona FPU - Cuba	Golden Title(1)	1988-93

WORK EXPERIENCE

1	Lecturer	(Renewable Energy Programme)	University of Zimbabwe	1999 to date
2	Meteorologist	(Radar and Electronics Dept.)	Govt. of Zimbabwe	1997-99
3	Industrial Trainee	(GEF Solar Project)	UNDP/Govt. of Zimbabwe	1996-7
4	Teacher	('O' level Science and Maths)	Min Education-Zimbabwe	1993-94
5	Student Teacher	(Pre-University Physics)	Min Education-Cuba	1992-93

PROFESSIONAL MEMBERSHIP: German Physical Society (member number 039716)
HOBBIES: Reading, listening to music, athletics

* * *

Erklärungen

Ich erkläre hiermit, dass ich die vorliegende Dissertation weder in ihrer Gesamtheit noch in Teilen einer anderen wissenschaftlichen Hochschule zur Begutachtung in einem Promotionsverfahren vorliegt oder vorgelegen hat.

Oldenburg, den 16. November 2004.

....
(Zivayi Chiguvare)

Ich erkläre hiermit, dass ich die vorliegende Arbeit bereits in Teilen veröffentlicht wurde.

Oldenburg, den 16. November 2004.

....
(Zivayi Chiguvare)

Ich erkläre hiermit, dass ich die vorliegende Arbeit selbst verfasst und nur die im Literaturverzeichnis angegebenen Quellen und Hilfsmittel benutzt habe.

Oldenburg, den 16. November 2004.

....
(Zivayi Chiguvare)